



British
Geological
Survey

Industrial Decarbonisation Research and Innovation Centre project: Hydrogen storage in porous media: Pre- and post-batch experiment assessment of borehole samples

Decarbonisation and Resource Management Programme
Open Report OR/23/022

If you have a cover picture delete this text and insert it here.
Scale the picture to fit the cell

The National Grid and other
Ordnance Survey data
© Crown Copyright and
database rights 2021.
Ordnance Survey Licence
No. 100021290 EUL.

Keywords

Hydrogen storage; porous
rocks; petrography; X-ray
diffraction; microbial
response; experimental
design.

Bibliographical reference

ROCHELLE, CA, LIDDY, TJ,
RUSHTON, JC, KEMP, SJ,
PEARSON, M, GREGORY, S,
MACKIE, J, CRIPPS, C, HASLAM,
RB, WILLIAMS, PJ, MA, L,
BRAID, H, TAYLOR, KG &
Hough, E. 2023.
Industrial Decarbonisation
Research and Innovation
Centre project: Hydrogen
storage in porous media: Pre-
and post-batch experiment
assessment of borehole
samples. *British Geological
Survey Open Report*,
OR/23/022. 128pp.

Copyright in materials derived
from the British Geological
Survey's work is owned by
UK Research and Innovation
(UKRI) and/or the authority
that commissioned the work.
You may not copy or adapt
this publication without first
obtaining permission. Contact
the BGS Intellectual Property
Rights Section, British
Geological Survey, Keyworth,
e-mail ipr@bgs.ac.uk. You
may quote extracts of a
reasonable length without
prior permission, provided a
full acknowledgement is given
of the source of the extract.

Maps and diagrams in this
book use topography based
on Ordnance Survey
mapping.

Industrial Decarbonisation Research and Innovation Centre project: Hydrogen storage in porous media: Pre- and post-batch experiment assessment of borehole samples

CA Rochelle, TJ Liddy, JC Rushton, SJ Kemp, M Pearson, S
Gregory, J Mackie, C Cripps, RB Haslam, PJ Williams, L Ma,
H Braid, KG Taylor & E Hough

BRITISH GEOLOGICAL SURVEY

The full range of our publications is available from BGS shops at Nottingham, Edinburgh, London and Cardiff (Welsh publications only) see contact details below or shop online at www.geologyshop.com

The London Information Office also maintains a reference collection of BGS publications, including maps, for consultation.

We publish an annual catalogue of our maps and other publications; this catalogue is available online or from any of the BGS shops.

The British Geological Survey carries out the geological survey of Great Britain and Northern Ireland (the latter as an agency service for the government of Northern Ireland), and of the surrounding continental shelf, as well as basic research projects. It also undertakes programmes of technical aid in geology in developing countries.

The British Geological Survey is a component body of UK Research and Innovation.

British Geological Survey offices

**Nicker Hill, Keyworth,
Nottingham NG12 5GG**

Tel 0115 936 3100

BGS Central Enquiries Desk

Tel 0115 936 3143

email enquiries@bgs.ac.uk

BGS Sales

Tel 0115 936 3241

email sales@bgs.ac.uk

**The Lyell Centre, Research Avenue South,
Edinburgh EH14 4AP**

Tel 0131 667 1000

email scotsales@bgs.ac.uk

**Natural History Museum, Cromwell Road,
London SW7 5BD**

Tel 020 7589 4090

Tel 020 7942 5344/45

email bgs-london@bgs.ac.uk

**Cardiff University, Main Building, Park Place,
Cardiff CF10 3AT**

Tel 029 2167 4280

**Maclean Building, Crowmarsh Gifford,
Wallingford OX10 8BB**

Tel 01491 838800

**Geological Survey of Northern Ireland, Department of
Enterprise, Trade & Investment, Dundonald House,
Upper Newtownards Road, Ballymiscaw,
Belfast, BT4 3SB**

Tel 01232 666595

www.bgs.ac.uk/gsni/

**Natural Environment Research Council, Polaris House,
North Star Avenue, Swindon SN2 1EU**

Tel 01793 411500

Fax 01793 411501

www.nerc.ac.uk

**UK Research and Innovation, Polaris House,
Swindon SN2 1FL**

Tel 01793 444000

www.ukri.org

Website www.bgs.ac.uk

Shop online at www.geologyshop.com

Acknowledgements

We acknowledge funding through the Industrial Decarbonisation and Research Innovation Centre (IDRIC, Multidisciplinary Integrated Programme 7, project 059), co-ordinated by Heriot-Watt University.

Contents

Acknowledgements	i
Contents	ii
Non-technical summary: Enabling hydrogen storage near industrial clusters	1
Summary	3
1 Introduction.....	5
2 Sample selection	7
3 Borehole descriptions.....	12
3.1 Sherwood Sandstone.....	12
3.2 Lower Greensand/Chalk	13
4 Petrography.....	15
5 X-ray diffraction	36
5.1 Sample preparation	36
5.2 analysis	36
5.3 Results.....	37
6 Specific surface area analysis	40
6.1 Methodology	40
6.2 Results.....	40
7 Porosity and permeability measurements	42
7.1 Methods.....	42
7.2 Porosity.....	42
8 X-ray computerised tomography.....	44
8.1 Methods.....	44
8.2 Other Analytical Techniques	47
8.3 Results.....	48
9 Experimental design and geochemistry.....	53
9.1 Methodologies	53
9.2 Results.....	61
10 Approach to understanding potential microbial response	76
10.1 Introduction.....	76
10.2 Methods.....	76
10.3 Results.....	77
11 National-scale mapping exercise	80
12 Discussion and conclusions.....	83
12.1 Petrography- discussion.....	83
12.2 X-ray diffraction- discussion.....	83
12.3 Porosity and permeability- discussion	84
12.4 X-ray computerised tomography- discussion	84
12.5 Experimental design and Geochemistry- Discussion.....	84

12.6	Microbiology response- discussion.....	84
12.7	National-scale mapping exercise- Discussion.....	85
Appendix 1	Images of core materials selected.....	86
Appendix 2	Sedimentary logs: Cretaceous borehole material.....	96
Appendix 3	Porosity and Permeability results.....	101
Appendix 4	Changes in water chemistry, pre- and post experiment.....	105
Appendix 5	Microbiological growth media.....	113
References	114

FIGURES

Figure 1:	National-scale assessment of areas of geology that may be suitable for hydrogen storage in porous rocks.....	2
Figure 2:	Map showing principal industrial clusters with a 3D facies map showing where the Sherwood Sandstone is present at surface and depth (including the Cheshire Basin), and absent over the London Platform, in England and Wales. <i>Contains Ordnance Survey data © Crown copyright and database right 2021.</i>	3
Figure 3:	location of bedrock samples taken for analysis. <i>Contains Ordnance Survey data © Crown copyright and database right 2021. Ordnance Survey Licence No. 100021290 EUL.7</i>	
Figure 4.	Summary of specific surface area data for the pre- and post-experimental samples.	41
Figure 5:	X-ray CT Sample Prep and Scanner.....	45
Figure 6:	X-ray CT Data Slices.....	46
Figure 7:	Non-Local Means Filter.....	46
Figure 8:	Segmented CT Data.....	46
Figure 9:	A: ResLab DHP-100 and B: ResLab DGP.....	48
Figure 10:	Ortho slices of pre-experiment scan and post-experiment scan of sample SSK138921 (Chester Formation).....	49
Figure 11:	Ortho slices of pre-experiment and post-experiment scan of sample SSK138924 (Hythe Formation).....	49
Figure 12:	Ortho slices of pre-experiment scan and post-experiment scan of sample SSK138926 (Sandgate Formation).....	50
Figure 13:	Ortho slices of pre-experiment scan and post-experiment scan of sample SSK138927 (Glauconitic Marl).....	50
Figure 14:	Fines migration shown in XY slice 433 of sample SSK138924 Hythe Formation.....	51
Figure 15:	Fines migration shown in 3D of sample SSK138924 Hythe Formation.....	52
Figure 16:	Schematic representation of the experimental approach.....	55
Figure 17:	Schematic diagram and photograph of a steel batch reactor, PTFE liner, and magnetic stirrer.....	56
Figure 18 :	Example of the range of ways samples were introduced into the reactors.....	58
Figure 19:	Samples as mounted inside the reactors, adjacent to the filter assembly on the dip tube.....	58
Figure 20:	Layout of several batch reactors inside the incubator.....	58

Figure 21: Sampling arrangement. Note syringe attached to sampling valve, and red gas monitor for hydrogen.	59
Figure 22: Typically, the rock samples appeared relatively unchanged at the end of the experiments.	60
Figure 23: Crystalline secondary minerals were visible at the end of the cement experiment (circled).	61
Figure 24: Schematic diagram of a pre-/post-reaction water chemistry plot. Chemical changes are evidenced by departures from the 1:1 line.	61
Figure 25: Evolution of pH and selected dissolved analytes upon reacting UKGEOS water with a red Permo-Triassic sandstone SSK138919.	62
Figure 26: Comparison plot of pre-/post-experiment (line vs blue dot) water chemistry when UKGEOS water is equilibrated with Sherwood Sandstone SSK138921 under N ₂ pressure (Run HIL59).	63
Figure 27: Comparison plot of pre-/post-experiment water chemistry when UKGEOS water is equilibrated with Sherwood Sandstone SSK138922 under N ₂ pressure (Run HIL60).	64
Figure 28: Comparison plot of pre-/post-experiment water chemistry when UKGEOS water is equilibrated with Sherwood Sandstone SSK138919 under N ₂ pressure (Run HIL73).	64
Figure 29: Comparison plot of pre-/post-experiment water chemistry when the NaCl solution is equilibrated with Hythe Formation sandstone SSK138924 under N ₂ pressure (Run HIL61).	65
Figure 30: Comparison plot of pre-/post-experiment water chemistry when the NaCl solution is equilibrated with Hythe Formation sandstone SSK138925 under N ₂ pressure (Run HIL62).	66
Figure 31: Comparison plot of pre-/post-experiment water chemistry when the NaCl solution is equilibrated with Sandgate Formation sandstone SSK138926 under N ₂ pressure (Run HIL63).	67
Figure 32: Comparison plot of pre-/post-experiment water chemistry when the NaCl solution is equilibrated with Glauconitic Marl chalk SSK138927 under N ₂ pressure (Run HIL64).	67
Figure 33: Comparison plot of pre-/post-experiment water chemistry when 'aged' UKGEOS water and Sherwood Sandstone SSK138921 is exposed to high pressure H ₂ pressure (Run HIL66).	68
Figure 34: Comparison plot of pre-/post-experiment water chemistry when 'aged' UKGEOS water and Sherwood Sandstone SSK138922 is exposed to high pressure H ₂ pressure (Run HIL67).	69
Figure 35: Comparison plot of pre-/post-experiment water chemistry when 'aged' UKGEOS water and Sherwood Sandstone SSK138919 is exposed to high pressure H ₂ pressure (Run HIL74).	69
Figure 36: Comparison plot of pre-/post-experiment water chemistry when 'aged' NaCl solution and Hythe Formation sandstone SSK138924 is exposed to high pressure H ₂ pressure (Run HIL68).	70
Figure 37: Comparison plot of pre-/post-experiment water chemistry when 'aged' NaCl solution and Hythe Formation sandstone SSK138924 is exposed to high pressure H ₂ pressure (Run HIL69).	71
Figure 38: Comparison plot of pre-/post-experiment water chemistry when 'aged' NaCl solution and Sandgate Formation sandstone SSK138926 is exposed to high pressure H ₂ pressure (Run HIL70).	72
Figure 39: Comparison plot of pre-/post-experiment water chemistry when 'aged' NaCl solution and Glauconitic Marl SSK138927 is exposed to high pressure H ₂ pressure (Run HIL71). ..	72
Figure 40: Comparison plot of pre-/post-experiment water chemistry when cement-equilibrated water and borehole cement are exposed to high pressure H ₂ pressure (Run HIL72).	73

Figure 41 MPN counts of SRB per ml starting fluid after 24 days anaerobic incubation at 50 °C. Starting fluid samples had a nitrogen headspace. 95% confidence intervals (Cornish & Fisher, 1938) indicated with error bars.	77
Figure 42. MPN counts of IRB per ml starting fluid after 25 days anaerobic incubation at 50 °C. Starting fluid samples had a nitrogen headspace. 95% confidence intervals (Cornish & Fisher, 1938) indicated with error bars.	77
Figure 43. Aerobic and anaerobic Miles Misra in colony forming units per ml fluid (CFU/ml) after 7 days incubation at 50 °C. Upper figure: Fluids taken from end of equilibration phase (nitrogen headspace). Lower: Fluid taken at end of experiment (hydrogen headspace).	78
Figure 44 Map showing closures identified from the BGS national scale upper surfaces of the Sherwood Sandstone and Lower Greensand. These are categorised by depth from surface. <i>Contains Ordnance Survey data © Crown copyright and database right 2021</i>	80
Figure 45: Analysis of closures within the Sherwood Sandstone, with closures categorised by depth from ground surface. <i>Contains Ordnance Survey data © Crown copyright and database right 2021</i>	81
Figure 46 Analysis of closures within the Lower Greensand, with closures categorised by depth from ground surface. <i>Contains Ordnance Survey data © Crown copyright and database right 2021</i>	82

PLATES

Plate 1: Experiment rock chip from Sherwood Sandstone SSK138919, pre-experiment, with analytical sites marked up on the whole chip SEM image (right).	17
Plate 2: Full section scans of all Sherwood Sandstone sample thin sections, with those taken forward for the experimental study highlighted (SSK138919, SSK138921 and SSK138922).	18
Plate 3: Combined petrography plate for SSK138919 PTS. Phase map key: Yellow: Quartz; Pink: K-feldspar; Dark Blue: Albite; Red: Biotite; Purple: Muscovite; Light green: Apatite; Mauve: Kaolinitic; Royal blue: Dolomite (Fe); Cyan: Calcitic; Red-pink: Mixed clays (Fe); Orange: Fe Sulphidic.....	19
Plate 4: SSK138921, SEM image from rock chip sample. A very fine-grained sandstone, with a lamination defined by aligned micas, detrital clay content and locally, accessory mineral enrichment (bright grains).	19
Plate 5: SSK138919, SEM image from rock chip sample. A moderately sorted fine-medium grained sandstone. Most grains are of quartz with rare overgrowths (qtz). Minor grain types include clay clasts (altered), tourmaline (tur, note Rare Earth Element inclusion). Box is site of Plate 6.....	20
Plate 6: SSK138919, SEM image from rock chip sample, showing typical K-feldspar grains with well-developed partial overgrowths (K feldspar). Diagenetic grain-coating clays are mostly well developed with a webbed-platy morphology. Box is site of Plate 7.	20
Plate 7: SSK138919, SEM image from rock chip sample. Detail of an area of diagenetic grain-coating clay, showing a box-work webbed-platy morphology. Microquartz overgrowths partially enclose the clays and are better developed where clay coverings are poorly developed (lower left).	21
Plate 8: SSK138920, SEM image from rock chip sample, showing an area of varied development of the grain-coating clays, sparse at the top, thick and well developed at the base. Note clays have formed at the edge of a muscovite (ms) mica.....	21
Plate 9: SSK138922, SEM image from rock chip sample showing an area of dolomite cement (dol). The uppermost dolomite surface is exposed to porosity and has a roughened surface with deeper incision along cleavage planes. The dolomite has partially enclosed an adjacent K-feldspar overgrowth (Kfs).....	22
Plate 10: SSK138919, SEM image from rock chip sample. A partially dissolved plagioclase (pl) with a patchy clay coating. A breach in the coating (centre; circled) reveals a microporous interior. Calcite (cal) cement displays pitting where exposed to porosity (base).	22

Plate 11: SSK138921, SEM image from rock chip sample. From the central boxed area in Plate 4. In this area clay matrix is absent and grain-coating clays are well developed. The multi-layer euhehedral and parallel oriented grain overgrowths (centre to bottom) are multiple developments of K-feldspar overgrowth (Kfp).	23
Plate 12: SSK138923, SEM image from rock chip sample. showing well developed quartz overgrowths (qtz) and authigenic quartz associated with an altered grain (right). Sparse, thin grain-coating clays are visible in overgrowth gaps.	23
Plate 13: Full section scans of all of the Lower Greensand / Chalk sample thin sections. All were taken forward for the experimental study.	24
Plate 14: Full section phase maps for the three Lower Greensand samples. Hythe Formation left and centre; Sandgate Formation right.	25
Plate 15: SSK138924 Hythe Formation, SEM image from rock chip sample. A moderately well-sorted medium-grained sandstone, with common subangular grains. Most are of quartz, with scattered glauconite (glt) and rare heavy minerals (HM). Most grains have thin diagenetic coatings of silica phases. Grain contacts are mostly point, porosity is high and well interconnected.	26
Plate 16: PPL image from PTS of SSK138926 Sandgate Formation. There is a high content of bioclasts including part-dissolved calcitic shell fragments (bio) and microporous sponge spicules (sp). Glauconite grains (glt) are typically fractured. The fabric is grain-supported but matrix is abundant. Most of the microporosity comprises isolated secondary pores (secondry) after spicule dissolution.	26
Plate 17: SSK138926 Sandgate Formation, SEM image from rock chip sample. Showing a calcite (cal) bioclast in clay matrix. In the lower left quadrant is dissolved bioclast with a relict structure of fibrous calcium carbonate (cal). Blocky authigenic zeolite (zeo) is associated.	27
Plate 18: SSK138924 Hythe Formation, SEM image from rock chip sample. From the large boxed area in Plate 15. This rare K-feldspar (Kfp) grain has been fractured by sample preparation, revealing minor internal dissolution. Adjacent grains are thinly coated by finely (<1 µm) textured silica, absent at grain contact sites.	27
Plate 19: SSK138924 Hythe Formation, SEM image from rock chip sample. From the small boxed area in Plate 15, showing the rod-like sub-µm form of much of the silica grain-coating, typically parallel-aligned in domains and stacks with subhedral forms.	28
Plate 20: SSK138925 Hythe Formation, SEM image from rock chip sample, illustrating different forms in the silica grain-coatings, also including two 'faceted' pits. The disc-like platelets (left side), also silica, contain radial fibres and stubby fibrous extensions.	28
Plate 21: SSK138926 Sandgate Formation, SEM image from rock chip sample. In the muddy bioclastic sample, bioclast chambers that are not filled with matrix are typically lined by botryoidal silica with stubby surface extensions. A rod-like cluster of framboidal pyrite (py) has probably formed replacively.	29
Plate 22: SSK138926 Sandgate Formation, SEM image from rock chip sample. The left part of the field of view is a cylindrical silica-based bioclast (sponge spicule) with a fibrous thin to botryoidal silica coating. Zeolite (zeo) has formed on the bioclast into a macropore. The matrix comprises silica, clays and coccoliths.	29
Plate 23: SSK138926 Sandgate Formation, SEM image from rock chip sample, showing detail of the matrix with resolvable coccolith remnants (arrowed). The rest of the matrix comprises silica and platy clays. Curled and webbed edges to detrital clay flakes indicate some diagenetic clay formation through alteration and overgrowth of detrital clays.	30
Plate 24: SSK138927 Glauconitic Marl Member, SEM image from rock chip sample. A limey mudstone with fine to coarse sand grains. In this field of view, the coarse grain at base is apatite (ap). The matrix is a mix of calcium carbonate (principally as micrite and coccolith fragments of a wide range of sizes and preservation) and silicates (quartz fragments, clay minerals).	31

Plate 25: SSK138927 Glauconitic Marl Member, SEM image from rock chip sample, from the central boxed area in Plate 24 showing detail of the matrix which contains abundant coccoliths. Clays dominantly have bridging webbed forms and as such are at least partially diagenetic. Some euhedral single crystal calcite (cal) is authigenic or neofomed. Clay-rich clast lower left is glauconite (glt).	31
Plate 26: SSK138927 Glauconitic Marl Member, SEM image from rock chip sample, from the larger boxed area in Plate 24. Here, a coarse calcite cement (cal) has formed enclosing some matrix components. Angular grain top right is quartz (qtz). Box is site of Plate 27.....	32
Plate 27: SSK138927 Glauconitic Marl Member, SEM image from rock chip sample, from Plate 26. Pyrite (py) is present as framboids and looser clusters of microcrystals, all with euhedral forms. A high proportion of the matrix comprises coccoliths, showing a wide range of types and sizes. The clays show evidence of some diagenetic alteration from detrital origins in the webbed edge morphologies.	32
Plate 28: Comparative panel for pre-post imagery, whole sample SEM images of SSK138919 Sherwood Sandstone, post is after experimental run HIL74.	33
Plate 29: Comparative panel for pre-post imagery, selected area SEM images of SSK138919 Sherwood Sandstone from the boxed areas in Plate 28, equivalent to site 003 in Plate 1. .	34
Plate 30: Comparative panel for pre-post imagery, selected area SEM images of SSK138927 Glauconitic Marl, showing several modes of change that have affected this sample post HIL71.	35
Plate 31: Type G cement, post test HIL71, showing surface portlandite precipitates.	35

TABLES

Table 1: Location metadata and summary description for samples used in this study	8
Table 2: Samples prepared per sample point.....	9
Table 3. Summary of whole-rock XRD analyses.....	38
Table 4. Summary of <2 µm clay mineral XRD analyses.....	39
Table 5. Summary of sample surface area data	40

Table 6: Volume fractions of different phases in four selected samples.....	51
Table 7: Metadata of sample material	54
Table 8: Summary experiment details	54
Table 9: Analyses of headspace gas compositions at the end of the experiments (as a percentage of total gas analysed).....	74
Table 10: Porosity data of 9 rock samples: pre-batch experiments.....	101
Table 11: Permeability data of 9 rock samples: pre-batch experiments.....	102
Table 12: Porosity data of 9 rock samples: post-batch experiments	103
Table 13: Permeability data of 9 rock samples: post-batch experiments	104
Table 14: Starting solutions and nitrogen runs: geochemical changes	105
Table 15: Nitrogen equilibrium test: geochemical changes.....	107
Table 16 : Final hydrogen runs: geochemical changes.....	109

Non-technical summary: Enabling hydrogen storage near industrial clusters

The storage of large amounts of energy is recognised as an important part of meeting low-carbon ambitions. Energy- in the form of thermal (heat and cool), mechanical (pressure, motion) and chemical, (e.g., methane, hydrogen), can be released over various timescales, although many forms of geological storage are more suitable for “Long-Duration” energy storage. This means that discharge times will typically vary from a few days to seasons, allowing geological storage to contribute to effective energy management in response to fluctuating demand and supply at those timescales. Hydrogen is one of the longer-term energy solutions, and can allow the transport, storage and use of energy that is derived from other sources (e.g., reformation of methane). There are several large concentrations of industry (so-called ‘industrial clusters’) that account for a significant proportion of the UK CO₂ emissions (see <https://idric.org/>), and these areas are likely early adopters to reduce emissions using hydrogen. The storage of hydrogen will be a critical part of the supply chain required to reduce carbon emissions, and geological storage – in bedrock layers deep underground – can accommodate the large volumes of hydrogen that will be needed for industrial-scale use.

Current options for the geological storage of hydrogen include pumping the gas into large holes dissolved into naturally occurring beds of rock salt underground. However, these are limited by the distribution of suitable accumulations of rock salt, meaning this ‘cavern storage’ is not possible everywhere in the UK (notably industrial clusters at the Black Country, South Wales and Grangemouth in east Scotland). Storage of hydrogen in porous rocks (where gas is stored in the tiny spaces between individual grains of sand that make up sandstone) may give an alternative option to cavern storage when located close to industrial areas.

However, hydrogen storage is not commercially employed in porous rocks anywhere in the world, and there are processes including geochemical and microbial reactions in the rocks that can be enhanced in the presence of hydrogen which means concerns have been raised relating to containment and contamination of the stored hydrogen. Consequently, to support the uptake of porous storage, there is an urgent need to understand the behaviour of these rocks in terms of their effectiveness and efficiency. Laboratory-based experiments that address these questions could increase investor confidence and move porous storage potential beyond proof-of-concept.

In response to this need, the British Geological Survey (BGS) has recently completed a collaboration with the University of Manchester to investigate the behaviour of hydrogen in the laboratory using samples of porous rocks that may be considered for future storage. Experiments targeted two of the principal water producing rocks (aquifers) in the UK - the Triassic Sherwood Sandstone and Cretaceous Lower Greensand which underlie large areas of England (see figure below).

Results of the laboratory experiments found no major changes to rock structure or composition following exposure to hydrogen at elevated temperatures and pressures. Some of the subtle changes observed could be attributed to tolerances in the analytical techniques used, and it is also possible that the experimental design itself may have contributed to some or all of the changes observed. While this study did not identify major changes in rock samples, there remains the possibility for geochemical reactions or microbial growth in rocks with different compositions.

Full details of the research, including a downloadable research report and slide pack are available from the project website: <https://idric.org/project/mip-7-4/>; general information regarding the Industrial Decarbonisation Research and Innovation Centre is available here: <https://idric.org/>.

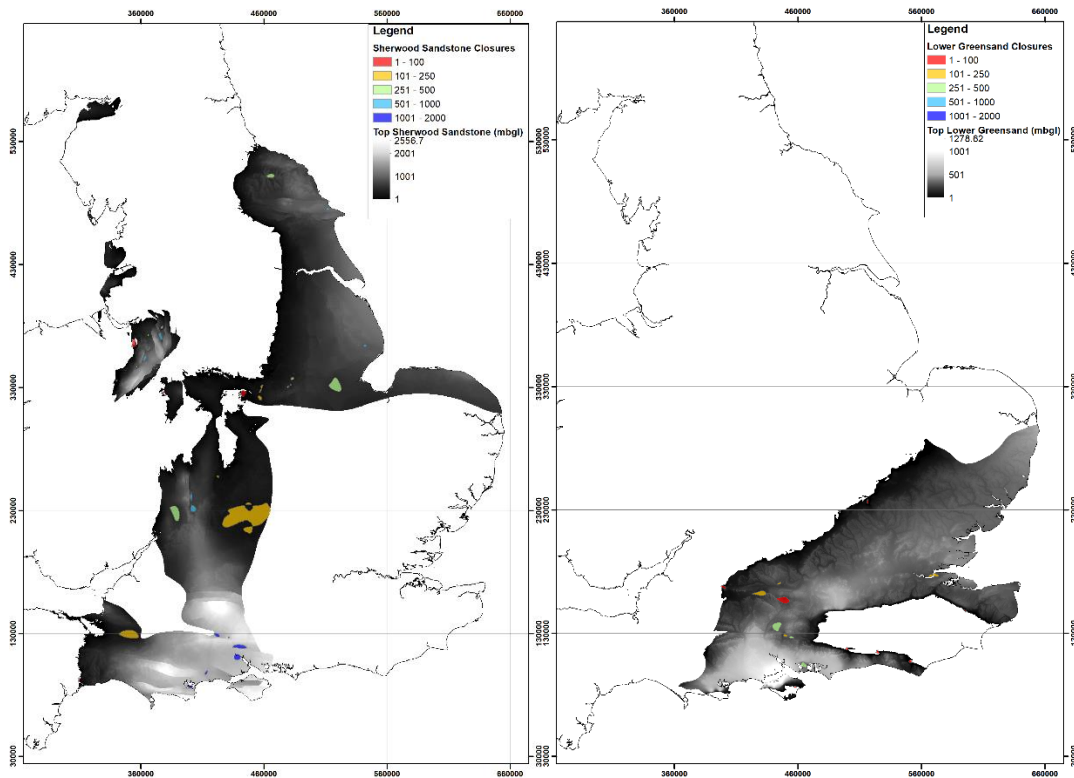


Figure 1: National-scale assessment of areas of geology that may be suitable for hydrogen storage in porous rocks

In the images above we have mapped two principal aquifers that may be suitable in some areas for the underground storage of hydrogen (the Triassic Sherwood Sandstone- left, and Cretaceous Lower Greensand- right) (Figure 1). The upper surface of both rock units has been interrogated to identify natural closures that may represent areas of structural closure that may represent potential storage areas suitable for further exploration. A depth cut-off has not been applied to these areas, although it is acknowledged that some closures are shallower than 100 m and may therefore be technically or commercially unsuitable for storage.

Summary

This report is the published product of a study by the British Geological Survey (BGS) working in collaboration with the University of Manchester. This report provides an initial laboratory-based assessment of the changes in rock properties of three porous rock units that may be caused by exposure to hydrogen at elevated temperatures and pressures. The rock materials analysed are considered representative of possible targets for the onshore storage of hydrogen in the UK.

The utilization of hydrogen as a fuel is one way to enable the decarbonisation of industrial clusters and domestic heating. This report describes an assessment of the potential for subsurface storage of hydrogen in porous rocks and relation to existing industrial clusters; if onshore storage becomes a plausible option then it would help avoid the need for surface storage facilities (Figure 2). Although gas storage is commercially undertaken in engineered caverns in halite, this is only possible in certain areas of the UK where there are suitable beds of halite (including Cheshire, Teesside, Lancashire), and results in cavern storage options nearby to the larger industrial clusters located near to Teesside, Humber and Merseyside. Additionally, the Southampton industrial cluster is located near to the Wessex Basin (Dorset Halite) which may be suitable for cavern construction (although caverns have not yet been developed in this area).

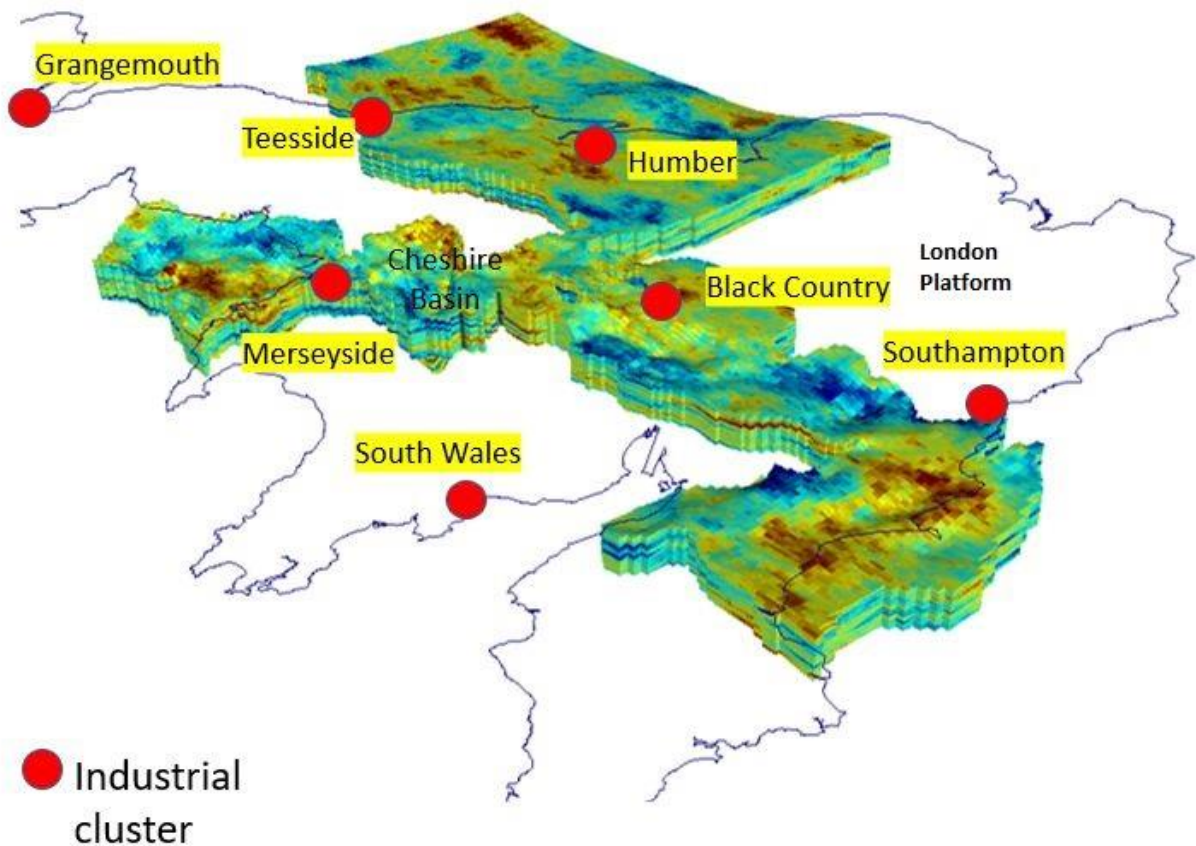


Figure 2: Map showing principal industrial clusters with a 3D facies map showing where the Sherwood Sandstone is present at surface and depth (including the Cheshire Basin), and absent over the London Platform, in England and Wales. *Contains Ordnance Survey data © Crown copyright and database right 2021.*

The industrial clusters located near to the Black Country, South Wales and Grangemouth are all located significant distances from naturally occurring beds of halite within which caverns could be constructed. For these areas, alternative storage options in porous/ fractured bedrock need to be identified to support the implementation of hydrogen into supply chains. For areas located

near to halite beds, the identification of porous rock storage sites would give alternative storage options to those clusters. Regional mapping by BGS indicates that one or more principal aquifers with porous storage potential (Sherwood Sandstone Group or Lower Greensand Formation) are located locally to all major industrial clusters with the exception of south Wales and Grangemouth. For these two areas, potential storage units may be located in alternative geological formations onshore (e.g., secondary aquifers such as the Carboniferous Coal Measures sandstone), or there may be offshore storage opportunities, although these are not considered in the current research.

Currently, hydrogen storage is not commercially employed in porous rocks anywhere in the world, and there are processes including geochemical and microbial reactions in the subsurface that can be enabled in the presence of hydrogen meaning questions concerning containment of hydrogen in porous rocks have been raised. Consequently, there is an urgent need to understand the behaviour of these porous rocks when acting as storage volumes for hydrogen on the effectiveness and efficiency of reservoirs for the storage of this important potential future energy need. This report outlines:

- An experimental method suitable for exposing rock samples to hydrogen at elevated temperatures and pressures;
- Rock materials selected for analysis;
- Characterisation of rock samples before and following exposure to a hydrogen-rich, high-temperature and high-pressure environment;
- Discussion on the potential effects of hydrogen on the porous rocks analysed;
- Maps of where hydrogen storage in the Sherwood Sandstone and Lower Greensand might be possible.

The study found no major changes to rock structure or composition following exposure to hydrogen at elevated temperatures and pressures, while subtle changes observed could be attributed to tolerances in the analytical techniques used. It is also possible that the experimental design itself may have contributed to some or all of the changes observed. While this study did not identify major changes in rock samples, there remains the possibility for geochemical reactions or microbial growth in rocks with a different composition that contain minerals that may be more prone to react with hydrogen (e.g., sulphate minerals; pyrite).

In terms of supporting the decarbonisation of industrial clusters, most such areas are located near to saline aquifers that may represent hydrogen storage targets. We have mapped two principal aquifers that may be suitable in some areas for the underground storage of hydrogen (the Triassic Sherwood Sandstone and Cretaceous Lower Greensand). The upper surface of both rock units has been interrogated to identify natural closures that may represent areas of structural closure that may represent potential storage areas suitable for further exploration. A depth cut-off has not been applied to these areas, although it is acknowledged that some closures are shallower than 100 m and may therefore be technically or commercially unsuitable for storage.

1 Introduction

The UK Government's hydrogen strategy¹ outlines an ambition for 10 GW of hydrogen production capacity by 2030 and acknowledges that storage is a critical part of the supply chain required to deliver this aim. Hydrogen storage in geological formations can provide the large volumes of storage that may be required to support the uptake of hydrogen on an industrial scale, and many studies acknowledge the role that storage must play to meet the projected demand for hydrogen and support increased uptake of renewable energy (e.g., Aftab et al., 2022; Heinemann et al., 2021; Mouli-Castillo et al., 2021).

The geological storage of natural gas (and to a lesser extent hydrogen) is currently employed in solution-mined caverns located in naturally occurring beds of halite - the distribution of halite of suitable thickness, composition and depth is therefore a limiting factor on the areas where cavern storage is possible. Alternative options for the geological storage of hydrogen include storage in porous rocks (either saline aquifers or depleted hydrocarbons reservoirs), but there is a limited understanding of the location and capacity of sites in the UK. The technology is considered to be at a low technology readiness level of 2-4 (Van Gessel & Hajibeygi, 2023), and experiments that prove some aspects of feasibility with laboratory-based studies could increase investor confidence and move the storage potential beyond proof-of-concept. Another consideration is that hydrogen may in certain circumstances react with host rocks, cap rocks and borehole infrastructure (including cements), and may encourage the growth of microbial communities. Such processes have the potential to affect the quality of the stored gas, impact reservoir integrity and/or affect cap rock and borehole sealing of the storage unit.

This study had the following objectives:

- To establish an experimental method suitable for exposing rock samples to hydrogen at elevated temperatures and pressures;
- To select rock samples from geological units that may represent plausible hydrogen storage units;
- To characterise rock samples before and following exposure to a hydrogen-rich, high-temperature and high-pressure environment;
- To better understand the potential effects of hydrogen on the porous rocks analysed;
- A first-pass mapping exercise to identify areas in the UK which may be favourable for hydrogen storage in the Sherwood Sandstone and Lower Greensand.

The Sherwood Sandstone, Lower Greensand and Chalk were selected for analysis in this study. The Sherwood Sandstone and Lower Greensand are plausible candidates for hydrogen storage given their favourable aquifer properties and distribution beneath many parts of northern, central and south-eastern England. Understanding the reactivity of Chalk with hydrogen is relevant as gas/hydrocarbons storage in fractured chalk has been carried out in both the UK and France, so could represent a target for future storage (Evans & West, 2008).

In this study, 7 rock samples and one cement sample were selected for multi-technique characterisation both before and following exposure to a hydrogen-rich environment at elevated temperatures and pressures of 50 degrees C and 150 bar in a series of laboratory-based batch experiments. Samples were selected from rock types considered likely targets for hydrogen storage, focussing on principal aquifers of the Sherwood Sandstone and Lower Greensand (one sample of Chalk was also analysed). Within this study, access to a recently drilled section of Sherwood Sandstone core was possible. This allowed corresponding pore fluids to be acquired that have been used for the calibration of experiments using that material. Characterisation of samples included:

- Petrography and SEM analysis;
- Mineralogy with X-ray diffraction;
- Porosity and permeability;
- X-ray computerised tomography*;

¹https://assets.publishing.service.gov.uk/government/uploads/system/uploads/attachment_data/file/1011283/UK-Hydrogen-Strategy_web.pdf

- Analysis for changes in microbial populations

*: analysis carried out at the University of Manchester.

The experiments were designed to evaluate the response of rock samples to hydrogen storage in terms of geochemical, mineralogical and microbial change, and small-scale structural changes that may affect reservoir performance (including porosity and permeability changes). An associated part of the study was the development of models that show the potential geological/structural closures in the Sherwood Sandstone and Lower Greensand that represent possible areas that may be suitable as hydrogen stores (subject to the uncertainties associated with evaluating sites at a national scale).

2 Sample selection

This study focusses on the potential for hydrogen storage in porous rocks to support decarbonisation of industrial clusters. In the UK, there are 5 principal onshore aquifers that are dominated by porous storage: Carboniferous Fell Sandstone Formation, Permian sandstones, Triassic Sherwood Sandstone Group, Cretaceous Spilsby Sandstone Formation, and Cretaceous Lower Greensand Group.

The BGS holds numerous borehole core samples from the Sherwood Sandstone, Lower Greensand and Chalk. Groundwater chemistry is a relevant parameter in experimental design as it allows samples to be calibrated with appropriate fluid chemistries (depending on composition, the chemistry of fluids may promote or attenuate reactions with hydrogen in the subsurface). Importantly, recently acquired fluid samples were available to calibrate the Sherwood Sandstone samples chosen for this study.

The Triassic Sherwood Sandstone is local at subcrop near to the Humber, Teesside, Black Country, Southampton and Merseyside industrial clusters, and samples for use in this study were prioritised from this unit (Figure 2). Additionally, the Cretaceous Lower Greensand is present in the south-east of the UK and may give opportunities for hydrogen storage in this region (where there are few other obvious geological storage options in the subsurface). One sample of Chalk, located close to the Lower Greensand, was also selected for analysis.

The BGS on behalf of NERC had recently drilled a borehole in the Sherwood Sandstone at Ince Marshes, Cheshire. As well as giving the opportunity for fresh core samples, borehole fluids were also available for the site which allow for calibration of samples fluids during experiments. Five bedrock sample points from the UKGEOS Ground Investigation Borehole A101 (SJ47NE/141) were identified (Figure 3).

Borehole sample points of the Lower Greensand were identified from two boreholes: A3 Hindhead SU83/17, Laporte 360 TQ25SE/247. A sample of chalk (Glaucconitic Marl) was obtained from the Faircross Borehole (SU66SE/21); Figure 3.

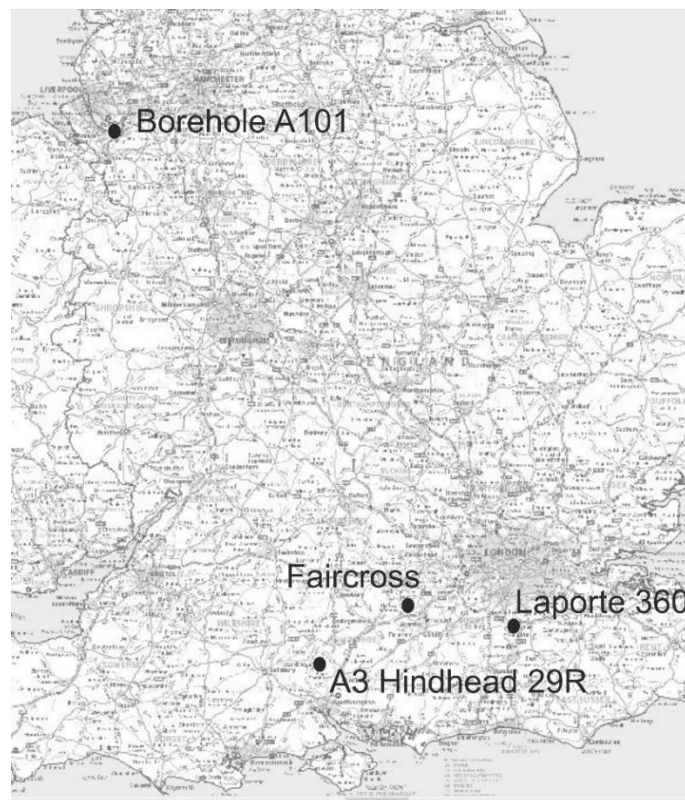


Figure 3: location of bedrock samples taken for analysis. *Contains Ordnance Survey data © Crown copyright and database right 2021. Ordnance Survey Licence No. 100021290 EUL*

Table 1 gives the location data and summary description for these sample points. Nine bedrock samples were selected, from which 7 were analysed along with a sample of borehole cement (see also Appendix 1).

Table 1: Location metadata and summary description for samples used in this study

Borehole Name	BGS reference number	Subsample number	Depth interval (m)	Lithology	Rock unit
UKGEOS CHESHIRE A-101	SJ47NE141.	SSK138919	78.00 – 78.06	Sandstone, red-brown, mottled pale pink, fine-medium-grained, low-angle cross-bedded (channel fill)	Chester Formation
UKGEOS CHESHIRE A-101	SJ47NE141.	SSK138920	81.70 – 81.80	Sandstone, red-brown, moderately sorted, fine-medium-grained, low-angle cross-bedded (channel fill)	Chester Formation
UKGEOS CHESHIRE A-101	SJ47NE141.	SSK138921	89.97 – 90.07	Sandstone, red-brown, fine-grained, cross-laminated, micaceous (channel base)	Chester Formation
UKGEOS CHESHIRE A-101	SJ47NE141.	SSK138922	106.42 – 106.52	Sandstone, red-brown and yellow-brown; medium-grained, planar lamination (some minor soft sediment deformation in this unit); common mud-clasts (channel fill)	Chester Formation
UKGEOS CHESHIRE A-101	SJ47NE141.	SSK138923	117.73 – 117.83	Sandstone, red-brown and yellow-brown, fine-medium grained, moderately sorted, sub-rounded grains, low-angle cross-bedded with mudflakes up to 20 mm; deformation bands in this unit (Channel fill)	Chester Formation
A3 HINDHEAD 29R	SU83NE17.	SSK138924	47.01 – 41.11	Sandstone, yellow, coarse-grained, friable	Hythe Formation (Lower Greensand Group)
A3 HINDHEAD 29R	SU83NE17.	SSK138925	51.55 – 51.65	Sandstone, yellow, coarse-grained, friable	Hythe Formation (Lower Greensand Group)

Borehole Name	BGS reference number	Subsample number	Depth interval (m)	Lithology	Rock unit
LAPORTE 360	TQ25SE247.	SSK138926	33.90 – 34.30	Sandstone, grey, calcareous, very fine-fine grained, bioturbated	Sandgate Formation (Lower Greensand Group).
FAIRCROSS	SU66SE21.	SSK138927	320.30 – 320.40	Cementstone	Glauconitic Marl Member, West Melbury Chalk Formation, Grey Chalk Subgroup, Chalk Group

For each sample point, a series of sub-cores and offcuts were prepared for analysis (Table 2).

Table 2: Samples prepared per sample point

Borehole Name	BGS reference number	Subsample number	Depth interval (m)	Samples prepared
UKGEOS CHESHIRE A-101	SJ47NE141.	SSK138919	78.00 – 78.06	25 mm diameter plug: Poroperm 25 mm diameter plug: contingency 18 mm diameter plug: Micro-CT 2 x 18 mm plug: contingency Offcuts: XRD, surface area analysis (powder); SEM
UKGEOS CHESHIRE A-101	SJ47NE141.	SSK138920	81.70 – 81.80	25 mm diameter plug: Poroperm 25 mm diameter plug: contingency 18 mm diameter plug: Micro-CT 2 x 18 mm plug: contingency Offcuts: XRD, surface area analysis (powder); SEM
Borehole Name	BGS reference number	Subsample number	Depth interval (m)	Samples prepared

UKGEOS CHESHIRE A-101	SJ47NE141.	SSK138921	89.97 – 90.07	25 mm diameter plug: Poroperm 25 mm diameter plug: contingency 18 mm diameter plug: Micro-CT 2 x 18 mm plug: contingency Offcuts: XRD, surface area analysis (powder); SEM
UKGEOS CHESHIRE A-101	SJ47NE141.	SSK138922	106.42 – 106.52	25 mm diameter plug: Poroperm 25 mm diameter plug: contingency 18 mm diameter plug: Micro-CT 2 x 18 mm plug: contingency Offcuts: XRD, surface area analysis (powder); SEM
UKGEOS CHESHIRE A-101	SJ47NE141.	SSK138923	117.73 – 117.83	25 mm diameter plug: Poroperm 25 mm diameter plug: contingency 18 mm diameter plug: Micro-CT 2 x 18 mm plug: contingency Offcuts: XRD, surface area analysis (powder); SEM
A3 HINDHEAD 29R	SU83NE17.	SSK138924	47.01 – 41.11	25 mm diameter plug: Poroperm 25 mm diameter plug: contingency 18 mm diameter plug: Micro-CT 2 x 18 mm plug: contingency Offcuts: XRD, surface area analysis (powder); SEM
A3 HINDHEAD 29R	SU83NE17.	SSK138925	51.55 – 51.65	25 mm diameter plug: Poroperm 25 mm diameter plug: contingency 18 mm diameter plug: Micro-CT 2 x 18 mm plug: contingency Offcuts: XRD, surface area analysis (powder); SEM
LAPORTE 360	TQ25SE247.	SSK138926	33.90 – 34.30	Narrow diameter core so 25 mm plugs could not be prepared: 4 x 18 mm plugs taken
Borehole Name	BGS reference number	Subsample number	Depth interval (m)	Samples prepared
FAIRCROSS	SU66SE21.	SSK138927	320.30 – 320.40	25 mm diameter plug: Poroperm 25 mm diameter plug: contingency

				18 mm diameter plug: Micro-CT 2 x 18 mm plug: contingency Offcuts: XRD, surface area analysis (powder); SEM
--	--	--	--	--

3 Borehole descriptions

Cores adjacent to the sample points described in Section 2 were logged to give sedimentological and structural context to the samples (Appendix 2).

3.1 SHERWOOD SANDSTONE

The Sherwood Sandstone samples (Borehole A101) are described in the UKGEOS data pack for that borehole² (UKGEOS, 2022). These samples are from the Chester Formation of the Cheshire Basin and are available for inspection at the National Geological Repository at the British Geological Survey.

Permo-Triassic age sandstones (and associated lithofacies) are present under large areas of England, stretching from the south-west, through the Midlands and into north-western and north-eastern areas; they are not present in the south-east of England due to non-deposition as they onlap onto the London-Brabant Massif. The British onshore Permo-Triassic records a near continuous record of sedimentary infill, beginning in the Permian with deposition of mostly arid and aeolian deposition (Appleby and Cumbrian Coast Groups), through to non-marine fluvial and aeolian deposition in the Early Triassic (Sherwood Sandstone Group) to a fully marine incursion in the Late Triassic (Penarth Group).

The Early to Middle Triassic Sherwood Sandstone Group (SSG) is designated a Principal Aquifer by the Environment Agency due to its general high porosity, permeability, and favourable hydrogeological characteristics including high transmissivities and high yields of groundwater. The Sherwood Sandstone Group represents deposition of a series of quasi-cyclical fluvial pebbly sandstones, conglomerates and fluvio-aeolian sandstones, that were isolated from marine influence (Newell, 2018). They were deposited in a series of linked and rapidly subsiding fault bounded extensional basins, that developed in response to the break-up of Pangaea, by a major river drainage system (termed the 'Budleighensis River') that flowed northwards from the south, sourced around present-day northern France.

The Cheshire Basin is located in Cheshire and parts of Shropshire and Staffordshire. Structurally, the basin is fault bounded to the east and south-east and is partially separated from the East Irish Sea Basin to the north-east by the Llŷn–Rossendale ridge. The Cheshire Basin covers an area approximately of 3500km² and contains the thickest continuous Permo-Triassic sedimentary succession in England at around 4km (Plant et al, 1999 and Newell, 2018). The SSG of the Cheshire Basin comprises the following formations (oldest first): the Kinnerton Sandstone; Chester; Wilmslow; and Helsby Sandstone formations. The formations generally represent a series of alternating continental lithofacies ranging from fully aeolian (Kinnerton Sandstone Formation) to mixed aeolian-fluvial (Wilmslow Formation, Helsby Formation) to fully fluvial sedimentary deposition (Chester Formation).

In the deepest part of the Cheshire Basin, the Chester Formation is very broadly 500m thick (Newell, 2018). Across the basin in general, it comprises a series of red-brown conglomerates, pebbly sandstones, and sandstones with subordinate dark reddish-brown mudstone interbeds. In addition, within the gravel and sandstone lithofacies, it is characterised by planar and trough cross-stratification, which indicate deposition by low - to medium-sinuosity braided river systems in an arid continental setting (Howard et al, 2007). Due to the nature of the sedimentary deposition, it is anticipated that the lithofacies alternate in a broadly cyclical manner; this is because the braided river channels and inter-channel dune areas shifted and eroded/deposited across an arid dynamic landscape (Hetherington et al, 2022). Typical lithofacies include cross-bedded gravel, interpreted as representing mid-channel bars in confined braided channels; cross-bedded pebbly sandstones interpreted as representing transverse bars and dunes of a braided river system; silts and mudstone interbeds, interpreted as representing interdune or interchannel areas or periods of low flow velocity (Plant et al, 1999).

² <https://data.ukgeos.ac.uk/geonetwork/srv/eng/catalog.search#/metadata/e79c782b-f0fd-0491-e053-0937940aa9e3>

3.1.1 Samples SSK138919 - SSK138923: UKGEOS Ground Investigation Borehole A101 [BGS ID SJ47NE/141]

The UKGEOS Ground Investigation Borehole A101 is located in the northern part of the Cheshire Basin and proves part of the central part of the Chester Formation, with core retrieved between borehole depths of 51.0 -121.2 m (Figure 3). Five sample points (Table 2) were identified from channel base and channel fill facies, representative of the majority of the cored succession (Table 1). These are typically red-brown, fine to medium grained, moderately sorted sandstone, with low angle cross-bedding. In addition, there is some nodules of post diagenetic white cement.

3.2 LOWER GREENSAND/CHALK

Borehole logs for the Cretaceous samples analysed as part of this project are in Appendix 1.

Lower Cretaceous sandstones cover a large swathe of south-east England; they outcrop around the Weald and underlie areas to the north and south of the London Basin. Cretaceous sandstones are notably absent across the London Platform (Anglo-Brabant Massif) due to non-deposition. The Lower Greensand Group of the Wealden Basin is 50-215m thick (Hopson et al., 2008), and is a predominant lithofacies of the Lower Cretaceous sandstones. In general, the Lower Greensand comprises unconsolidated sands and sandstones of various grain-sizes, interbedded with subordinate siltstones and mudstones. In addition, there is usually a component of glauconite (a dark green mineral), often as visible grains, giving rise to the Lower Greensand's name and characteristic greenish hue. Glauconite is found exclusively in marine settings, particularly continental shelf shallow marine environments with slow rates of sediment accumulation. The Lower Greensand was primarily deposited in a continental shelf shallow marine setting during Early Aptian to Early Albian times. Following a small unconformity and a global sea-level rise, the Gault Formation (Selborne Group) was deposited. The Gault Formation comprises a thick dark grey mudstone; it was deposited in a mid to outer shelf edge marine environment and blankets the London Platform. During Late Albian times, the Upper Greensand Formation (Selborne Group) was deposited in a shallow marine setting and is the final sandstone of the Lower Cretaceous; it is a glauconitic fine - grained sandstone. It grades upwards from the muds of the Gault Formation into the sands of the Upper Greensand Formation. It then passes conformably upwards into the overlying Glauconitic Marl Member and this marks the base of the West Melbury Chalk Formation, a major chalk lithofacies of England (Hopson, 2008). In this context, Chalk is typically a micritic limestone of biogenic origin. The chalk represents a return to a deeper typically open marine environment, and dominates the Upper Cretaceous of England.

Three samples (SSK138924, SSK138925, and SSK138926) were taken spanning the Lower Greensand Group sandstones of the Wealden Basin, and they are from the Sandgate and Hythe Formations. A further sample (SSK138927) was obtained from the Glauconitic Marl Member (SSK138927), which is from the very base of the Upper Cretaceous.

3.2.1 Samples SSK138924 and SSK138925: A3 Hindhead 29R Borehole [BGS ID SU83NE/17]

Two samples were taken from this borehole, both in the Hythe Formation of the Lower Greensand Group. The Hythe Formation is the second oldest of the Lower Greensand in the Wealden Basin, and is Early to Late Aptian in age. The lithological characteristics of the Hythe formation in the borehole where the samples were taken is as follows. The sandstone is generally a friable (and sometimes quite loose) pale cream and buff coloured, glauconitic, well-sorted, fine- to medium grained sand and sandstone. It is trough and planar bedded. It can be intensely (30-40%) glauconitic in places. The Hythe Formation at this location is interpreted as being deposited in a shallow marine environment, dominated by high energy currents which give rise to the planar and trough cross-bedding.

3.2.2 Sample SSK138926: Laporte 360 Borehole [BGS ID TQ25SE/247]

The sample was taken in the Sandgate Formation of the Lower Greensand Group. The Sandgate Formation immediately follows the underlying Hythe Formation, in a transgressive fashion, and is Late Aptian in age. The Sandgate Formation in the Laporte Borehole comprises sandstones and silty sandstones. The sandstones are pale green-grey, glauconitic, and

massive. In addition, they are fossiliferous and bioturbated, although species and types of fossils/bioturbation were not seen. The sandy siltstones are medium grey-green, massive (structureless) and friable with an absence of fossils/bioturbation. The Sandgate Formation is interpreted as being deposited in a shallow marine environment (similar to the Hythe Formation), and this is clearly evidenced by the glauconite and fossiliferous/bioturbated nature of the sediments.

3.2.3 Sample SSK138927: Faircross Borehole [BGS ID: SU66SE/21]

The sample was taken at 320.3m – 320.4m which was in the Glauconitic Marl Member, West Melbury Chalk Formation, Grey Chalk Subgroup, from the base of the Chalk Group. The basal unit in this borehole is the Upper Greensand Formation, a poorly consolidated, glauconitic, silty to very fine sandstone, with fossils and bioturbation. This is interpreted as being deposited in a shallow marine environment. The overlying unit, the Glauconitic Marl Member (basal member of the West Melbury Chalk Formation), rests disconformably, and marks the passage into the Upper Cretaceous in the Cenomanian. The Glauconitic Marl member is a heavily glauconitic, calcareous, silty, sandy marl; it passes conformably upward into the West Melbury Chalk Formation proper, marked by a rapid decrease in glauconite. The West Melbury Chalk Formation is a predominately pale to medium grey, marly, chalk with some fossil fragments and bioturbation with a wispy appearance. The West Melbury Chalk Formation (including the Glauconitic Marl Member) was deposited in an open marine environment.

4 Petrography

Petrographic analysis was used:

- to characterise rock samples petrographically through analysis of thin sections and rock chips,
- to assess the effects of the experimental programme using pre-post same-site, high resolution imagery of selected rock chips used in the experiments.

The cement sample was not characterised petrographically and was only examined as a post-experimental chip.

4.1 METHODS

Petrographic analysis utilises a combination of several microscopy methodologies, principally based on optical and scanning electron microscope techniques.

4.1.1 Sample preparation

Polished thin-sections (PTS) oriented in the vertical plane were prepared from selected core samples. These were made from sample portions that were impregnated with an epoxy-resin with added blue dye to enable porosity to be readily identified and distinguished under the optical petrographic microscope. PTS were thinned and polished to a standard thickness of 30 μm .

After preparation, low magnification images of the PTS were recorded by digital scanning using an Epsom Perfection 1240U flatbed scanner equipped with a transmitted light (transparency) scanning attachment. Scanned whole-section images were recorded at a resolution of 1200 dpi.

Rock chips were taken from unimpregnated sample remnants and mounted on 12 mm diameter aluminium pin stubs using carbon paint with freshly exposed surfaces presented uppermost for analysis.

The rock chips examined as part of the pre-post experimental analysis were not mounted and the only preparation pre-experimentally was to ensure all loose surface grains were removed.

The mounted rock chips, and selected PTS, were coated with carbon using the using an AGAR Turbo Carbon Coater, evaporation-coating unit, to a thickness of 25 nm, prior to analyses by scanning electron microscope. This type of coating is applied as an electrically conductive layer to facilitate removal of electrons from the sample surfaces. The pre-post rock chips were analysed (both pre- and post-experiment) without such coatings.

4.1.2 Optical microscopy

The system used for the optical microscopy of selected PTS, was a Zeiss Axio Imager A2m optical petrographic polarising microscope with a Zeiss AxioCam 305 color digital camera attachment driven by Zeiss Zen Pro (v2.5) software. Images were recorded as 24-bit JPG format files. Analytical modes used included transmissive plain-polarised light (PPL) and cross-polarised light (XPL), and reflective plain-polarised light (RF).

4.1.3 Scanning electron microscopy

Scanning electron microscope (SEM) techniques were used to assess the sedimentary textures of the samples, obtain a modal mineralogy (using large area phase mapping), identify mineral phases exposed to the pore system and determine their morphological and compositional characteristics from both PTS and mounted rock chip analyses. These were examined under high vacuum conditions ($<10^{-4}$ Torr), at accelerating voltages of 10-20 keV, using an FEI Company Quanta 600 environmental scanning electron microscope (ESEM) and a Zeiss Sigma 300 field emission SEM. The FEI ESEM is fitted with an Oxford Instruments X-Max 50 mm^2 SDD energy dispersive X-ray (EDX) detector running with Oxford Instruments INCA (v4) software, whilst the Zeiss SEM is fitted with twin Bruker Xflash 6|30, 30 mm^2 , 129 eV, EDX detectors running with Zeiss' Mineralogic phase-mapping software and Bruker's Esprit microanalytical software.

EDX systems are used to identify the elemental compositions from where the electron beam is interacting with points and areas of surfaces, as an aid to phase identification and to map out phase and element distributions. The detector determines the energies of X-rays that are emitted by elements under the imaging electron beam. The EDX systems are capable of identifying elements from atomic number 4 (B) to atomic number 92 (U), and have detection limits of the order of 0.2 to 0.5 wt% for most common elements. As X-rays generated from rough surfaces can be variably attenuated through absorption by material adjacent to the analysis sites, EDX analysis is qualitative when used on samples with rough, unpolished, surfaces.

Images were obtained with secondary electron (SE) and backscatter electron (BSE) imaging techniques. The brightness of a phase under BSE imaging is proportional to its mean atomic number. This means that many minerals can be distinguished by differences in brightness. Additionally, porosity in a PTS impregnated by a carbon-rich resin, typically shows as black or near-black and has a strong brightness contrast with most mineral phases. Consequently, BSEM images are very good for showing mineral phase distributions and variations in chemistry, but are less good at showing surface topography. SEM photomicrographs obtained under BSE and SE conditions were recorded as 8-bit greyscale TIF format digital images.

For the pre-post experiment comparative petrography, detailed SEM imagery and phase characterisation were undertaken from selected surface sites of one rock chip sample from each of the experimental runs. This work was performed in the FEI ESEM using variable pressure (VP) conditions with a chamber atmosphere of water at a pressure of 0.6 Torr to prevent electron charge build-up. BSE imagery was collected using the conventional BSE detector, SE imagery using the VP-specific large field detector (LFD) system. EDX was used for qualitative compositional analysis as an aid to phase identification and characterisation.

4.1.4 Phase mapping and modal analysis

PTS samples were mapped using the Zeiss Mineralogic system over selected areas, at least 5 x 5 mm in size, up to and including full section areas (23 x 36 mm). These were run with the SEM operating at 20 kV, with the 120 μm aperture and 'beam boost' on to give a nominal beam current of 10 nA. Mapping was performed with a beam step size of ~10 to 5 μm and a dwell time of 10 ms. Phase identifications were based on normalised quantitative EDX data passed through expert-user-defined filters. Outputs were formed by combining data from multiple adjacent fields of view, mosaicked into phase map images with associated BSE images. Additionally, quantitative modal data was derived from the same source.

Milodowski and Rushton (2008) reviewed differences between conventional modal analysis and a similar SEM-EDX approach, pointing out that conventional modal analysis (by optical microscope hosted point-counting), differentiates grain types such as lithic clasts (rock fragments), chert, polycrystalline quartz and monocrystalline quartz. However, modal analysis by an SEM-EDX phase mapping technique uses chemistry to differentiate components. Consequently, polymineralic lithic clasts will be determined as their component minerals rather than as discrete particles, and polycrystalline grains will not be recognised. As a result, the modal analyses determined by the above described phase mapping underestimate the significance of lithic components normally considered in sandstone classification systems (e.g. Hallsworth and Knox, 1999). Monocrystalline quartz, polycrystalline quartz and chert are all essentially composed of SiO_2 , and are therefore grouped with "quartz". Similarly, no differentiation can be made between primary sedimentary and secondary or authigenic generations of the same mineral using SEM-EDX phase mapping, and in the current study, this is particularly relevant to quartz and K-feldspar, both of which have minor overgrowth development throughout the SSG interval.

The principal advantage of the SEM-EDX modal analysis is the representativeness of the data and a greater certainty in phase identification. Conventional modal analysis is typically based on a few hundred grains, whilst the smallest areas mapped in this study contain thousands of grains. Another advantage is the output of phase map images which display the distribution of minerals and their relationships with each other, and the with the pore system. This contextualisation of the dataset adds considerably to its usefulness.

4.1.5 Pre-post experiment petrography

Normal post-experiment analysis always leaves interpretive uncertainty as the typical natural variations in mineral distributions, habits and compositions prevent definitive identifications of changes at the pore scale. Microscopic observations are needed to help explain changes to bulk properties and fluid chemistries.

To overcome this uncertainty, rock chip samples were taken from the experimental sample set pre-experiment, and were analysed by SEM using the VP capabilities of the FEI Quanta 600. In this form, the sample does not need any special surface coatings or preparations. Several sites on each sample surface were visited, analysed, and the sites marked-up on a full sample image (Plate 1). The samples were then returned and included in the full experimental process. Post-experiment, the same chips were retrieved and, using the pre-experiment imagery, the same sites were revisited, if they had not been lost or obscured.

Comparing images and microanalytical data then shows any definitive changes that have occurred.



Plate 1: Experiment rock chip from Sherwood Sandstone SSK138919, pre-experiment, with analytical sites marked up on the whole chip SEM image (right).

4.2 RESULTS

4.2.1 Sherwood Sandstone characterisation

Of five initial samples selected from the Sherwood Sandstone Group (SSG), three were selected to go through the experimental programme (SSK SSK138919, SSK138921 and SSK138922). Here, full characterisation is described for the three samples which underwent the experimental programme, some of the general observations recorded are obtained from analysis of all five samples.

The five samples are all SSG sandstones, mostly moderately sorted with grain sizes ranging from fine to medium sand (Plate 2, Plate 3, Plate 5). SSK138921 is strongly laminated with a very fine grain size and a lamination-controlled content of detrital clay matrix (Plate 2). Grains are subrounded to subangular, with the latter dominant. Quartz is the dominant detrital grain type (Plate 3), with lesser but common feldspars (mostly K-feldspar; the less abundant plagioclase is largely albite). Micas are minor constituents apart from in SSK138921, where they are common and aligned with the lamination (Plate 4). Scattered accessory minerals include zircon, apatite, tourmaline, spinel and iron-titanium oxides. Accessory minerals are concentrated in some of the laminations in SSK138921 (Plate 4). Compaction is moderate with point and short edge grain contacts dominant. Many detrital sand grains have red-stained, patchy, inherited grain-coating clays.

Carbonate minerals are the dominant diagenetic phases in the SSG samples, with considerable variation in content from sample to sample. Dolomite is most common, being present in all samples, locally concentrated in areas rich in detrital clays, but also as a widespread pore-filling cement of rhombic crystals up to 300 μm across. Dolomite crystal surfaces exposed to open pores were noted to have notched and pitted surfaces (Plate 9). Some samples have common calcite as mm-scale nodules where it completely occludes porosity (SSK138919, Plate 3). The calcite cement displays rough faces where it has formed against grains with clay coatings, and

deep pitting (Plate 10), where exposed to porosity. The pitting of carbonate cement faces suggest minor diagenetic dissolution has affected them.

The most abundant diagenetic silicate mineral, by area exposed on pore walls, is a grain-coating clay. This was observed throughout the sample set as a webbed-platy morphology (Plate 6) and a composition (from EDX analysis) that suggests it is an illite-smectite. It has a patchy distribution in terms of grain-surface coverage and thickness, both within and between samples (Plate 7, Plate 8). It can be up to 25 μm thick, but is more normally 10-15 μm thick. It has formed over the inherited clay coatings, which have smoother surface morphologies and more illitic compositions. Both calcite and dolomite formation post-date the grain-coating clay formation and there is evidence of some of the diagenetic clay having been compacted around the margins of grain contact sites.

There are minor amounts of diagenetic quartz and feldspar overgrowth. These have both formed as fine euhedral extensions formed through and around the grain-coating clays. K-feldspar overgrowths are dominant and most extensively developed typically partially developed locally as multiple fine euhedral forms (Plate 6, Plate 11). Quartz overgrowth is locally well developed, typically where the grain-coating clays are sparse (Plate 12).

Grain dissolution and alteration has affected some grains, with accessory mineral and feldspar grains most affected. This has crated minor secondary porosity.

Porosity is high to moderate, mostly primary intergranular macropores, lowest in SSK138921 where the clay matrix has facilitated a greater degree of compaction. In the other samples, outside of the carbonate cemented areas, pores are open and moderately well interconnected, although the diagenetic grain-coating clay considerably constricts some pore throats and roughens pore walls (Plate 6, Plate 8). The carbonate cements only form local barriers to pore interconnectivity.

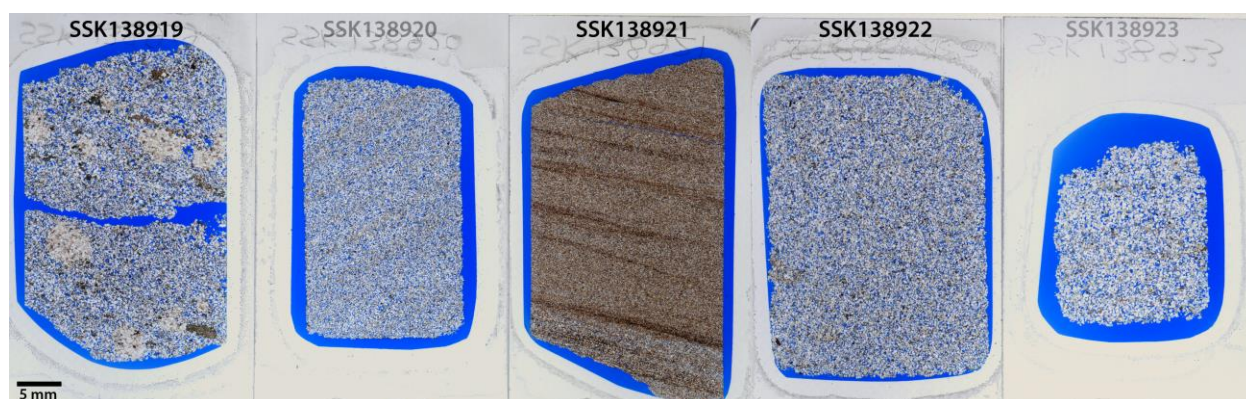


Plate 2: Full section scans of all Sherwood Sandstone sample thin sections, with those taken forward for the experimental study highlighted (SSK138919, SSK138921 and SSK138922).

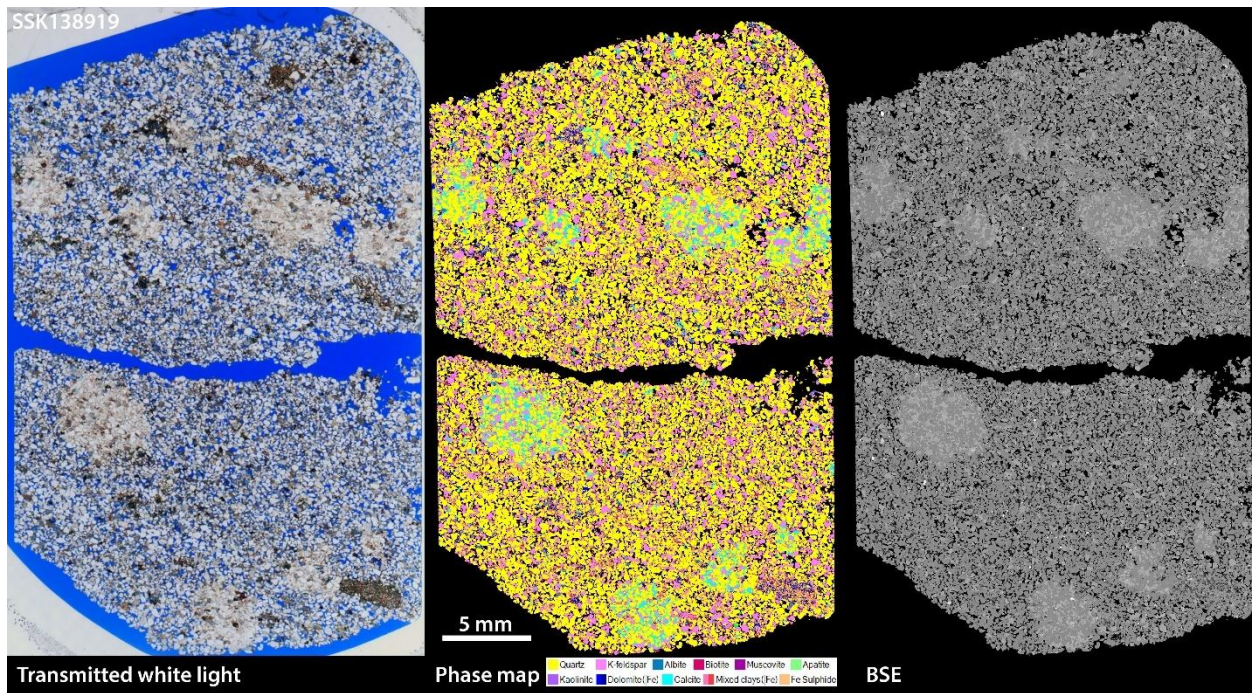


Plate 3: Combined petrography plate for SSK138919 PTS. Phase map key: Yellow: Quartz; Pink: K-feldspar; Dark Blue: Albite; Red: Biotite; Purple: Muscovite; Light green: Apatite; Mauve: Kaolinitic; Royal blue: Dolomite (Fe); Cyan: Calcitic; Red-pink: Mixed clays (Fe); Orange: Fe Sulphidic.

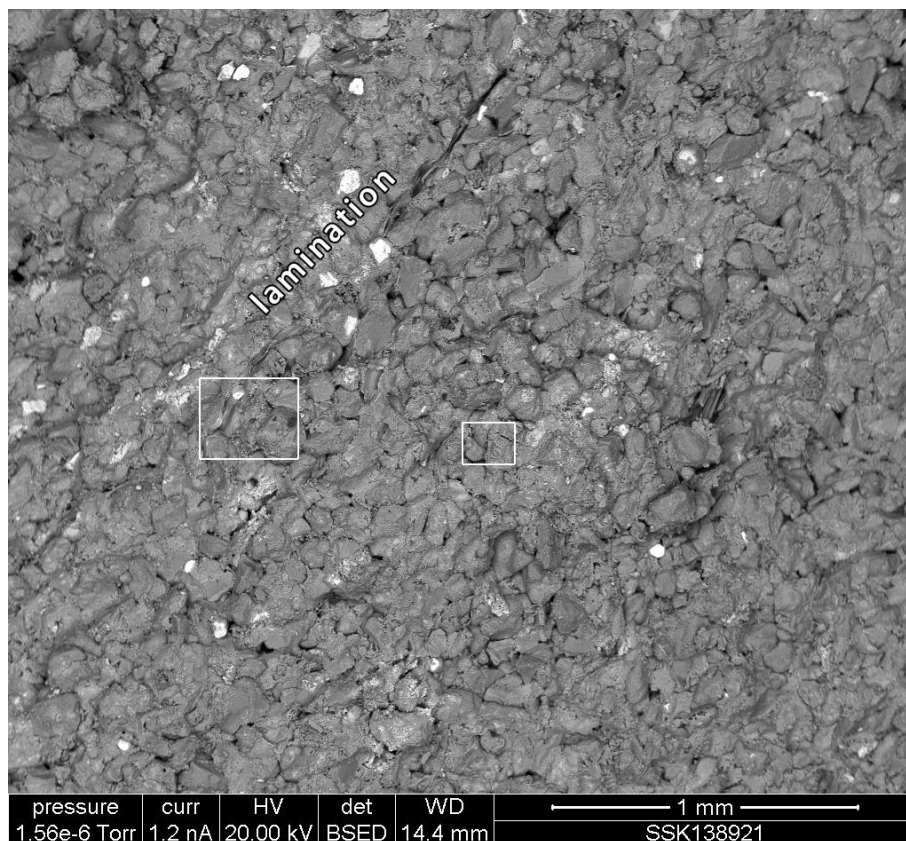


Plate 4: SSK138921, SEM image from rock chip sample. A very fine-grained sandstone, with a lamination defined by aligned micas, detrital clay content and locally, accessory mineral enrichment (bright grains).

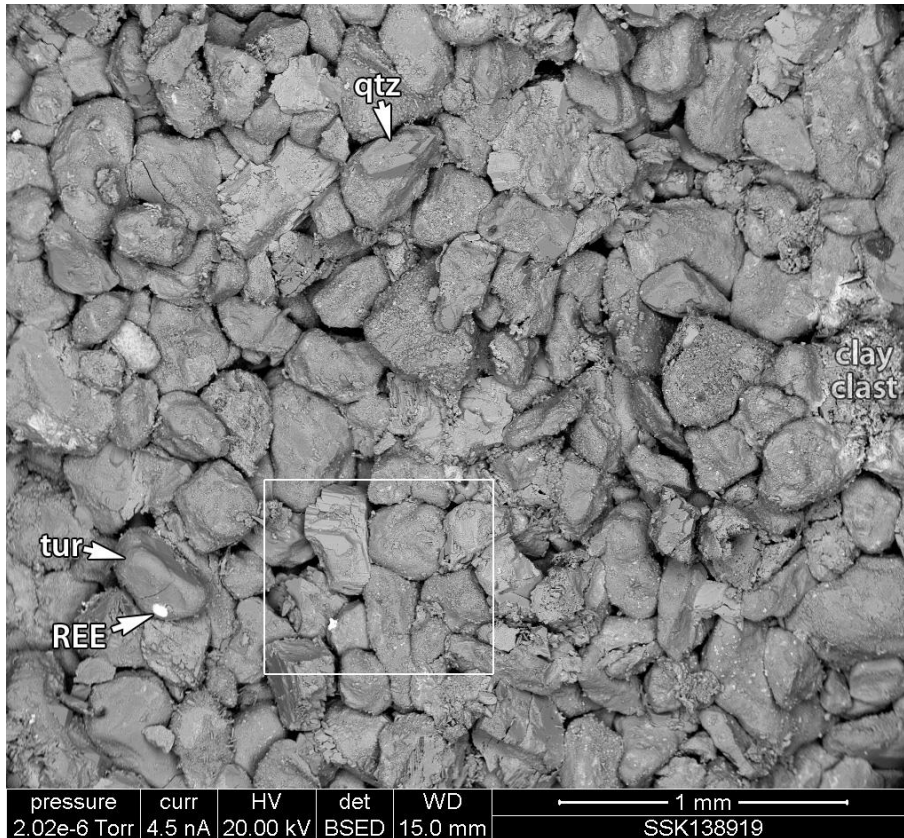


Plate 5: SSK138919, SEM image from rock chip sample. A moderately sorted fine-medium grained sandstone. Most grains are of quartz with rare overgrowths (qtz). Minor grain types include clay clasts (altered), tourmaline (tur, note Rare Earth Element inclusion). Box is site of Plate 6.

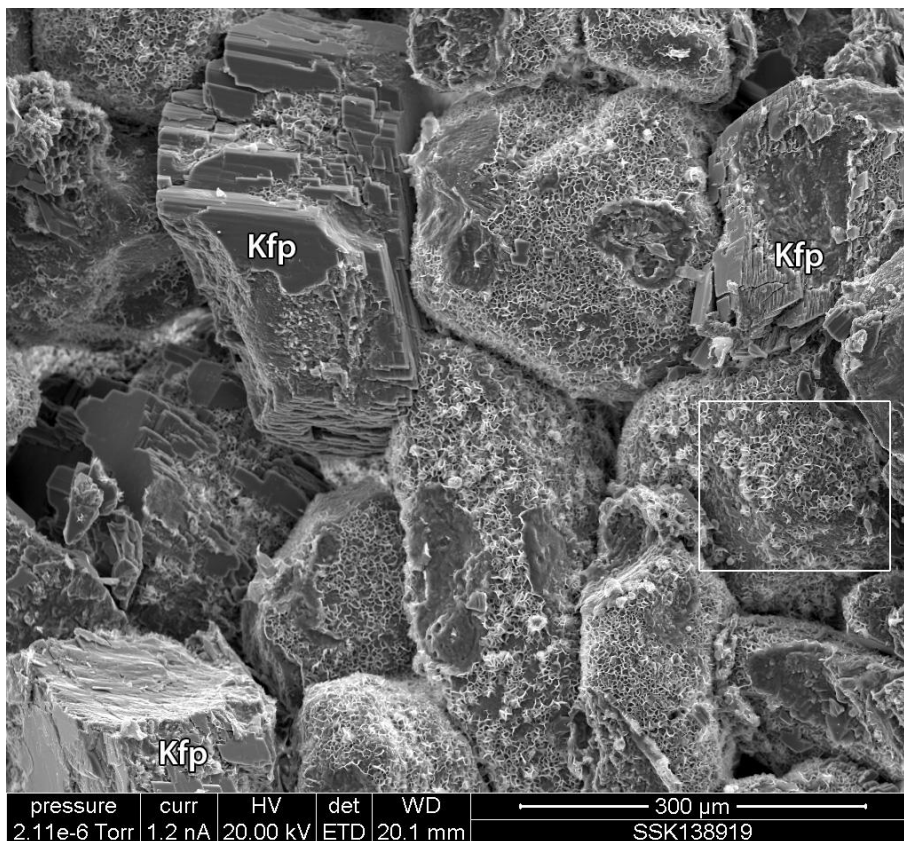


Plate 6: SSK138919, SEM image from rock chip sample, showing typical K-feldspar grains with well-developed partial overgrowths (K feldspar). Diagenetic grain-coating clays are mostly well developed with a webbed-platy morphology. Box is site of Plate 7.

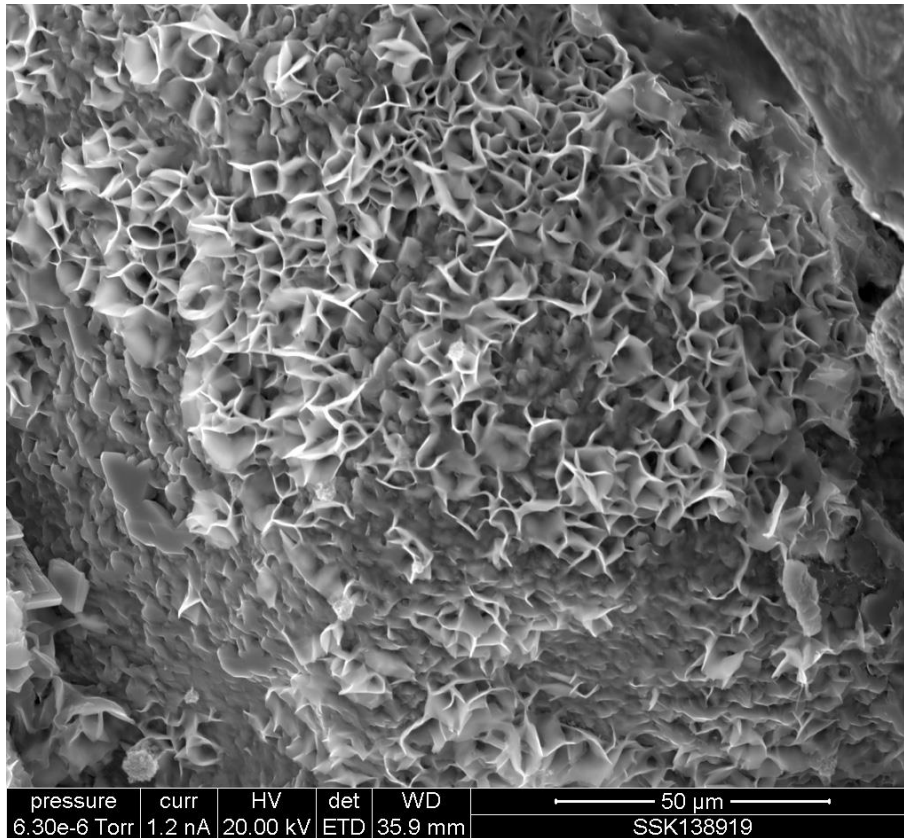


Plate 7: SSK138919, SEM image from rock chip sample. Detail of an area of diagenetic grain-coating clay, showing a box-work webbed-platy morphology. Microquartz overgrowths partially enclose the clays and are better developed where clay coverings are poorly developed (lower left).

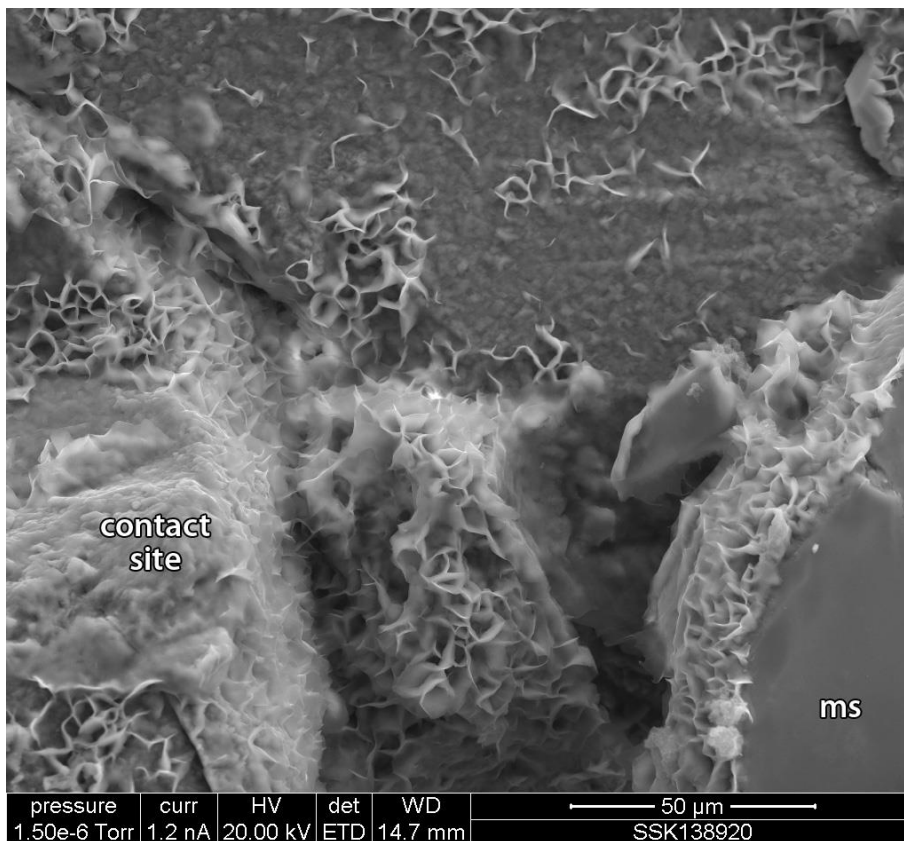


Plate 8: SSK138920, SEM image from rock chip sample, showing an area of varied development of the grain-coating clays, sparse at the top, thick and well developed at the base. Note clays have formed at the edge of a muscovite (ms) mica.



Plate 9: SSK138922, SEM image from rock chip sample showing an area of dolomite cement (dol). The uppermost dolomite surface is exposed to porosity and has a roughened surface with deeper incision along cleavage planes. The dolomite has partially enclosed an adjacent K-feldspar overgrowth (Kfs).

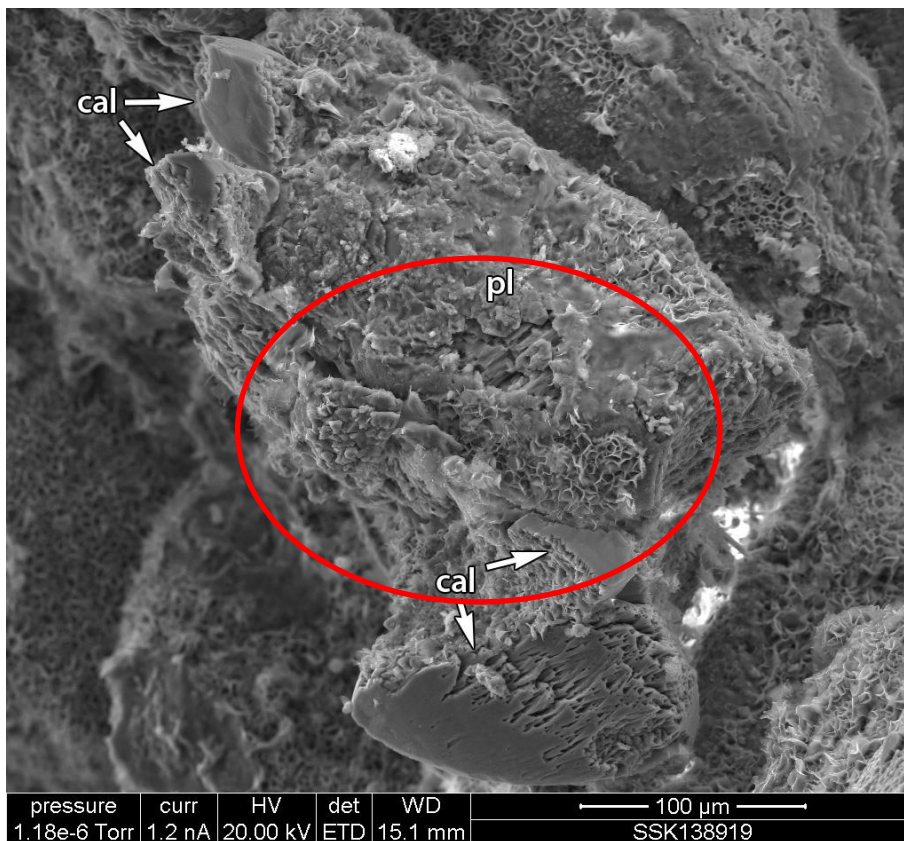


Plate 10: SSK138919, SEM image from rock chip sample. A partially dissolved plagioclase (pl) with a patchy clay coating. A breach in the coating (centre; circled) reveals a microporous interior. Calcite (cal) cement displays pitting where exposed to porosity (base).

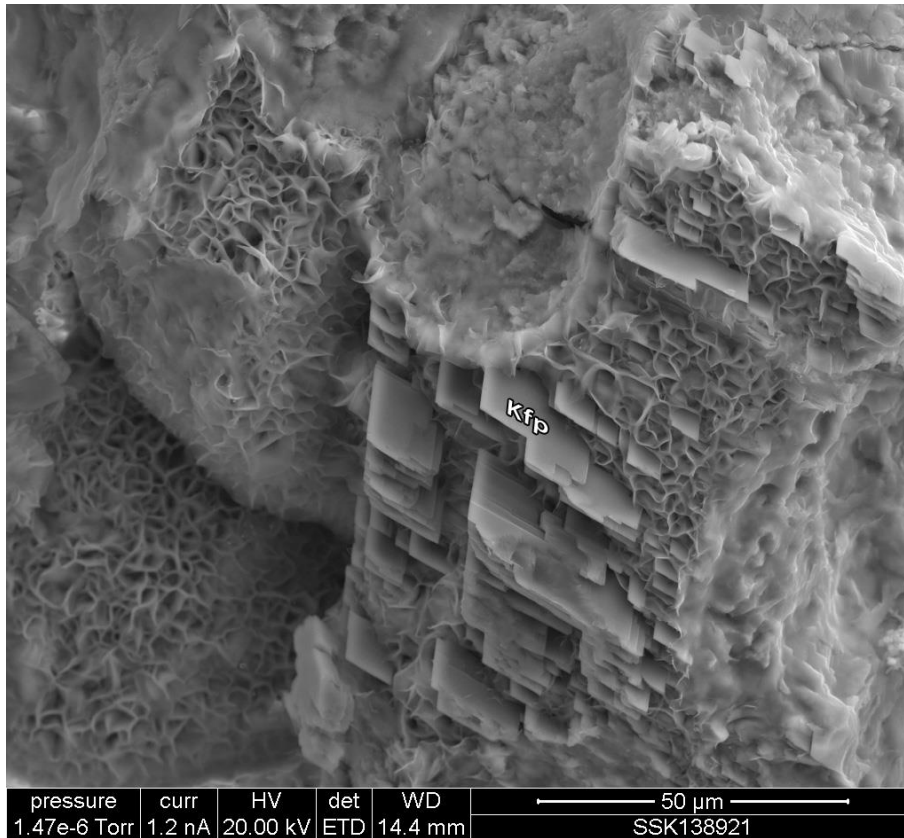


Plate 11: SSK138921, SEM image from rock chip sample. From the central boxed area in Plate 4. In this area clay matrix is absent and grain-coating clays are well developed. The multi-layer euhedral and parallel oriented grain overgrowths (centre to bottom) are multiple developments of K-feldspar overgrowth (Kfp).

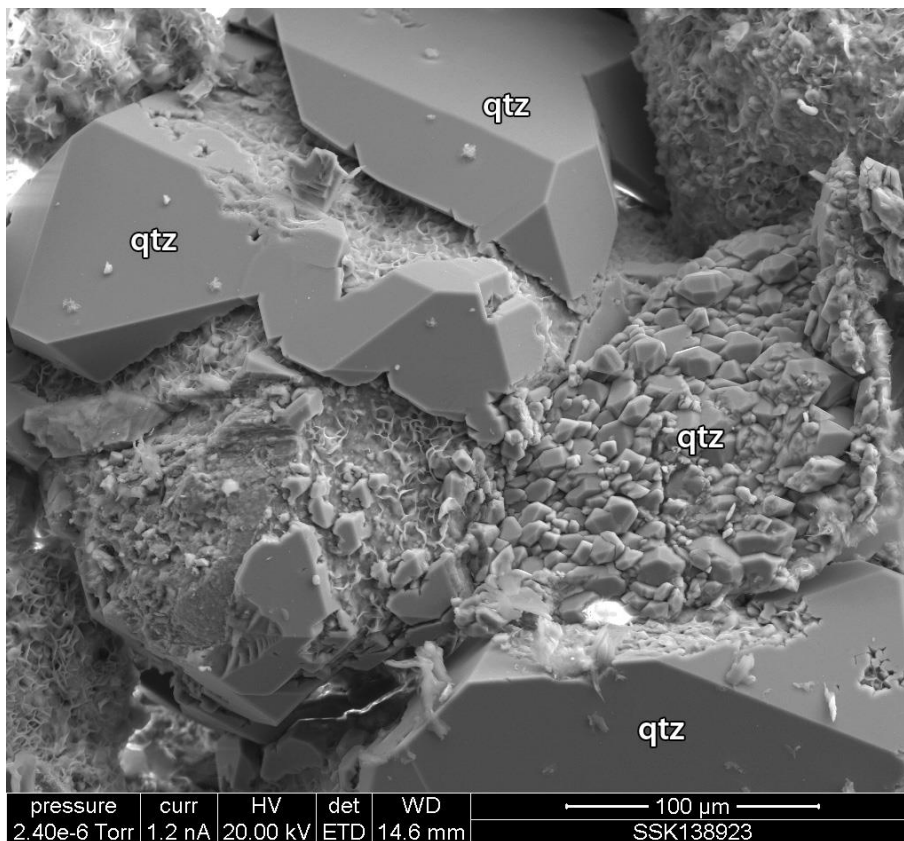


Plate 12: SSK138923, SEM image from rock chip sample. showing well developed quartz overgrowths (qtz) and authigenic quartz associated with an altered grain (right). Sparse, thin grain-coating clays are visible in overgrowth gaps.

4.2.2 Lower Greensand / Chalk characterisation

This set of samples represent both potential storage (Lower Greensand) and cap rock (Chalk) lithologies (Plate 13).

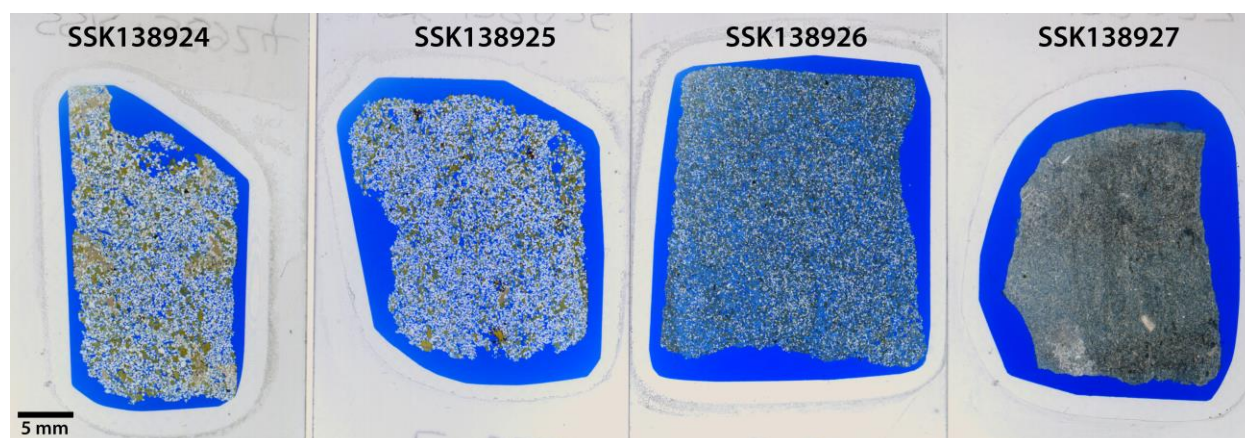


Plate 13: Full section scans of all of the Lower Greensand / Chalk sample thin sections. All were taken forward for the experimental study.

4.2.2.1 LOWER GREENSAND

Two of these samples (SSK138924, SSK138925 both Hythe Formation) are moderately to moderately-well sorted fine to medium grained sandstones with quartz and glauconite. The dominant detrital grain types (Plate 14) include local patches of detrital matrix. Both have high contents of well-interconnected macropores (Plate 15). The third sample (SSK138926 Sandgate Formation) is a moderately poorly sorted muddy bioclastic fine grained sandstone, which mostly comprises quartz, bioclasts (mostly calcitic shell fragments and sponge spicules) and glauconite in a detrital matrix (Plate 16, Plate 17); its porosity is dominated by micropores and common poorly interconnecting secondary macropores (Plate 14, Plate 16). All three samples have high contents of subangular grains (Plate 15, Plate 16)

Diagenesis in the two sandstone samples is dominated by the formation of grain-coating and pore-lining silica-based phases. These are present as both a finely ($<1 \mu\text{m}$) textured thin layer (5-10 μm thick) absent at grain contact sites and with common scattered $\approx 5 \mu\text{m}$ diameter pits (Plate 18), and as scattered more coarsely textured patches with a mix of granular to platy habits (Plate 18, Plate 20). In detail, the former comprises domains and stacks of subhedral, rod-like, sub-micron forms, typically locally parallel-aligned (Plate 19). The coarser textured patches also commonly contain sub-micron subhedral forms as well as fibrous and platy morphologies (Plate 20). Some of the equant pits appear to have faceted outlines (Plate 20). All of these constituents are speculatively identified as forms of opaline silica.

Outside of the silica formation, most other diagenesis involves dissolution of detrital phases. The rare feldspar grains typically show evidence of slight dissolution. There are also common elongate secondary macropores (sub-millimetre scale; Plate 14) the outlines of which are consistent with typical spicule morphologies. These secondary pores have most likely formed through the dissolution of silica-based sponge spicules and this silica is a likely source for the at least some of the grain-coating silica. In these samples the secondary macropores significantly contribute to both the volume and interconnectivity of the pore system.

The pore system in these two samples are therefore mainly lined by silica phases, most likely opaline.

The muddy bioclastic sandstone sample has some diagenesis in common with the two sandstones, principally in the widespread formation of silica phases and the dissolution of siliceous bioclasts. In this instance the deposited silica phases are on most surfaces exposed to macropores, including secondary pore walls and bioclast chamber walls, with a range of morphologies from botryoidal to fibrous (Plate 21, Plate 22). Dissolution again appears to be largely of spicule forms. Additionally, there has been widespread, but to variable extent, dissolution of the calcitic bioclasts (Plate 16, Plate 17); there is also evidence of dissolution to the coccoliths present as part of the matrix (Plate 23).

Other diagenetic phases identified in the muddy bioclastic sandstone sample are zeolite, pyrite and some clay minerals. The zeolite is present as an overall minor phase, but is widespread as fine (mostly <30 µm) euhedral crystals lining macropore walls, also associated with some of the partially dissolved calcitic bioclasts (Plate 22 and Plate 17 respectively). Microanalysis suggests it is clinoptilolite. Pyrite is scattered throughout, present as microcrystals and framboids in the matrix, also lining bioclast chambers. Some of the pyrite forms suggest it has formed replacively after bioclastic or organic constituents (Plate 21). The curled and webbed edges to detrital clay flakes indicate some diagenetic clay formation through alteration and overgrowth of these matrix constituents (Plate 23).

The pore system in this sample is highly complex, comprising a wide range of pore sizes, dominated by micropores with scattered poorly interconnected macropores. Many different mineral phases are exposed in the pore system, in contrast to the other two samples of Lower Greensand, with widespread silica, but also carbonate, zeolite, pyrite and clay minerals.

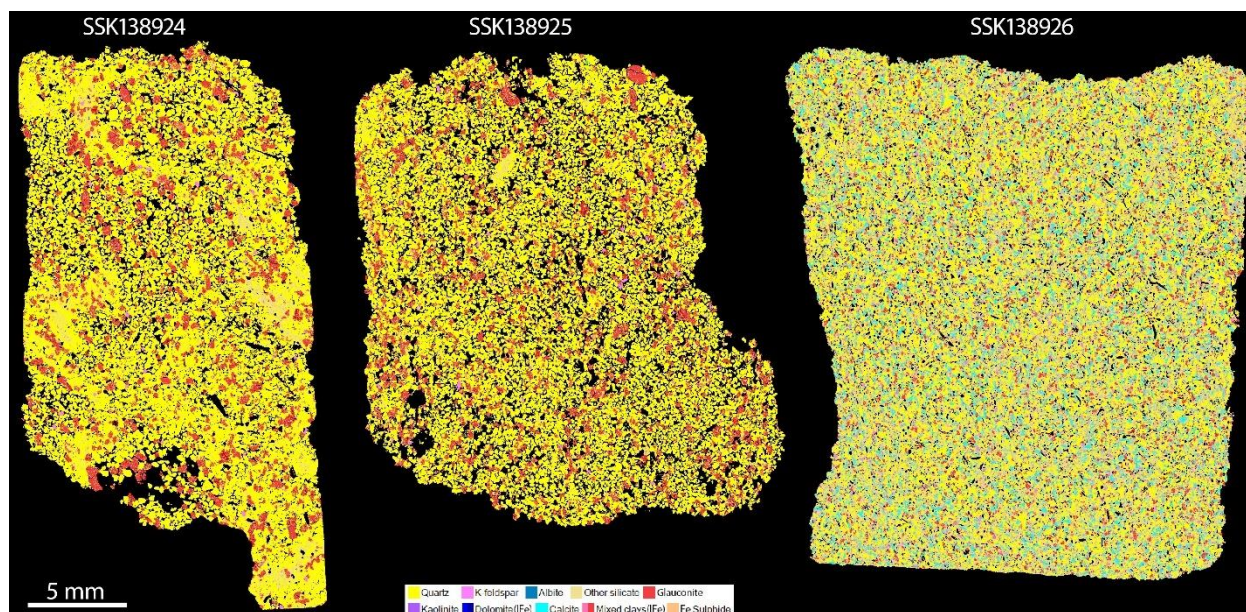


Plate 14: Full section phase maps for the three Lower Greensand samples. Hythe Formation left and centre; Sandgate Formation right.

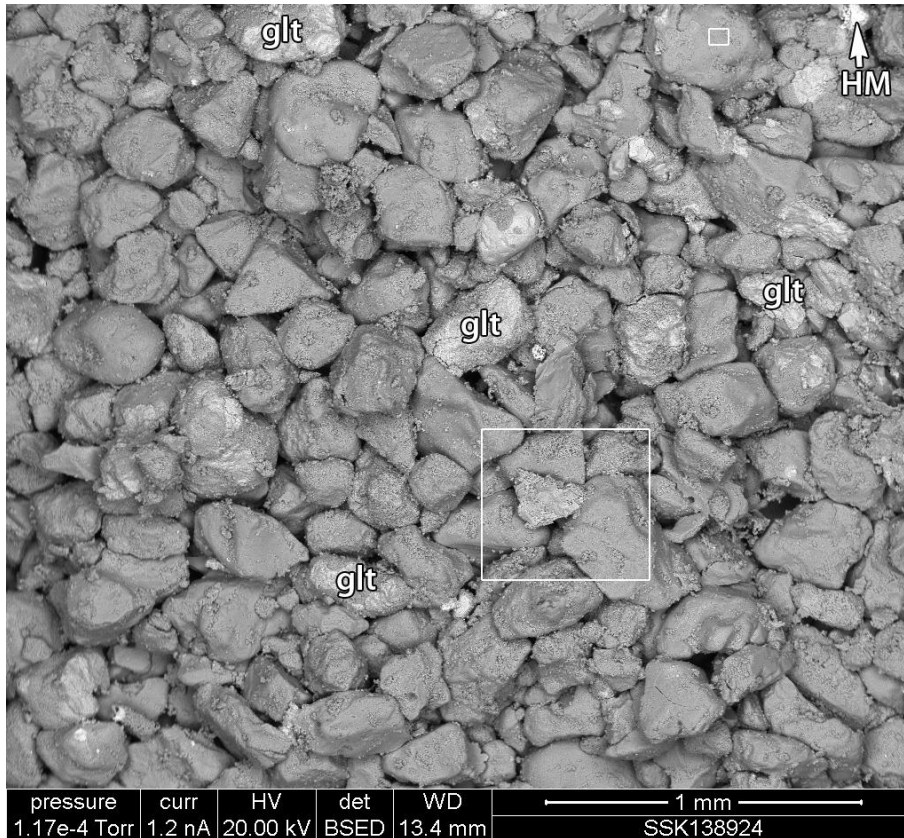


Plate 15: SSK138924 Hythe Formation, SEM image from rock chip sample. A moderately well-sorted medium-grained sandstone, with common subangular grains. Most are of quartz, with scattered glauconite (glt) and rare heavy minerals (HM). Most grains have thin diagenetic coatings of silica phases. Grain contacts are mostly point, porosity is high and well interconnected.

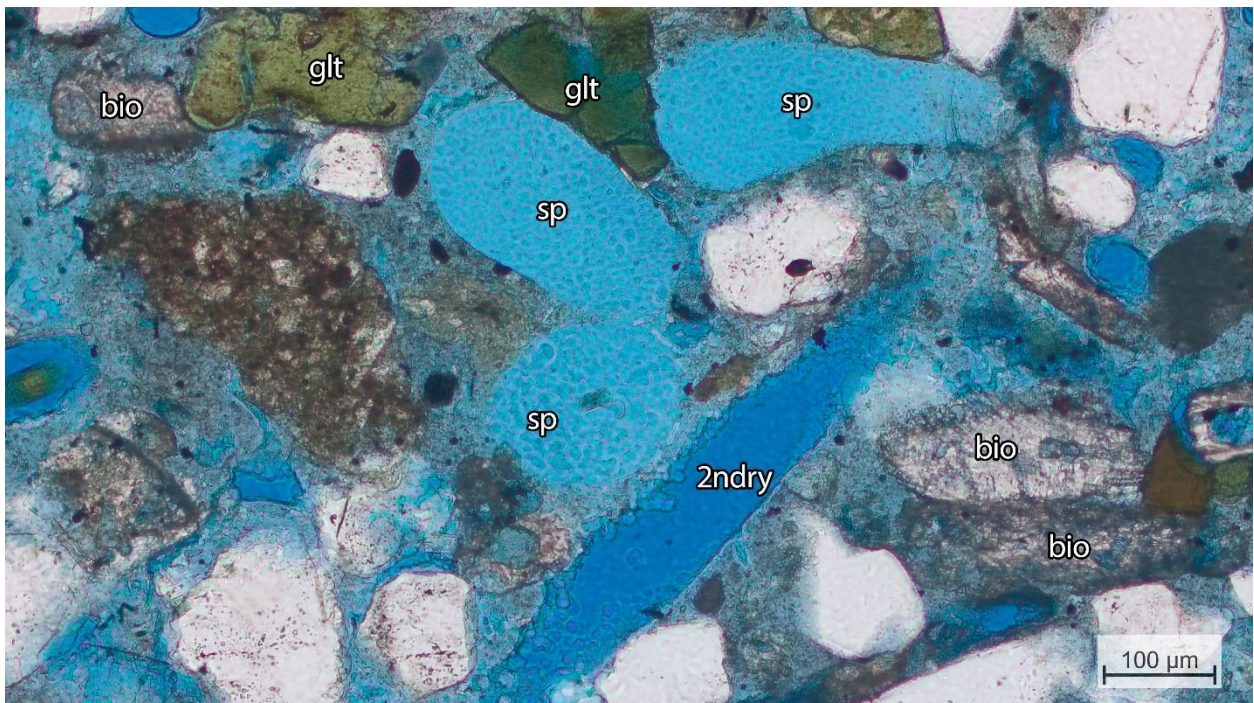


Plate 16: PPL image from PTS of SSK138926 Sandgate Formation. There is a high content of bioclasts including part-dissolved calcitic shell fragments (bio) and microporous sponge spicules (sp). Glauconite grains (glt) are typically fractured. The fabric is grain-supported but matrix is abundant. Most of the microporosity comprises isolated secondary pores (secondry) after spicule dissolution.

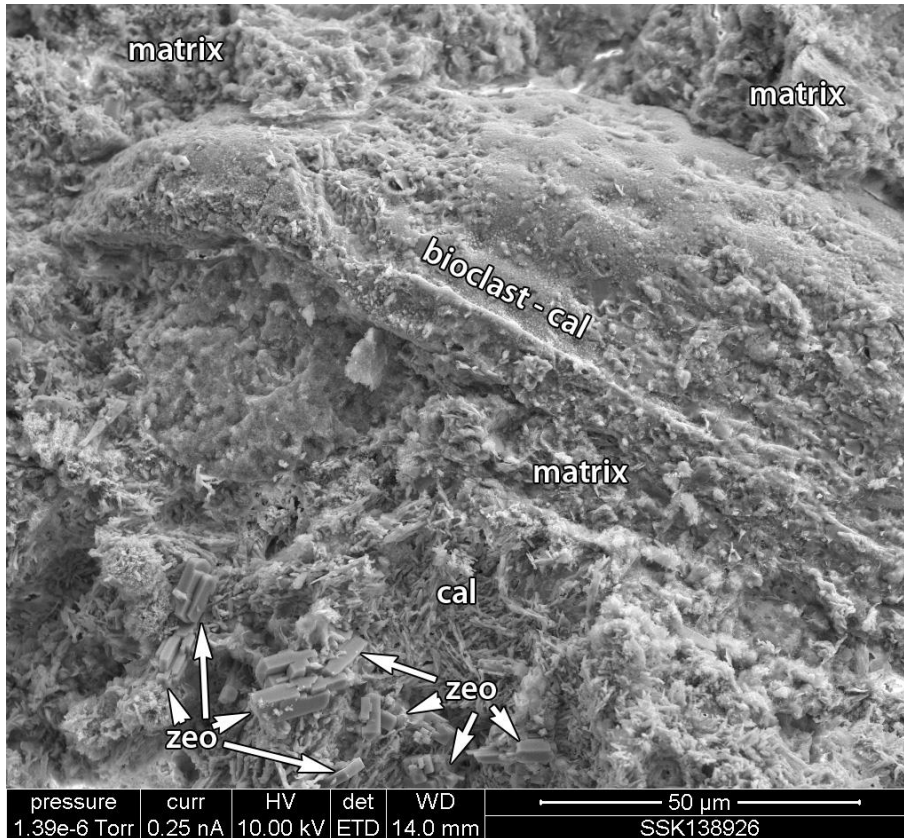


Plate 17: SSK138926 Sandgate Formation, SEM image from rock chip sample. Showing a calcite (cal) bioclast in clay matrix. In the lower left quadrant is dissolved bioclast with a relict structure of fibrous calcium carbonate (cal). Blocky authigenic zeolite (zeo) is associated.

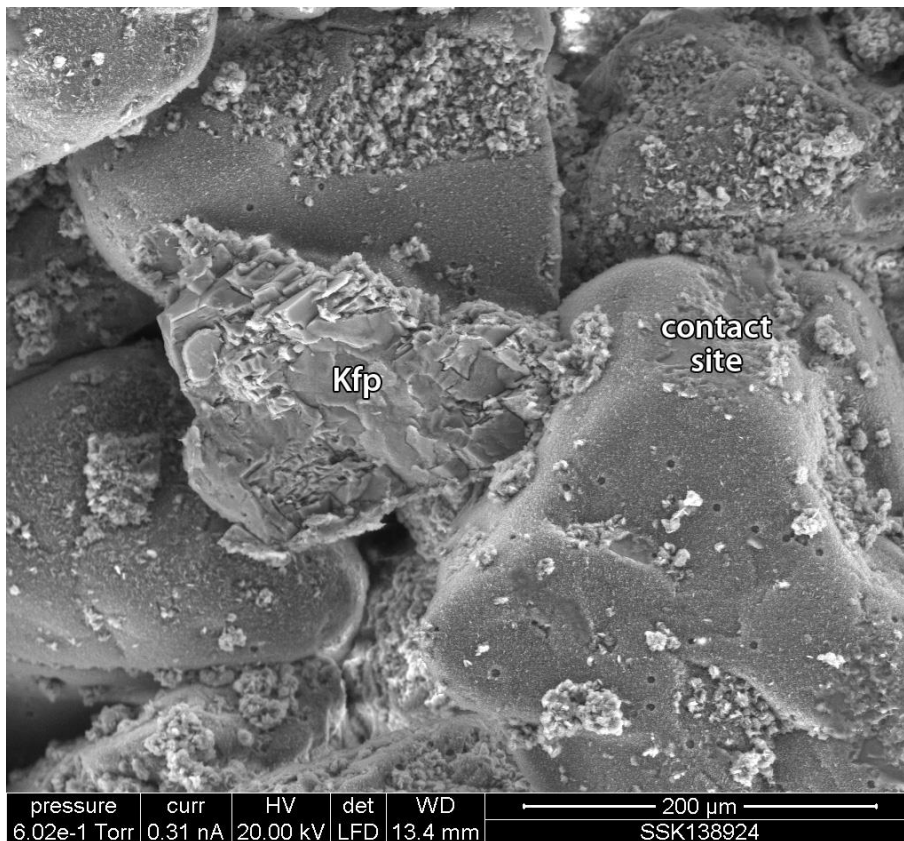


Plate 18: SSK138924 Hythe Formation, SEM image from rock chip sample. From the large boxed area in Plate 15. This rare K-feldspar (Kfp) grain has been fractured by sample preparation, revealing minor internal dissolution. Adjacent grains are thinly coated by finely (<1 μm) textured silica, absent at grain contact sites.

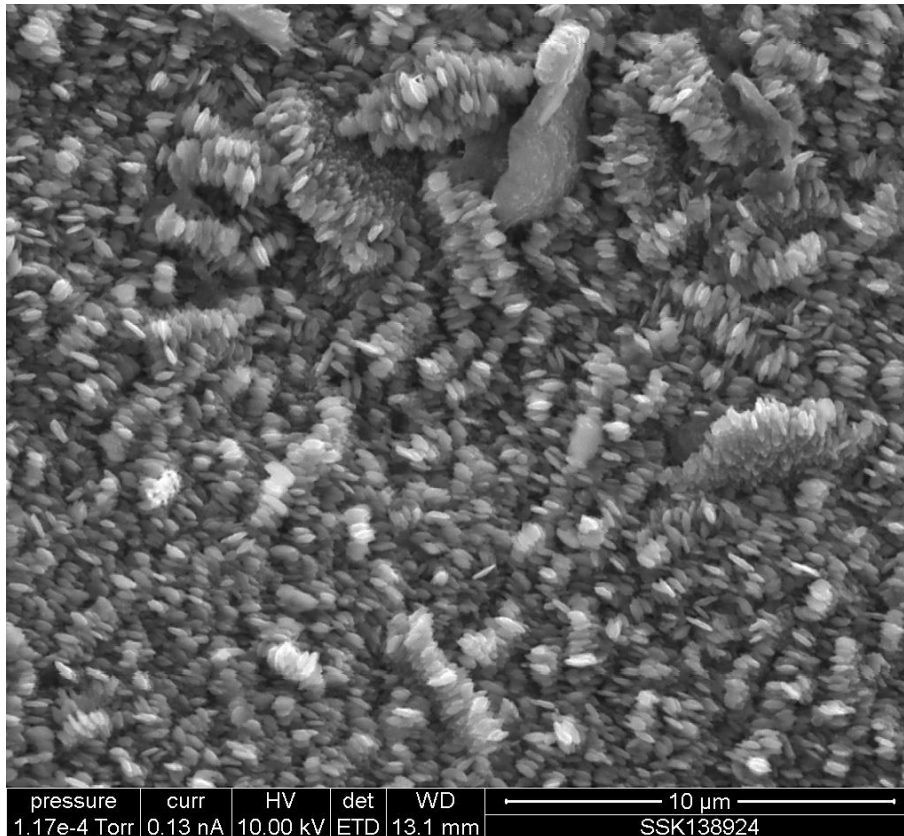


Plate 19: SSK138924 Hythe Formation, SEM image from rock chip sample. From the small boxed area in Plate 15, showing the rod-like sub- μm form of much of the silica grain-coating, typically parallel-aligned in domains and stacks with subhedral forms.

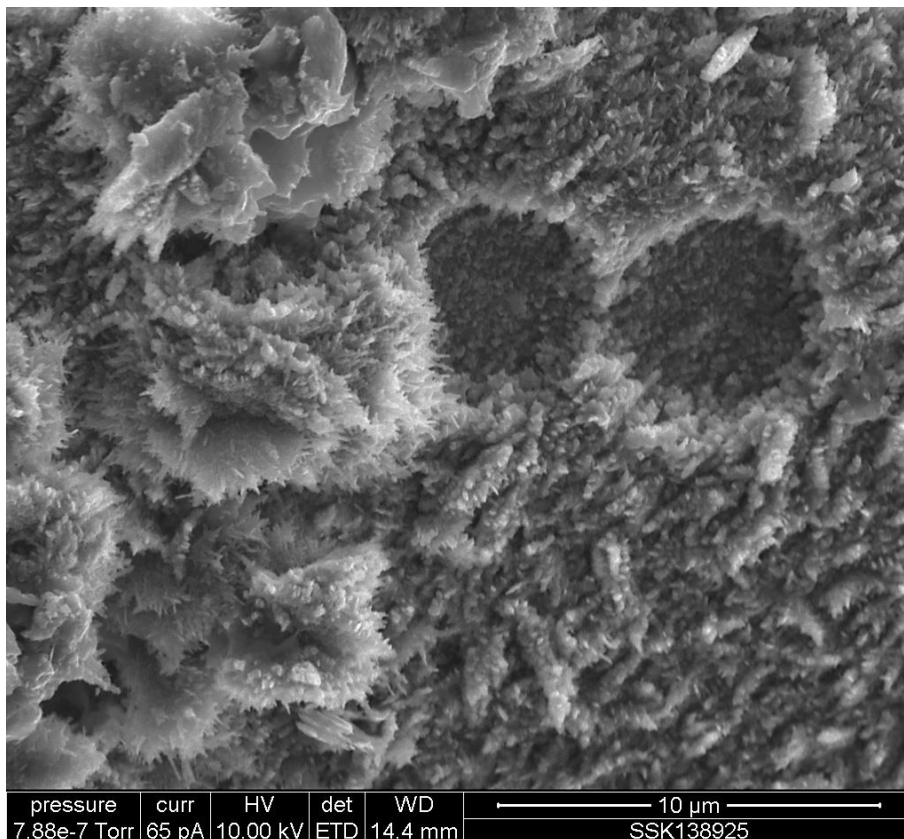


Plate 20: SSK138925 Hythe Formation, SEM image from rock chip sample, illustrating different forms in the silica grain-coatings, also including two 'faceted' pits. The disc-like platelets (left side), also silica, contain radial fibres and stubby fibrous extensions.



Plate 21: SSK138926 Sandgate Formation, SEM image from rock chip sample. In the muddy bioclastic sample, bioclast chambers that are not filled with matrix are typically lined by botryoidal silica with stubby surface extensions. A rod-like cluster of framboidal pyrite (py) has probably formed replacively.

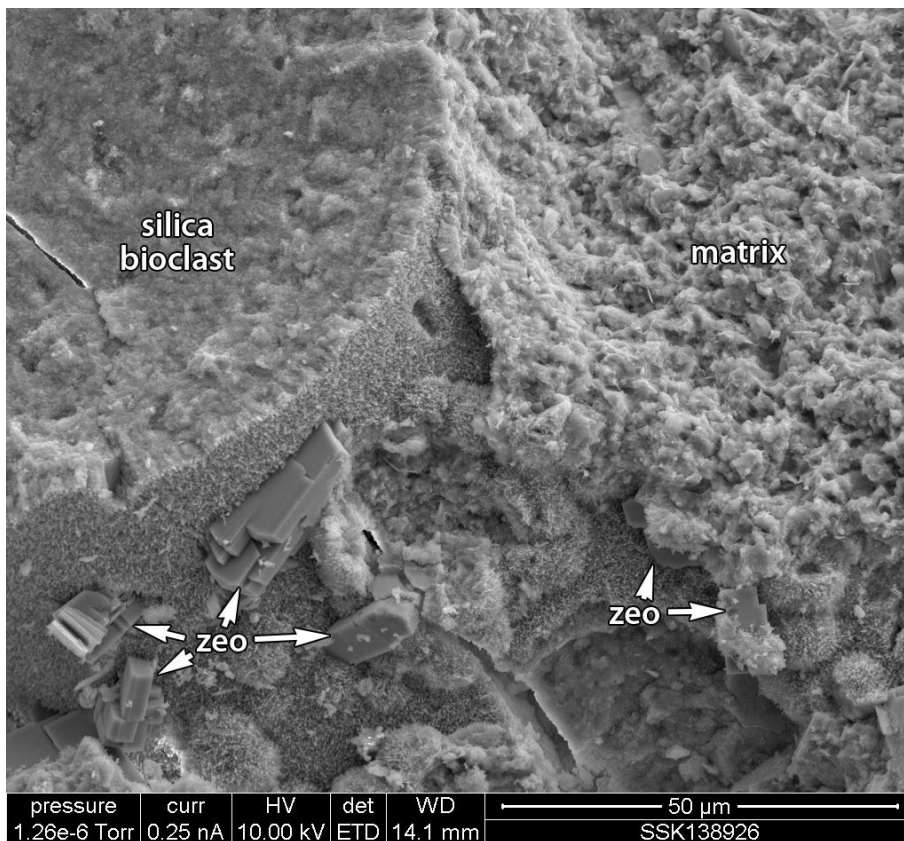


Plate 22: SSK138926 Sandgate Formation, SEM image from rock chip sample. The left part of the field of view is a cylindrical silica-based bioclast (sponge spicule) with a fibrous thin to

botryoidal silica coating. Zeolite (zeo) has formed on the bioclast into a macropore. The matrix comprises silica, clays and coccoliths.

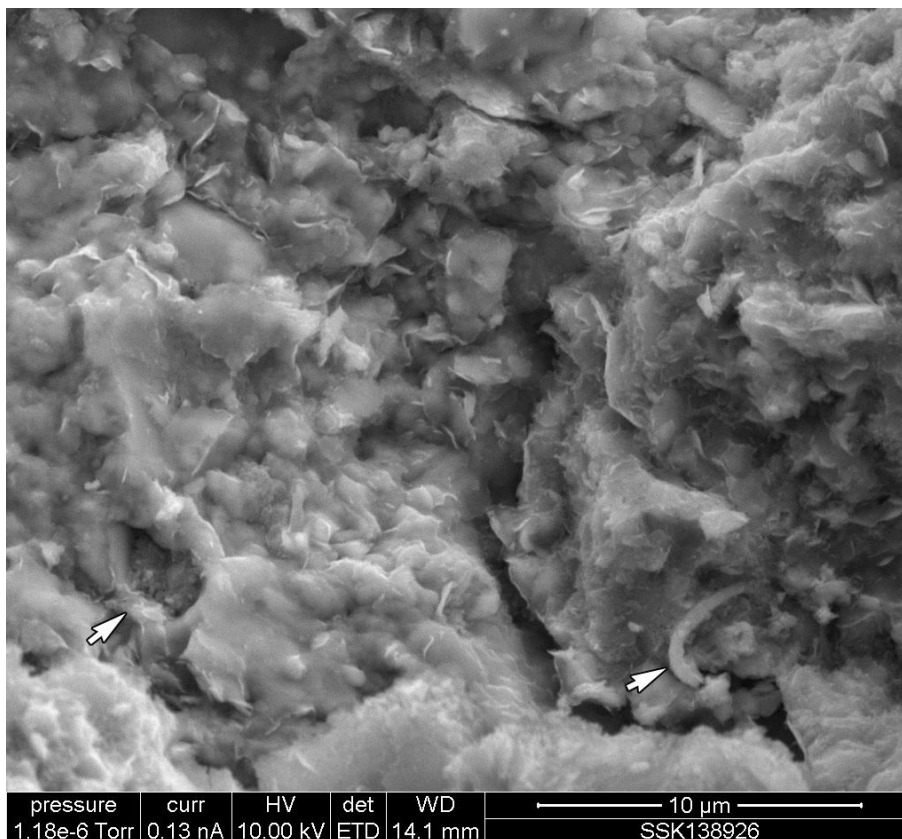


Plate 23: SSK138926 Sandgate Formation, SEM image from rock chip sample, showing detail of the matrix with resoluble coccolith remnants (arrowed). The rest of the matrix comprises silica and platy clays. Curled and webbed edges to detrital clay flakes indicate some diagenetic clay formation through alteration and overgrowth of detrital clays.

4.2.2.2 CHALK, GLAUCONITIC MARL MEMBER

This sample (SSK138927) is a limey mudstone containing scattered fine to coarse sand grains. Sand grain types include quartz, accessory minerals (e.g. apatite; Plate 24) and glauconite (Plate 25). Quartz is also present as scattered silt-sized grains, typically angular (Plate 26). The matrix is a mix of calcium carbonate (principally as micrite and coccolith fragments of a wide range of sizes and preservation) and silicate clay minerals (Plate 25, Plate 27).

There is widespread evidence of diagenesis. Calcite has formed as a local cement throughout, enclosing matrix components (Plate 26) and presenting some euhedral faces in rare macropores (Plate 25). The curled and webbed edges to many of the silicate detrital clay components, that locally bridge to other constituents and across micropores, are an indication of some diagenetic clay formation through alteration and overgrowth of detrital clays. Pyrite is present throughout as scattered microcrystal clusters and framboids (Plate 27).

Porosity in the sample is low and dominantly comprises fine micropores, poorly interconnected.

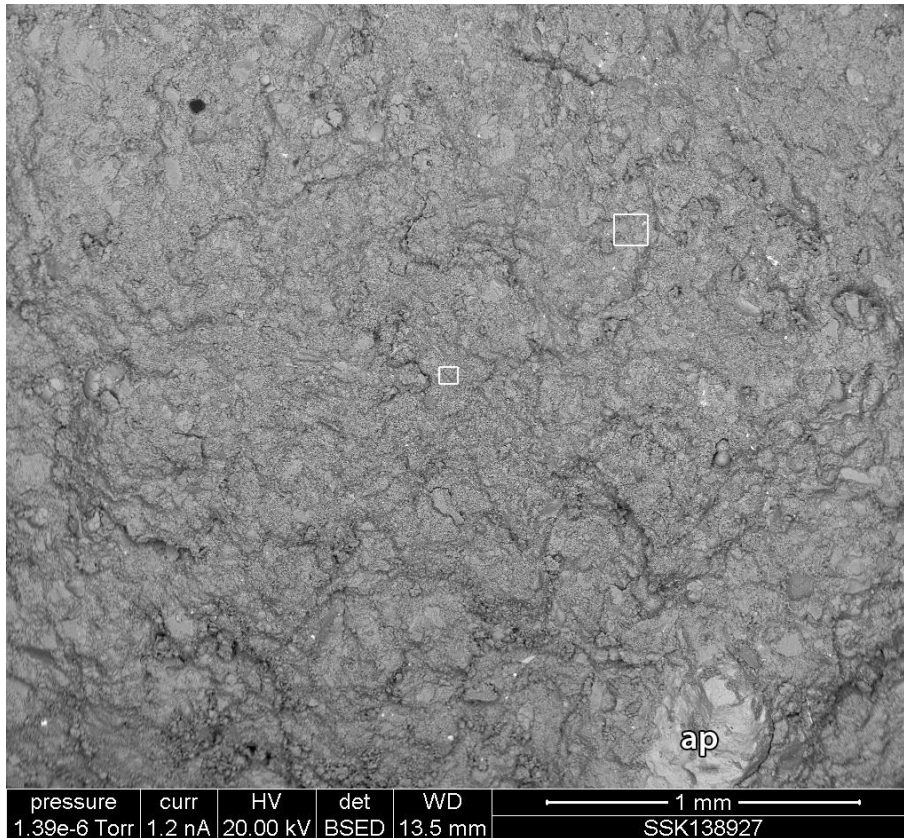


Plate 24: SSK138927 Glauconitic Marl Member, SEM image from rock chip sample. A limey mudstone with fine to coarse sand grains. In this field of view, the coarse grain at base is apatite (ap). The matrix is a mix of calcium carbonate (principally as micrite and coccolith fragments of a wide range of sizes and preservation) and silicates (quartz fragments, clay minerals).

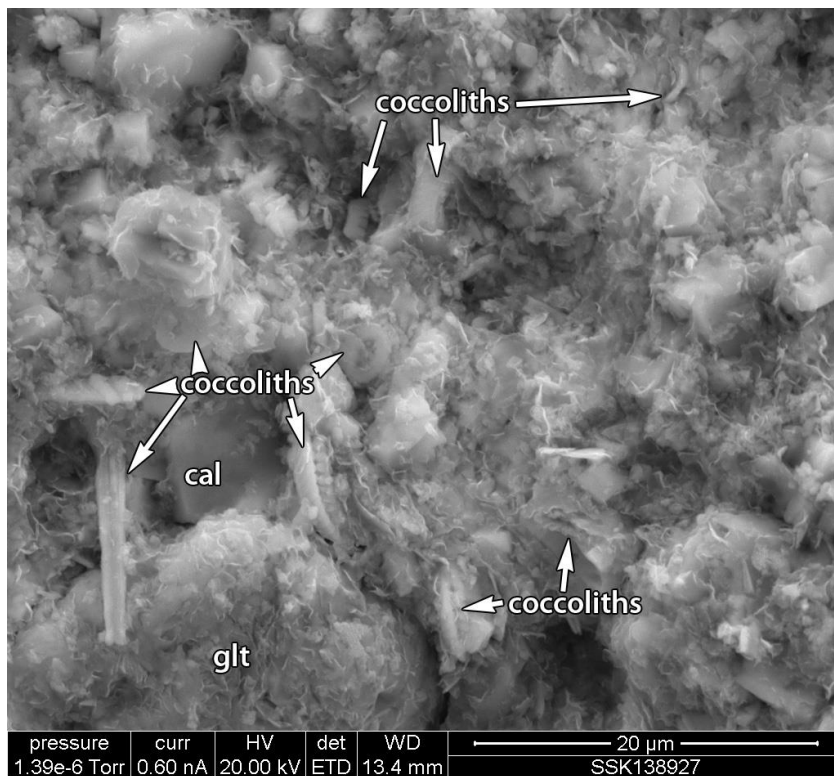


Plate 25: SSK138927 Glauconitic Marl Member, SEM image from rock chip sample, from the central boxed area in Plate 24 showing detail of the matrix which contains abundant coccoliths. Clays dominantly have bridging webbed forms and as such are at least partially diagenetic. Some euhedral single crystal calcite (cal) is authigenic or neoformed. Clay-rich clast lower left is glauconite (glt).

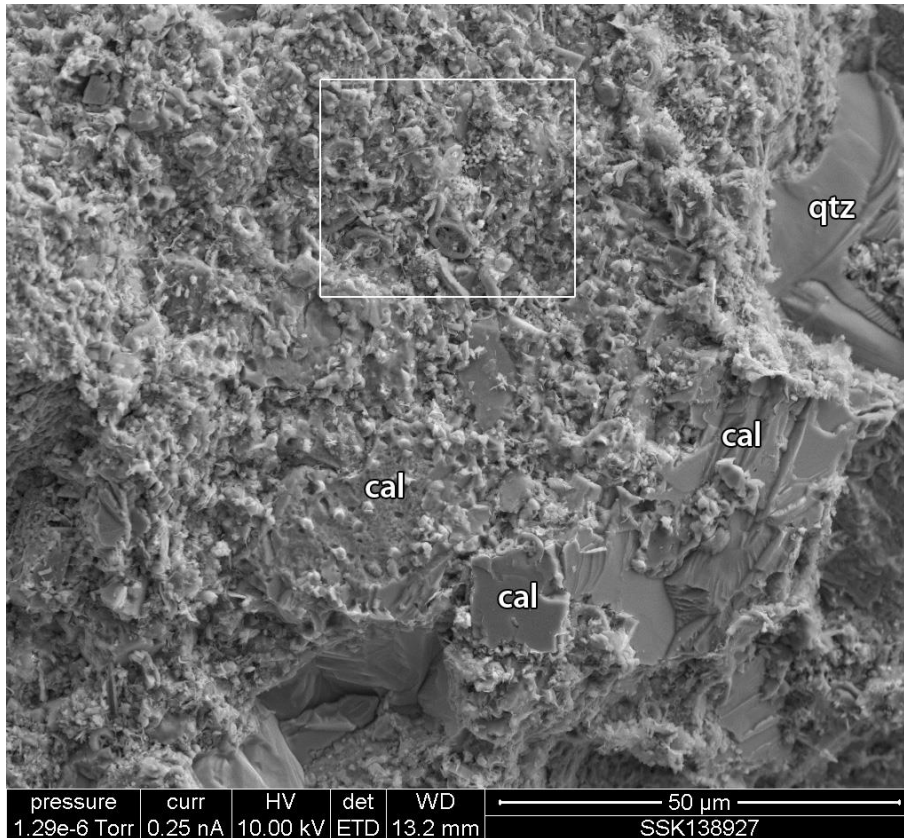


Plate 26: SSK138927 Glauconitic Marl Member, SEM image from rock chip sample, from the larger boxed area in Plate 24. Here, a coarse calcite cement (cal) has formed enclosing some matrix components. Angular grain top right is quartz (qtz). Box is site of Plate 27.

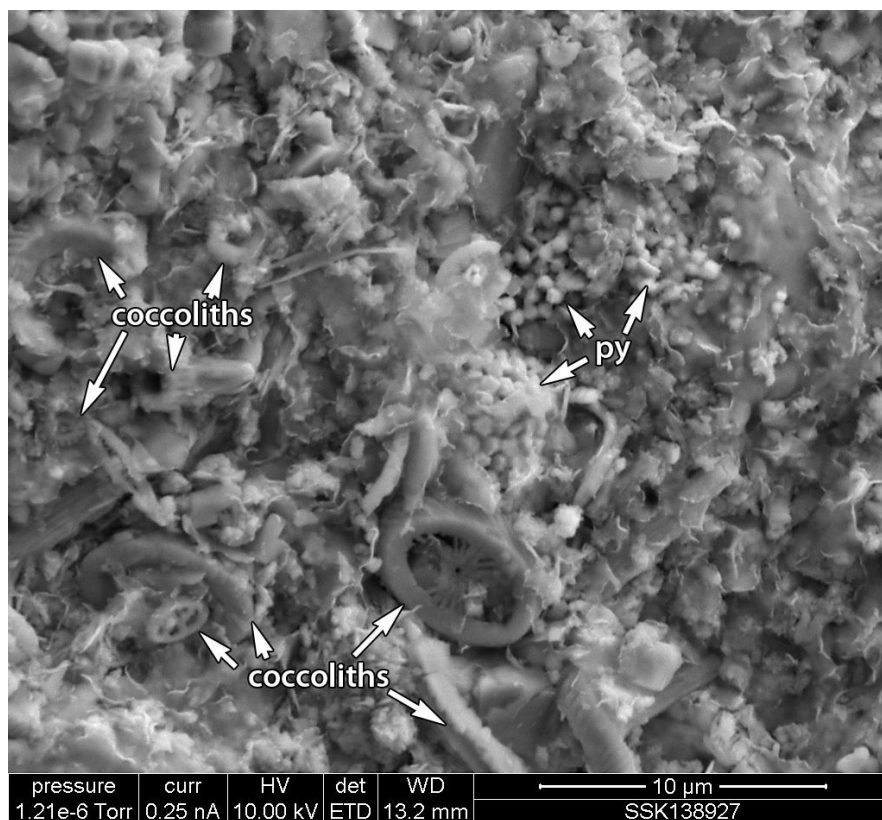


Plate 27: SSK138927 Glauconitic Marl Member, SEM image from rock chip sample, from Plate 26. Pyrite (py) is present as framboids and looser clusters of microcrystals, all with euhedral forms. A high proportion of the matrix comprises coccoliths, showing a wide range of types and sizes. The clays show evidence of some diagenetic alteration from detrital origins in the webbed edge morphologies.

4.2.3 Pre-Post experiment same site imagery

4.2.3.1 SHERWOOD SANDSTONE SAMPLES

For these samples, three main changes were noted:

1. Loss of sand grains from the corner and edge sites of the rock chips (Plate 28).
2. Movement of 'fines' (both loss and accumulation in new sites). Fines include fragmentary debris from the original coring, from sample handling and also from fragmentation of friable grains within the sample.
3. Detachment of areas of the diagenetic grain-coating clays (Plate 29).

The loss of grains is to be expected from friable sandstone samples; the loss could occur as a result of percussive interactions during the experimental program. Fines mobilisation is also not a surprise in an experiment with moving fluids.

The loss of grain-coating clay was seen in all three samples and was noted to be a common feature in most of the sites revisited. This change is not likely to result from percussive interactions, since many loss sites were observed to be in sheltered locations. Two possible mechanisms have been identified and would need further investigations to resolve:

- Change in volume of the clays (since they are a swelling clay type) due to changes in physical and / or chemical conditions during testing, has loosened them sufficiently to detach.
- Degassing of experimental fluids on release of the pressure at the end of the experiment has resulted in bubbles forming beneath the clays and pushing patches off.

Whichever mechanism is responsible, the experiments have identified a sample sensitivity. It is noted that change of clay volume is a mechanism that could also loosen surface grains, so could also explain some of the whole grain loss.

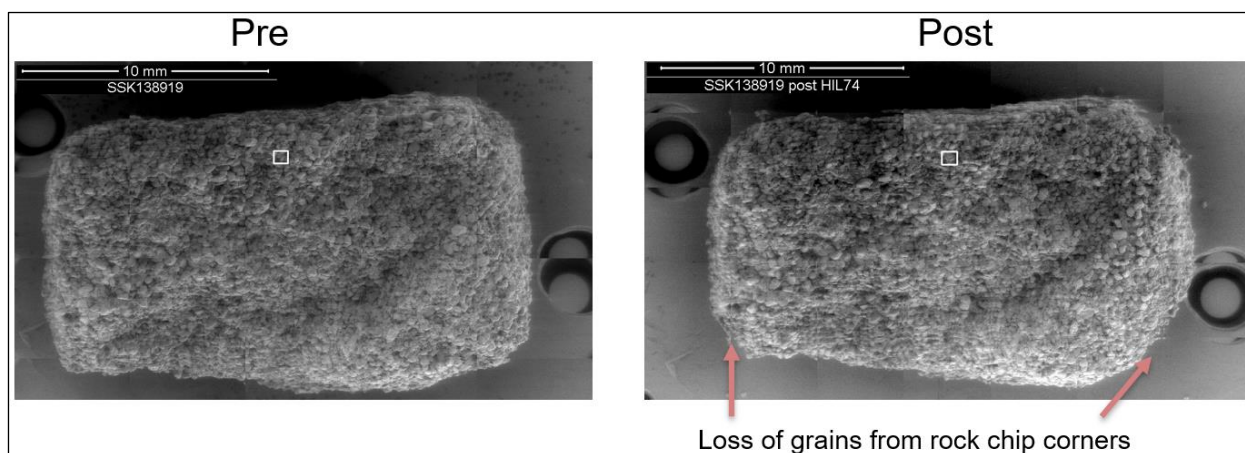


Plate 28: Comparative panel for pre-post imagery, whole sample SEM images of SSK138919 Sherwood Sandstone, post is after experimental run HIL74.

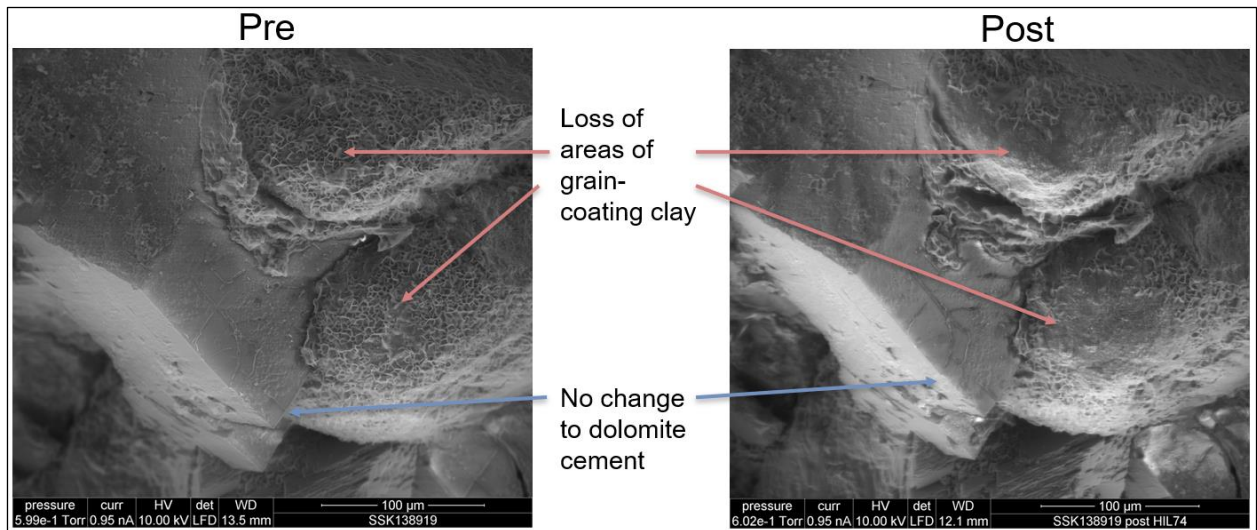


Plate 29: Comparative panel for pre-post imagery, selected area SEM images of SSK138919 Sherwood Sandstone from the boxed areas in Plate 28, equivalent to site 003 in Plate 1.

4.2.3.2 LOWER GREENSAND / CHALK SAMPLES

For these samples, five main changes were noted:

1. Loss of sand grains from the corner and edge sites of the rock chips.
2. Movement of 'fines' (both loss and accumulation in new sites; Plate 30). Fines include fragmentary debris from the original coring, from sample handling and also from fragmentation of friable grains and material (e.g. matrix) within the sample.
3. Minor evidence of change in volume of some small clay patches (Plate 30)
4. Possible local alteration of pyrite (Plate 30)
5. Slight dissolution of some coccoliths

Of these mechanisms, the first three affected the Lower Greensand samples, but mechanism 3 only affected sites with some matrix clays. Within these samples, there were no discernible differences to the silica grain coatings. All of the mechanism affected the chalk sample, and mechanism 5 was observed in the matrix-rich Lower Greensand sample (SSK138926 Sandgate Formation, post test HIL70).

As with the Sherwood sandstone samples, mechanisms 1 and 2 are likely due to a mix of percussive interactions and fluid flow. With a wide mix of clays, including swelling clay types, a change in volume is to be expected. Pyrite alteration (Plate 30) is a result of interest as it can lead to generation of hydrogen sulphide (H₂S) and deserves further investigation.

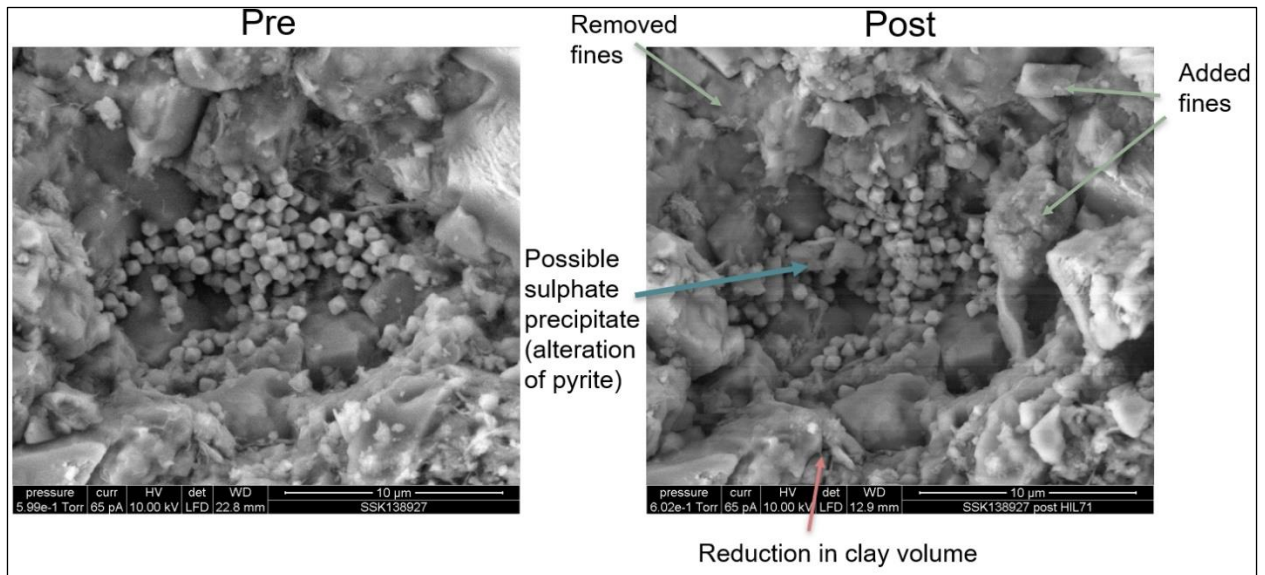


Plate 30: Comparative panel for pre-post imagery, selected area SEM images of SSK138927 Glauconitic Marl, showing several modes of change that have affected this sample post HIL71.

4.2.4 Post-test analysis of cement

Post-test examination of a fragment of cement and associated precipitate fines after test HIL72 revealed that euhedral plates of portlandite ($\text{Ca}(\text{OH})_2$) had formed (Plate 31). This was identified using a combination of EDX-derived microanalysis (showing the presence of Ca and O), and comparative backscatter brightness analysis.

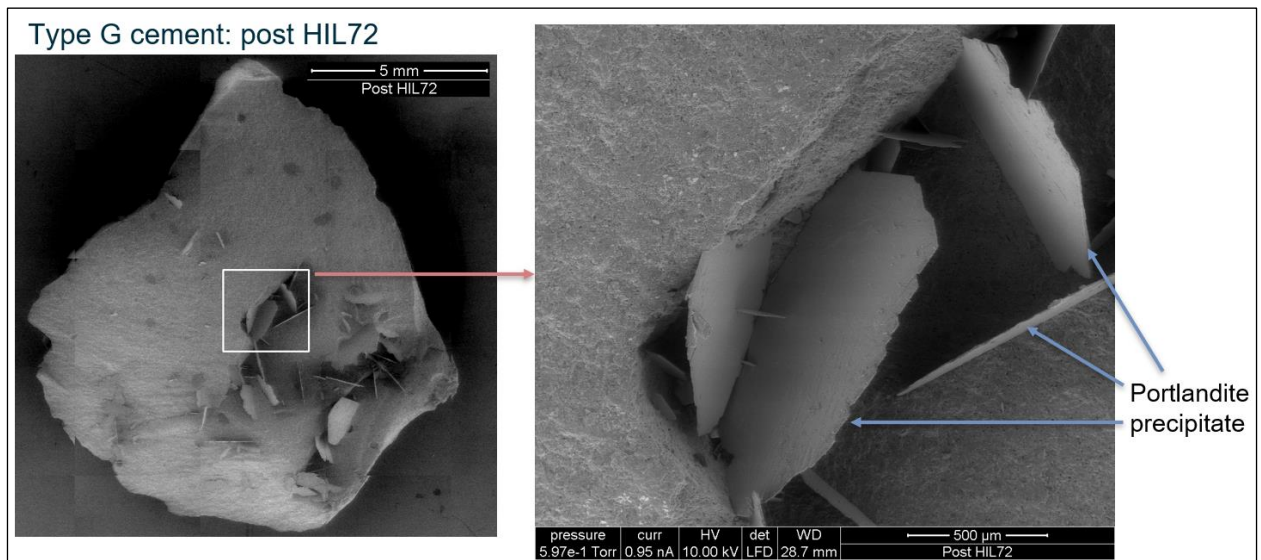


Plate 31: Type G cement, post test HIL71, showing surface portlandite precipitates.

5 X-ray diffraction

5.1 SAMPLE PREPARATION

The received pre- and post-experimental materials were ball-milled to a coarse powder. In order to provide a finer and uniform particle-size for powder X-ray diffraction (XRD) analysis, a 2.7 g portion of the milled powder was micronised under distilled water for 10 minutes with 10% (0.3 g) corundum (American Elements - PN:AL-OY-03-P). The addition of an internal standard allows the validation of quantification results and also the detection of any amorphous species present in the samples. Corundum was selected as its principal XRD peaks are suitably remote from those produced by most of the phases present in the samples. The pre-experimental micronised samples were then spray-dried following the method and apparatus described by Hillier (1999). The spray-dried material was then front-loaded into a standard, stainless steel sample holder for analysis. The smaller volume of post-experimental material available was not spray-dried but simply dried at 40°C in a moisture extraction oven, disaggregated and back-loaded into standard stainless steel sample holders for analysis.

To separate a fine fraction for clay mineral XRD analysis, further portions of the samples were dispersed in distilled water using a reciprocal shaker combined with ultrasound treatment. The suspensions were then sieved on 63 µm and the <63 µm material placed in a measuring cylinder and allowed to stand. In order to prevent flocculation of the clay crystals, 1 ml of 0.1M 'Calgon' (sodium hexametaphosphate) was added to each suspension. After a time period determined from Stokes' Law, a nominal <2 µm fraction was removed and dried at 55°C. Approximately 100 mg of the <2 µm material was then re-suspended in a minimum of distilled water and pipetted onto a ceramic tile in a vacuum apparatus to produce an oriented mount. The mounts were Ca-saturated using 0.1M CaCl₂·6H₂O solution, washed twice to remove excess reagent and allowed to air-dry overnight.

Where available, approximately 100 mg of the dried <2 µm material was re-suspended in a minimum of distilled water and pipetted onto a ceramic tile in a vacuum apparatus to produce oriented mounts. The mount was Ca-saturated using 2 ml 0.1M CaCl₂·6H₂O solution, washed twice to remove excess reagent and allowed to air-dry overnight. Where <100 mg of the dried <2 µm material was available, the dispersed material was Ca-saturated and the suspension deposited on the surface of a silicon crystal 'zero background' substrate and allowed to dry overnight.

5.2 ANALYSIS

XRD analysis was carried out using a PANalytical X'Pert Pro series diffractometer equipped with a cobalt-target tube, X'Celerator detector and operated at 45kV and 40mA. The micronised powder samples were scanned from 4.5–85°2θ at 2.06°2θ/minute. Diffraction data were initially analysed using PANalytical X'Pert HighScore Plus version 5.1 software coupled to the latest version of the International Centre for Diffraction Data (ICDD) database.

Following identification of the mineral species present in the samples, mineral quantification was achieved using the Rietveld refinement technique (e.g. Snyder & Bish, 1989) using the same HighScore Plus software. This method avoids the need to produce synthetic mixtures and involves the least squares fitting of measured to calculated XRD profiles using a crystal structure databank. Errors for the quoted mineral concentrations calculated from synthetic mixtures of minerals, are better than ±1% for concentrations >50 wt %, ±5% for concentrations between 50 and 20 wt % and ±10% for concentrations <10 wt % (Kemp *et al.*, 2016). Where a phase was detected but its concentration was indicated to be below 0.5%, it is assigned a value of <0.5%, since the error associated with quantification at such low levels becomes too large.

The <2 µm oriented mounts were scanned from 2–40°2θ at 1.02°2θ/minute after air-drying, after glycol-solvation and after heating to 550°C for 2 hours.

In order to gain further information about the nature of the clay minerals present in the samples, modelling of the XRD profiles was carried out using Newmod II™ software (Reynolds & Reynolds, 2013). Modelling was also used to assess the relative proportions of clay minerals present in the <2 µm fractions by comparison of sample XRD traces with Newmod II™ modelled profiles. The modelling process requires the input of diffractometer, scan parameters and a

quartz intensity factor (instrumental conditions), and the selection of different sheet compositions and chemistries. In addition, an estimate of the crystallite size distribution of the species may be determined by comparing peak profiles of calculated diffraction profiles with experimental data. By modelling the individual clay mineral species in this way, *mineral reference intensities* were established and used for quantitative standardization following the method outlined in Moore & Reynolds (1997).

5.3 RESULTS

The results of whole-rock and <2 µm clay mineral XRD analyses are summarised in Tables 3 and 4.

5.3.1 Pre-experiment

Whole-rock powder XRD analyses suggest that the pre-experimental Triassic Sherwood Sandstone samples (SSK138919, 138920, 138921 and 138922) are predominantly composed of quartz (>74.9%) ± minor proportions of feldspar (plagioclase and K-feldspar), carbonates (calcite and dolomite), phyllosilicates/clay minerals (see next section) and traces of hematite, pyrite, and halite. Clay mineral assemblages are dominated by approximately similar proportions of illite and smectite/chlorite (R0-ordered, 90%smectite, 10% chlorite interlayers) with trace amounts of discrete chlorite. Possible traces of palygorskite were also detected.

In comparison, the pre-experimental Cretaceous Hythe Formation (SSK138924 and 138925) are composed of greater proportions of quartz (>92.7%) with minor quantities of phyllosilicates/clay minerals ± zeolite and traces of K-feldspar and pyrite. The clay mineral assemblages are solely or predominantly composed of illite/smectite (R1-ordered, 85% illite, 15% smectite interlayers) glauconite with traces of discrete smectite.

The pre-experimental SSK138926 Sandgate Formation and 138927 Glauconitic Marl show different whole-rock mineralogies. SSK138926 Sandgate Formation is composed of 53.5% quartz with subordinate calcite, opal-CT, phyllosilicates/clay minerals (see next section) and traces of pyrite. However, SSK13827 is predominantly composed of calcite (88.6%) with minor proportions of quartz and traces of phyllosilicates/clay minerals. Clay mineral assemblages are composed of illite and smectite with the addition of minor amounts of chlorite in sample 138926. The proportion of smectite is also higher in sample 138927 than in sample 138926.

5.3.2 Post-experiment

In general terms and despite the small amount of material available post-experiment and the necessarily slightly different preparation and mounting method employed, the mineralogies of the post-experimental samples show little, if any, change from the pre-experimental analyses. The differences in concentrations detected are generally within the analytical error of the method. However, the post-experimental samples show slightly higher quartz and lower phyllosilicate/clay mineral concentrations compared to the pre-experimental materials.

Table 3. Summary of whole-rock XRD analyses

Description	SSK	Pre/Post expt	Silicates					Phyllosilicates/clay minerals				Carbonates		Others		
			quartz	plagioclase	K-feldspar	Opal C-T	zeolite	'mica'	chlorite	smectite	glaucanite	dolomite	calcite	hematite	pyrite	halite
Sherwood Sandstone (Chester Formation)	138919	Pre	81.8	0.6	8.0	nd	nd	2.1	<0.5	nd	nd	1.2	5.3	<0.5	0.9	nd
		Post	87.2	nd	7.6	nd	nd	1.4	nd	nd	nd	1.2	1.8	0.6	<0.5	<0.5
	138920	Pre only	81.3	<0.5	12.3	nd	nd	2.6	<0.5	nd	nd	2.7	nd	nd	0.9	<0.5
	138921	Pre	74.9	1.4	7.0	nd	nd	11.8	<0.5	nd	nd	<0.5	<0.5	4.2	nd	nd
		Post	78.8	nd	6.7	nd	nd	8.4	nd	nd	nd	<0.5	1.8	3.9	nd	<0.5
	138922	Pre	84.3	0.6	5.8	nd	nd	2.1	<0.5	nd	nd	5.3	<0.5	1.7	nd	nd
Post		87.5	nd	4.7	nd	nd	1.0	nd	nd	nd	5.0	<0.5	1.3	nd	<0.5	
138923	Pre only	86.5	<0.5	4.1	nd	nd	1.3	<0.5	nd	nd	5.5	0.6	1.1	0.6	nd	
Hythe Formation (Lower Greensand)	138924	Pre	92.7	nd	<0.5	nd	nd	6.3	nd	nd	0.6	nd	nd	nd	<0.5	nd
		Post	95.0	nd	<0.5	nd	nd	4.8	nd	nd	nd	nd	nd	nd	nd	nd
138925	Pre	96.6	nd	<0.5	nd	nd	2.3	nd	<0.5	0.7	nd	nd	nd	<0.5	nd	
	Post	98.0	nd	<0.5	nd	nd	1.3	nd	nd	<0.5	nd	nd	nd	<0.5	nd	
Sandgate Formation (Lower Greensand)	138926	Pre	53.5	nd	nd	20.0	1.9	7.3	<0.5	<0.5	nd	nd	16.7	nd	<0.5	nd
		Post	60.2	nd	nd	16.3	nd	6.1	nd	nd	nd	nd	17.3	nd	<0.5	<0.5
Chalk	138927	Pre	11.4	nd	nd	nd	nd	nd	nd	<0.5	nd	nd	88.6	nd	nd	nd
		Post	11.9	nd	nd	nd	nd	nd	nd	nd	nd	nd	88.0	nd	nd	<0.5

'mica' = non-differentiated mica species possibly including muscovite, biotite, illite,
nd = not detected

Table 4. Summary of <2 µm clay mineral XRD analyses

Description	SSK no.	Pre/Post expt.	Proportion of the clay minerals in the <2 µm fraction (%)					Nature of interlayered species	Non-layered clay minerals	Non clay mins in the <2 µm fraction	
			illite	ill/smec	chl	kaol	smec/chl				smec
Sherwood Sandstone (Chester Formation)	138919	Pre	42	nd	1	nd	57	nd	R0 90%S 10%C	?palygorskite	qtz, K-feld, plag, dol, hem
		Post	43	nd	1	nd	56	nd		-	qtz, hem
	138920	Pre only	40	nd	1	nd	59	nd	R0 90%S 10%C	?palygorskite	qtz, K-feld, plag, hem
	138921	Pre	73	nd	2	nd	26	nd	R0 90%S 10%C	?palygorskite	qtz, K-feld, plag, hem
		Post	48	nd	1	nd	51	nd		-	qtz, hem
138922	Pre	51	nd	1	nd	48	nd	R0 90%S 10%C	?palygorskite	qtz, K-feld, plag, dol, hem	
	Post	54	nd	<1	nd	46	nd		-	hem	
138923	Pre only	65	nd	1		34	nd	R0 90%S 10%C	-	qtz, K-feld, plag, dol, hem	
Hythe Formation (Lower Greensand)	138924	Pre	nd	100	nd	nd	nd	nd	R1 85%I 15%S	-	qtz
		Post	nd	90	nd	1	nd	9		-	qtz
138925	Pre	nd	92	nd	nd	nd	8	R1 85%I 15%S	-	qtz, K-feld, plag	
	Post	nd	91	nd	nd	nd	9		-	qtz	
Sandgate Formation (Lower Greensand)	138926	Pre	63	nd	9	nd	nd	29	-	-	qtz, opal-CT, plag, calc, pyrite, zeolite
		Post	63	nd	6	nd	nd	31	-	-	qtz, opal-CT, plag, calc, pyrite, zeolite
Chalk	138927	Pre	20	nd	nd	nd	nd	80	-	-	calc, qtz
		Post	49	nd	nd	<1	nd	49	-	-	calc, qtz

nd = not detected

6 Specific surface area analysis

6.1 METHODOLOGY

The surface area of the samples was determined using the amount of nitrogen adsorbed onto a solid surface at monolayer coverage from a multipoint plot of adsorption isotherm data using the BET/N₂ method, named after its inventors Brunauer, Emmett and Teller (Brunauer et al., 1938).

Approximately 2 g subsamples were degassed overnight in a vacuum oven at 60°C and then further degassed using a Micromeritics Gemini VacPrep for a least 1 hour at 60°C prior to analysis. Surface area analyses were conducted using a Micromeritics Gemini VI 2385C system. The samples were run on a 10-point adsorption pressure point program with a 10-second equilibration time.

6.2 RESULTS

The results of surface area analyses are summarised in Table 5 and Figure 4.

Table 5. Summary of sample surface area data

Description	SSK	Pre-/Post-experiment	SA (m ² /g)	Error (±)
Sherwood Sandstone (Chester Formation)	SSK138919	Pre-	3.3612	0.0288
		Post-	2.9180	0.0324
	SSK138921	Pre-	9.5682	0.064
		Post-	7.5881	0.0673
Hythe Formation (Lower Greensand)	SSK138922	Pre-	3.1086	0.0279
		Post-	2.1426	0.0206
Hythe Formation (Lower Greensand)	SSK138924	Pre-	16.661	0.099
		Post-	11.7345	0.0898
Hythe Formation (Lower Greensand)	SSK138925	Pre-	20.0883	0.0988
		Post-	15.6939	0.1023
Sandgate Formation (Lower Greensand)	SSK138926	Pre-	27.9018	0.1965
		Post-	25.5155	0.1914
Chalk	SSK138927	Pre-	5.7928	0.0315
		Post-	5.8714	0.0316

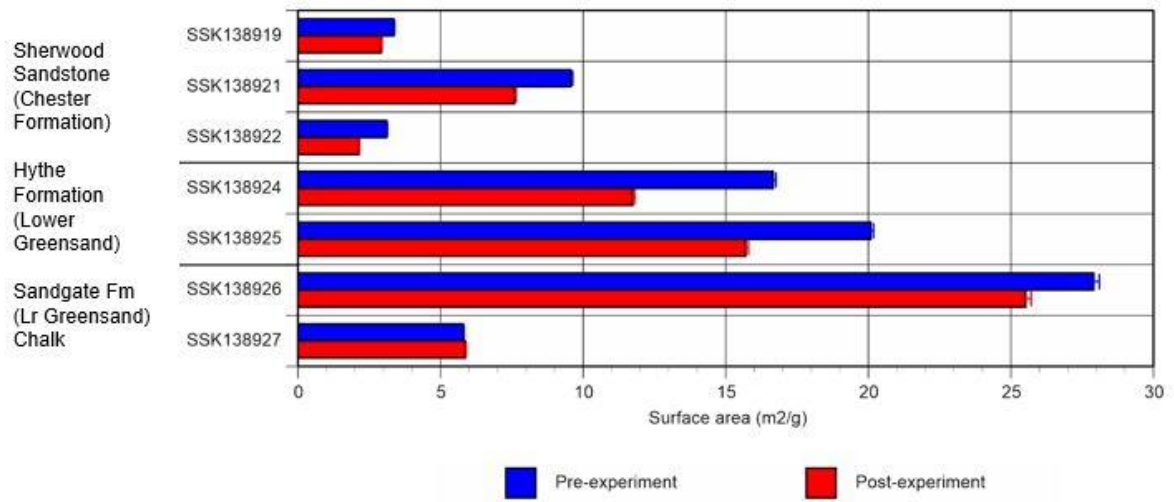


Figure 4. Summary of specific surface area data for the pre- and post-experimental samples

7 Porosity and permeability measurements

Prior to sample exposure to hydrogen, porosity measurements were made from SSK samples SSK138919 – 138927 and permeability measurements were made from all samples except SSK138926 due to sample condition. Samples were tested again following exposure to hydrogen.

7.1 METHODS

A standard liquid resaturation method was used to determine effective porosity, bulk and grain density (Bloomfield *et al.* 1995). Gas permeability was determined using nitrogen under steady state conditions and an equivalent liquid permeability calculated on the basis of a previous empirical correlation (Bloomfield & Williams 1995). Probe permeametry was performed using nitrogen as the permeant under steady state flow conditions and assuming radial flow geometry. Detail of each of the methods is given below.

7.2 POROSITY

Effective porosity, bulk density and grain density were measured using a liquid resaturation method based on the Archimedes principal. The methodology is described in detail in Bloomfield *et al.* (1995). A sample to be tested is weighed and then placed in a resaturation jar. The jar is evacuated then flooded with propanol. Propanol is used as it is relatively inert with respect to the core and reduces the potential for swelling clays to modify the porosity during testing. The sample is allowed to saturate for at least 24 hours. The saturated sample is then weighed, firstly immersed in the propanol and then, still saturated with propanol, in air. For each sample its dry weight (w), its propanol saturated weight in air (S_1) and its saturated weight immersed in propanol (S_2) are recorded, in addition the density of the propanol (ρ_f) is noted. From these values sample dry bulk density (ρ_b), grain density (ρ_g) and effective porosity (ϕ) can be calculated as follows:

$$\rho_b = (w\rho_f)/(S_1-S_2) \text{ g cm}^{-3} \quad (1)$$

$$\rho_g = (w\rho_f)/(w-S_2) \text{ g cm}^{-3} \quad (2)$$

$$\phi = (S_1-w)/(S_1-S_2) \quad (3)$$

The effective measurement errors on the porosity measurements are approximately +/- 0.5 porosity percent.

Permeability

Gas permeability tests were performed on samples under steady-state conditions. A full description of the methodology and discussion of the correlation between gas and liquid permeability in sandstones can be found in Bloomfield and Williams (1995). Samples were constrained in a core holder and a pressure-regulated supply of nitrogen gas was applied to one end of the sample (the downstream end of the sample was held at atmospheric pressure). A soap-foam flow meter was used to measure the outflow of nitrogen from the downstream end of the sample. Gas permeability was calculated using the measured sample dimensions, differential pressure, and the steady-state gas flow rate as follows

$$k_g = \mu Q L P_o/[A (P_i^2-P_o^2)] \quad (4)$$

where k_g is gas permeability, μ is gas viscosity, Q is the volumetric gas flow rate measured at atmospheric pressure, L and A are the sample length and area respectively, P_o is the downstream (atmospheric) pressure, and P_i (absolute pressure) is given by $P_i = P_o + P_g$, where P_g is the gauge pressure of the regulated nitrogen permeant. The effective measurement errors associated with the gas permeability measurements are about +/- 2.5% of measured sample permeability.

Results for porosity and permeability measurements taken before and following the batch experiments are given in Appendix 3.

8 X-ray computerised tomography

8.1 METHODS

X-ray computerised tomography (XCT) is a non-destructive technique that can give information regarding the internal structure of materials. In the case of porous rocks, the technique can image structures down to the pore-scale, allowing for the pore structures to be established. When run before and after sample exposure to hydrogen, changes to the rock structure at the pore-scale can be observed. X-ray computed tomography imaging transmits a beam of x-rays through a sample at all orientations to produce geometrically magnified radiographs, or shadow images, of the sample (Ketcham & Carlson, 2001). Different mineral phases have different characteristic x-ray attenuations, meaning the x-ray flux reaching the detector varies dependent on the sample composition, creating a grey scale of intensity (Ketcham & Carlson, 2001). Images are reconstructed into a stack of two-dimensional slices, revealing the internal structure of the sample in a non-destructive manner. This stack creates a three-dimensional dataset that can be manipulated in numerous ways depending on the research needs. Although the original CT dataset is qualitative, quantitative data can be produced such as measuring internal features of the sample like void fraction.

8.1.1 Sample Preparation

Due to size constraints of the experiment pressure vessels and the optimal geometric magnification required for XCT, 6mm sub-plugs were determined as optimal for imaging. Due to sample friability, samples were cut by hand using a bench-mounted saw into 6mm cuboids. Mechanical polishing was then attempted, but a high finish could not be achieved due to continual disaggregation of the samples. The original way up of samples was retained through tapering sample edges (producing a trapezoid-shaped sample), however this was not successful for all samples. Once all mechanical preparation was complete, samples were washing in an ultrasonic bath to remove any residual polish and unstable surface grains.

8.1.2 Data Acquisition

Scans were acquired in the Nikon Xtek 160kV/250kV/450W High Flux Bay at the Henry Moseley X-ray Imaging Facility (HMXIF, Figure 5a), with multiple scans undertaken initially to optimise the settings and produce the most coherent and clear dataset. This was an important step as reduced noise results in optimal scan data, and less computer processing is required afterwards. The 6mm cuboid samples (excluding SSK138920 and SSK138923, which were excluded from the pressure vessel experiments) were stacked together in two plastic tubes and attached to a sample holder (Figure 5b). This allowed multiple scans to be scheduled to run at once (e.g., overnight), rather than having to manually change samples following each scan, essential as the runtime for one sample was ~8hours. Cling film was used to steady the samples in the tube and separate them from one another to prevent any interference in the data acquisition from scattered x-rays passing through other samples.

Multiple two-dimensional projections (radiographs, Figure 6a) were collected as each sample rotated through 360° within the x-ray beam; this is the preliminary, unprocessed dataset for x-ray computed tomography. As each component of the sample (e.g., mineral phases, pore spaces) has a specific x-ray attenuation, the x-ray flux recorded at the detector varies as a direct result of what it has passed through. This allows the internal structure of the sample to be resolved, just as a medical x-ray images bone.



Figure 5: X-ray CT Sample Prep and Scanner (Image: University of Manchester)

(A): The High Flux Bay (HMXIF), the x-ray scanner used to acquire CT data of the samples.

(B): Samples stacked together in two plastic tubes to allow multiple scans to be completed without having to physically change samples in the bay (e.g., to run overnight). Within the tube samples were separated by clingfilm to keep them from touching which would cause interference in the data acquisition.

8.1.3 Image Processing

8.1.3.1 RECONSTRUCTION

Following acquisition, two-dimensional radiographs were reconstructed into two-dimensional slices through the X-Z plane of the sample (Figure 6b). This is a mathematical process done automatically by applying a computer algorithm, with options to reduce scan artefacts such as ring features. Once completed, the stack of two-dimensional slices can be loaded into Avizo software³, where the internal structure of the sample can be examined by loading three perpendicular ortho-slices (Figure 6c).

8.1.3.2 IMAGE FILTERING

To reduce noise, the grey scale was restricted to the samples' histogram of x-ray attenuation. This increased boundary definitions and made the images easier to examine. To further improve image quality, a deblur and non-local means filter were applied. This helped define the different components in the image and eliminate some residual noise, which can be seen in Figure 7. These are two of many filters that can be applied through Avizo, however it is important to remain cautious that the interpretation of images becomes more subjective as more image manipulation is done, and the data may become less representative of the original sample.

8.1.3.3 SEGMENTATION

Images were segmented into different components represented by the different grey scales seen in the images. This can be done by thresholding the different peaks present in the image histogram, and placing included voxels into separate groups, as shown in Figure 8. Although there are automated approaches to segmentation, manual approaches were also used; therefore there is an element of personal interpretation in the results. Once segmentation is completed, different components can be quantified and analysed (e.g., volume, geometry, length) and imaged separately. From here the porosity can be determined and imaged through a pore network model and measured.

³ <https://www.thermofisher.com/uk/en/home/electron-microscopy/products/software-em-3d-vis/avizo-software.html>

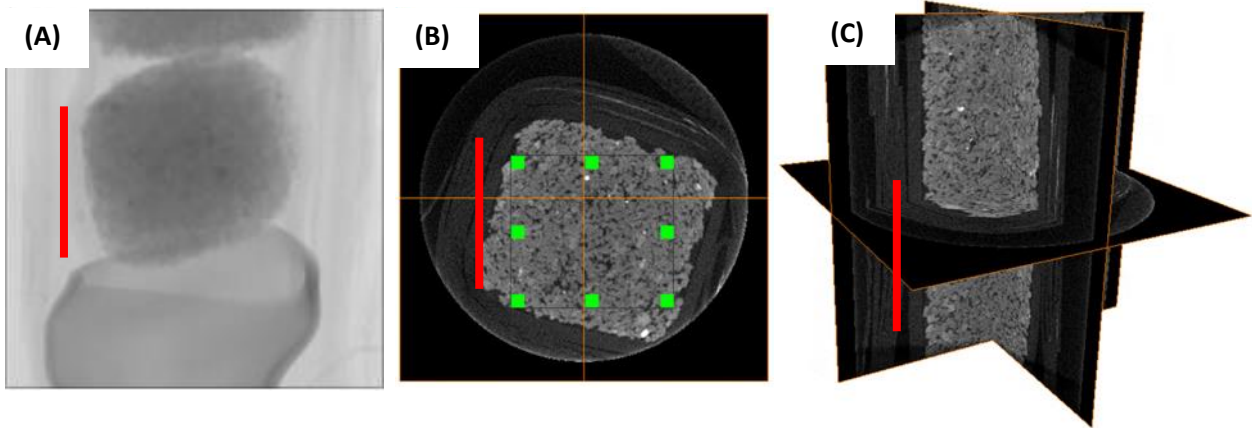


Figure 6: X-ray CT Data Slices (Image: University of Manchester)

(A): A single radiograph of sample SSK 1389 22 Sherwood Sandstone (the raw data acquired from the CT scan).

(B): A single X-Z plane slice through sample SSK 1389 22 Sherwood Sandstone (green boxed region indicates area to be cropped to).

(C): Three perpendicular slices through the same sample (SSK 1389 22 Sherwood Sandstone) showing the three-dimensional internal structure.

(Red scale bars are approximately 5mm)

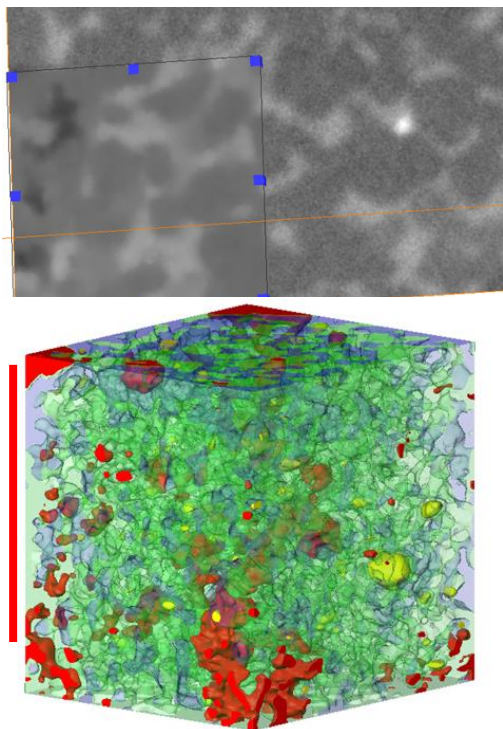


Figure 7: Non-Local Means Filter (Image: University of Manchester)

The region in the blue square shows the effect of the filter on eliminating noise from the original image (area not within the blue box). This example is from SSK 138919 Sherwood Sandstone.

Figure 8: Segmented CT Data (Image: University of Manchester)

This image of SSK 138919 Sherwood Sandstone shows four different components. Red represents the pore spaces and blue, green, and yellow show different mineral distributions. Different segments can be shown with different transparencies to help enhance different features.

(Red scale bar approximately 5mm)

8.1.4 Quantifying Change

Once pre- and post-scans had been processed, they were manually aligned to one another, so that the same grains occupied the same three-dimensional space within the voxel grid. This was followed by auto-alignment by applying a computer algorithm on Avizo, improving the accuracy of the affiliation between the two datasets. The new positions of the post-scans were registered to the pre-scans, and a sub-volume was cropped. This reduced error in component volume percentages, as some samples had suffered large degrees of grain loss between scans that

were not due to exposure to hydrogen but possibly due to the experimental design. The post-scans were then subtracted from the pre-scans to identify and quantify any changes that had occurred.

8.2 OTHER ANALYTICAL TECHNIQUES

Although XCT was the focus of the University of Manchester's involvement in this project, a selection of other analytical techniques were also undertaken. These provided comparative data to aid image interpretation and data analysis of the XCT.

(Porosity and Permeability)

Porosity and permeability measurements were taken on the original core samples prior to and after sample preparation, excluding SSK138926 (Sandgate Formation) due to its smaller diameter. Porosity was measured using a Digital Helium Porosimeter (ResLab DHP-100) and calculated using Boyle's Law. Permeability was measured by a Digital Gas Permeameter (ResLab DGP) and calculated using Darcy's Law (gas permeability) and the Klinkenberg Correction (absolute permeability). Images of both apparatuses can be found in Figure 9.

(Scanning Electron Microscopy (SEM))

Scanning electron microscopy was undertaken to provide compositional and textural context to be compared to the XCT data. Low-vacuum mode was employed on uncoated samples mounted on SEM stubs and secured with copper tape to prevent excessive charging on the poorly polished surfaces. Different SEM detector modes were used to provide different characterisation information: 1) Secondary electrons (SE) mode (spot size 3.5) to capture textural features on the samples surface; 2) Backscattered electrons (BSE) mode (spot size 3.5) to image variations in composition of the samples surface. And 3) Energy dispersive x-ray (EDX) mapping (spot size 6 to promote higher x-ray production) producing chemical maps of the samples surface, allowing some mineralogy to be determined. Multiple images were taken in both SE and BSE modes, with a maximum resolution reaction 2500x.

Plasma-focused Ion Beam (PFIB) SEM was attempted on samples to capture three-dimensional images of pores. The ion beam was used to mill the samples surface, so the attached SEM could acquire better images with less surface artefacts. Ion milling failed due to surface

charging deflecting the ion-beam considerably, resulting in a loss of focus on a single point and a difficulty in interpreting the acquired images.

8.3 RESULTS

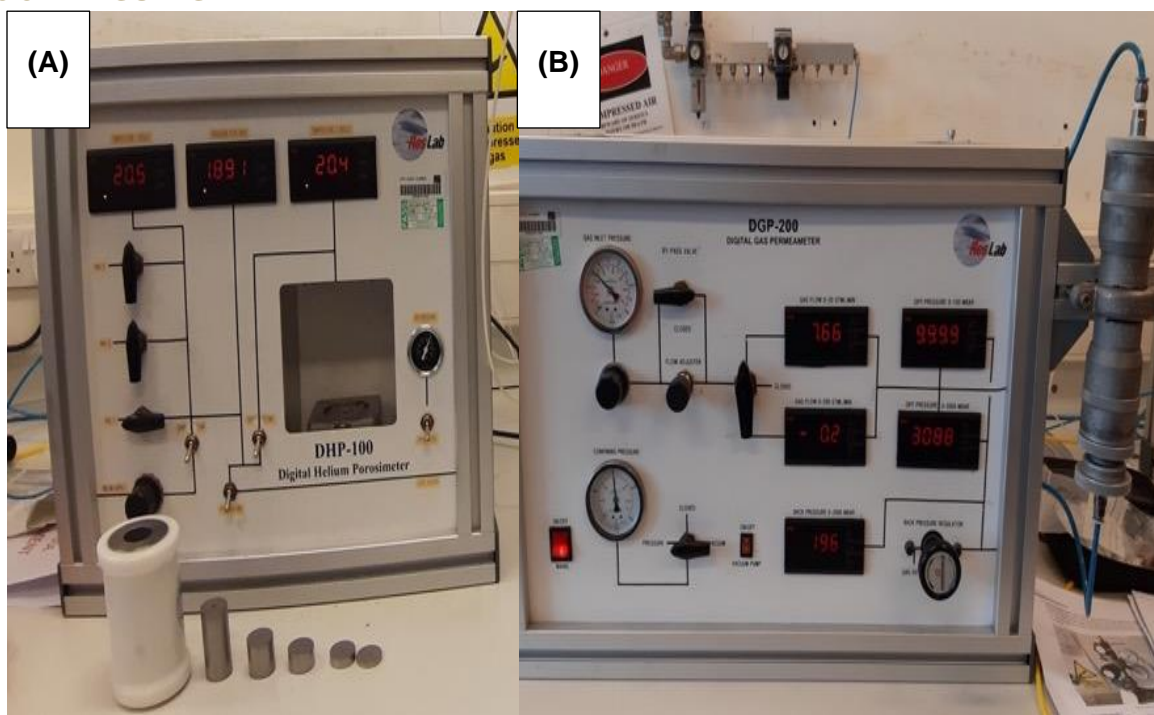


Figure 9: A: ResLab DHP-100 and B: ResLab DGP (Image: University of Manchester)

(A): Digital Helium Porosimeter used to measure the porosity of samples, included in the picture are the calibration disks which are essential to provide accurate calculations and sample cup to hold the 1" cores.

(B): Digital Gas Permeameter used to measure the permeability of samples, the samples fit in the protruding arm to the right-hand side of the photo.

The results presented here are from four of the samples that were exposed to hydrogen in the batch experiments (Sherwood Sandstone Group- SSK138921, Hythe Formation- SSK138924, Sandgate Formation- SSK138926, and Glauconitic Marl Member- SSK138927), one to represent each porous reservoir formation under investigation. Images of pre- and post-experiment samples were processed identically and segmented, allowing bulk volume fraction percentages to be determined to be compared. Post-scan images were then subtracted from corresponding pre-scan images to reveal any internal changes, such as fines migration.

8.3.1 Images of pre- and post- experiments

The qualitative pre- and post- segmented scan data is shown in Figure 10, Figure 11, Figure 12, Figure 13; which is used in the following sections to produce quantitative results. These images show the filtered pre- and post- scans on the left followed by the segmented scans respectively.

8.3.1.1 CHESTER FORMATION

The pre- and post- images in Figure 10 shows the same planes within the sample. Pore spaces (shown in black in scans, and red in segmented images) are well distributed throughout the sample. Heavy mineral grains (white in scans, yellow in segmented images) appear in parallel bands consisting of less porosity. This indicates some pre-existing texture in the sample, such as laminations.

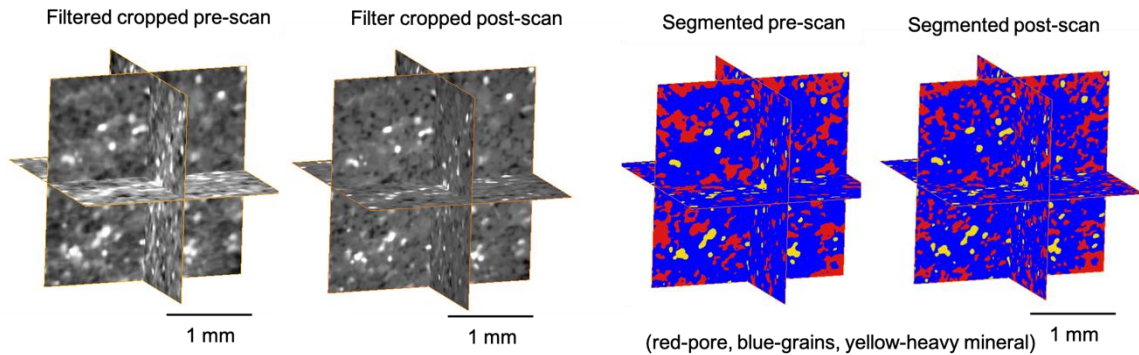


Figure 10: Ortho slices of pre-experiment scan and post-experiment scan of sample SSK138921 (Chester Formation) (Image: University of Manchester)

8.3.1.2 HYPHE FORMATION

The scan data in Figure 11 shows the coarse grain nature of the Hythe Formation samples. The porosity is well-distributed throughout the sample, as there is little to no cementation. Grains can be split into those predominantly silicates (shown in blue in segmented images) and heavy minerals (likely pyrite, yellow in segmented images). The sample appears moderately-well sorted with no evidence of any pre-existing sedimentary textures.

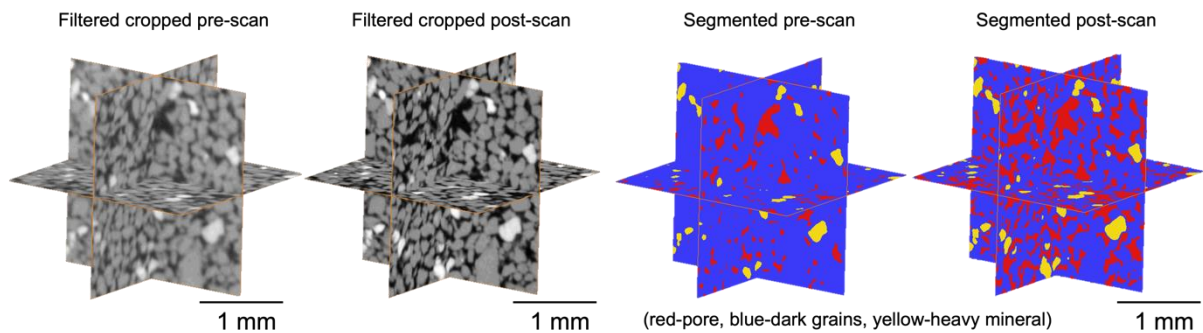


Figure 11: Ortho slices of pre-experiment and post-experiment scan of sample SSK138924 (Hythe Formation) (Image: University of Manchester)

8.3.1.3 SANDGATE FORMATION

The Sandgate Formation scan results (Figure 12) show a fine grained, mixed composition mineralogy (inferred from the variety of grey-scale/mottled pattern in scan images) surrounded by areas of much finer-grained carbonate matrix (shown in green in segmented images). The porosity is concentrated in areas containing grains rather than matrix, leading to an irregular distribution.

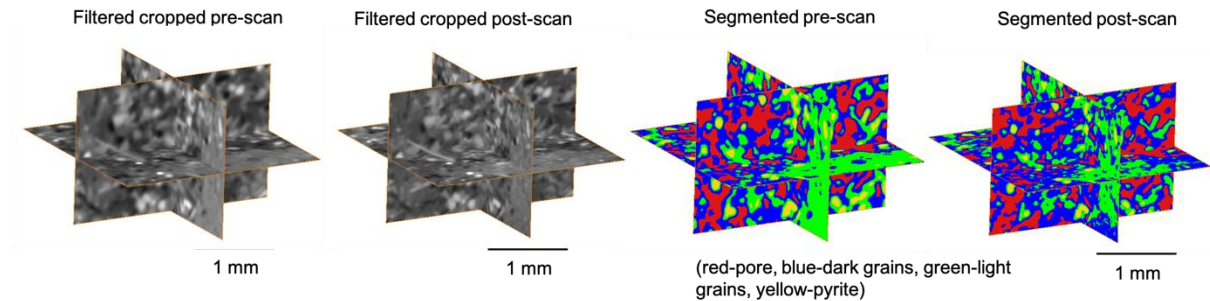


Figure 12: Ortho slices of pre-experiment scan and post-experiment scan of sample SSK138926 (Sandgate Formation) (Image: University of Manchester)

8.3.1.4 GLAUCONITIC MARL MEMBER (CHALK)

Figure 13 shows the extremely fine-grained nature of the Glauconitic Marl sample. Carbonates make up the majority of grains (green in segmented image), with silicates appearing in bands, inferring the transition period from sandstone to chalk reflective of borehole information. Porosity is contained within silicate areas and is often related to pre-existing fractures in the sample.

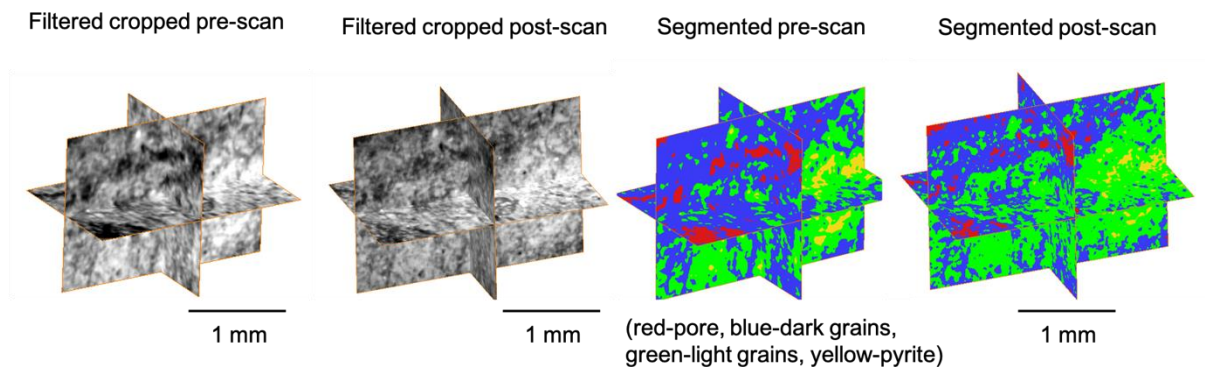


Figure 13: Ortho slices of pre-experiment scan and post-experiment scan of sample SSK138927 (Glauconitic Marl) (Image: University of Manchester)

8.3.2 Volume Changes

Only minor changes in bulk volume fractions can be found in these samples (Table 6). The volume percentage changes are all less than 5%, which is within the x-ray computed tomography image segmentation errors.

Table 6: Volume fractions of different phases in four selected samples

Sample Number	Formation	Pores (vol. %)			Grains (vol. %)			Heavy minerals (vol. %)		
		Pre-scan	Post-scan	±	Pre-scan	Post-scan	±	Pre-scan	Post-scan	±
SSK138921	Chester Formation	25.6	22.4	-3.2	71.3	73.6	+2.3	3.2	4.0	+0.8
SSK138924	Hythe Formation	34.3	31.2	-3.2	55.4	57.0	+1.6	10.1	11.8	+1.7
SSK138926	Sandgate Formation	21.2	18.5	-2.7	73.1	77.4	+4.3	5.7	4.1	-1.6
SSK138927	Glauconitic Marl	5.0	4.9	-0.1	92.9	93.9	+1.0	2.1	1.2	-0.9

8.3.3 Fine Migration

The movement of fine particles can be seen in some samples. Figure 14 shows a heavy mineral (likely pyrite), changing positions within a pore between the pre- and post- scans in a slice (XY plane). This movement can be further identified in the subtracted images in Figure 15, as identified by the red arrow.

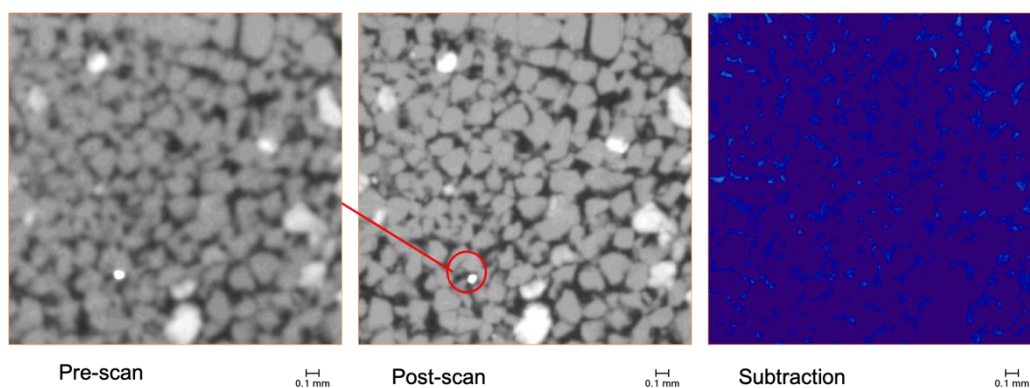


Figure 14: Fines migration shown in XY slice 433 of sample SSK138924 Hythe Formation (Image: University of Manchester)

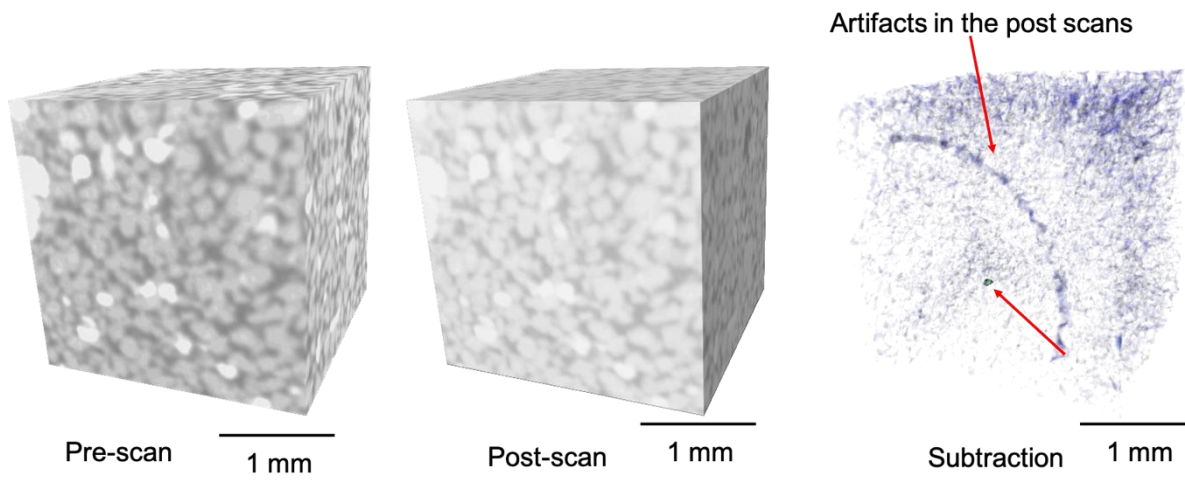


Figure 15: Fines migration shown in 3D of sample SSK138924 Hythe Formation (Image: University of Manchester)

9 Experimental design and geochemistry

A main objective of this project was to develop an experimental method that could expose rock samples to a hydrogen-rich environment at elevated temperatures and pressures in a laboratory environment. During the running of the experiments, changes in geochemistry were also measured, as part of the multi-analysis approach.

9.1 METHODOLOGIES

9.1.1 Preparation of starting materials

9.1.1.1 SOLIDS

The solid material used in the experimental work were seven samples of rock and one sample of borehole cement. These were used in 3 forms in the experiments:

- 1) A small core of material for pre-post-experiment poroperm testing
- 2) Chips of material for high-resolution imaging of surfaces and pore structure
- 3) Granulated material to monitor changes in surface area

Whilst it was recognised that having different shapes of solids in each experiment could complicate interpretation of, for example, rates of reaction, the broad similarities between the experiments enabled *relative* changes to be assessed – both in terms of evolution of each experiment and also between experiments. This experimental arrangement also allowed for a balance of different mineralogical and geochemical data to be generated, which addressed one of the main aims of the work to scope the broad types of reactivity of potential host formations (and one sample of borehole cement) for H₂ storage.

Details of the rock samples used are given in Table 1 and Table 7. In broad terms, the rocks used were of three main types:

- Red-brown coloured Permo-Triassic sandstones
- Cretaceous Greensands (both green (Hythe Formation)- and grey (Sandgate Formation)-coloured varieties were studied)
- Cretaceous Chalk Group

These types of rocks were chosen as they represent potential storage formations for aquifer storage of H₂; the Chalk represent a potential fractured storage reservoir. These rocks also have different compositions and mineral contents. In particular, the different oxidation state of Fe-minerals (hence red versus green colouration), and the potential for reduced and oxidised S in minerals (e.g. pyrite versus anhydrite).

The small cores of rock were used in the experiments 'as received', having previously had their poroperm properties measured (see Chapter 7). They came in one of two diameters, 18 mm and 25 mm, and were approximately 3 cm long.

The small chips were between 5 mm and 10 mm across, and taken from offcuts of the original borehole core adjacent to where the sub-cores were drilled.

The granulated material was generated using remaining material from cutting the small cores. This was made by careful crushing using an agate 'cone grinder' to obtain a powdered fraction of <600 µm that was used for all experimental and analytical work. It was this material was also used for characterisation by X-ray diffraction, for bulk composition, and BET (Brunauer–Emmett–Teller theory) for surface area.

The solids used were given different identifiers, linking to the borehole they came from, as well as laboratory numbers (see Table 8).

For use in experiments, solid samples were carefully weighed and added to the appropriate fluid. Given the different sizes and densities of the solid samples, the actual fluid:rock ratio is different between each experiment. Whilst this is not ideal, it was unavoidable given the health and safety requirement to minimise the volume of hydrogen gas in the experimental setup.

Batch experiments were run for approximately 9 – 12 weeks.

Table 7: Metadata of sample material

Sample details	Lithology	Starting water	Samples prepared & used	Pre-equilibration	H2 experiment
Full and abbreviated details UKGEOS Cheshire A-101 Depth: 78.00 – 78.06 m BGS ref: SJ47NEBJ141 Subsample: SSK138919	Sandstone, red-brown, mottled pale pink, fine-medium-grained, low-angle cross-bedded (channel fill), e.g. Chester Formation	Actual groundwater from sandstones at the UKGEOS site, or simplified saline water, or de-ionised water equilibrated with crushed cement.	25 mm diameter plug: Poroperm 25 mm diameter plug: contingency 18 mm diameter plug: Micro-CT 2 x 18 mm plug: contingency Offcuts: XRD, surface area analysis (powder); SEM; Micro-CT	150 bar N2, 50°C. Lab run numbers, larger autoclaves, water/rock ratio 12.5-25 / 1 (actually c. 250g / 10-20g)	150 bar H2, 50°C. Lab run numbers, smaller autoclaves, variable water/rock ratio (c. 1.8 - 2.5 / 1)
SSK138919	Sandstone, red	UKGEOS	25 mm plug; 2x chips; powder	Run HIL073, 250/15 **	Run HIL066, 1.9 / 1
SSK138920	Sandstone, red (N/U **)	-	-	-	-
SSK138921	Sandstone, red	UKGEOS	25 mm plug; 2x chips; powder	Run HIL059, 250/20	Run HIL066, 2.5 / 1
SSK138922	Sandstone, red (N/U **)	-	-	Run HIL060, 250/20	Run HIL067, 2.0 / 1
SSK138923	Sandstone, red	UKGEOS	25 mm plug; 2x chips; powder	-	-
SSK138924	Sandstone, yellow-green	35 g/L NaCl	25 mm plug; 2x chips; powder	Run HIL061, 250/10	Run HIL068, 2.3 / 1
SSK138925	Sandstone, yellow-green	35 g/L NaCl	25 mm plug; 2x chips; powder	Run HIL062, 250/10	Run HIL069, 3.1 / 1
SSK138926	Sandstone, grey	35 g/L NaCl	18 mm plug; 2x chips; powder	Run HIL063, 250/10	Run HIL070, 6.6 / 1
SSK138927	Chalk ('cementstone'), grey	35 g/L NaCl	25 mm plug; 2x chips; powder	Run HIL064, 250/20	Run HIL071, 1.8 / 1
Type G' cement as used in offshore boreholes (from the SECURE project)	-	Water already equilibrated with cement at 1 bar, 50°C	25 mm plug; 2x chips	-	Run HIL072, 2.6 / 1

Table 8: Summary experiment details

N2 'ageing' expt - Run HIL***	H2 reaction expt - Run HIL***	Pressure vessel BGS***	Type of sample (see earlier table)	Subsample number (with prefix)	MPLY ***	Basic fluid *
58 (failed)	Abandoned	063	Red Permo-Triassic sandstone	SSK138919	057	UKGEOS water
59	66	065	Red Permo-Triassic sandstone	SSK138921	059	UKGEOS water
60	67	066	Red Permo-Triassic sandstone	SSK138922	060	UKGEOS water
61	68	046	Green Cretaceous sandstone	SSK138924	062	35 g/L NaCl sln
62	69	047	Green Cretaceous sandstone	SSK138925	063	35 g/L NaCl sln
63	70	054	Grey Cretaceous sandstone	SSK138926	064	35 g/L NaCl sln
64	71	057	Grey Cretaceous sandstone	SSK138927	065	35 g/L NaCl sln
-	72	029	Borehole cement	-	-	Cement equilibrated DIW
73 (repeat of 58)	74	063	Red Permo-Triassic sandstone	SSK138919	057	UKGEOS water

* Pre-reacted for H2 expts

9.1.1.2 SOLUTIONS

Three solutions were used in the experiments, which consisted of:

- 1) Water extracted from UKGEOS ground investigation borehole A101 in Cheshire. This came from an open-hole section at approximately the same depth as some of the rock samples, and so it has been assumed that it is broadly in equilibrium with those rock samples (here we acknowledge the possibility of some uncertainty, for example from stratified water compositions, but have had to work within the boundaries of what fluids were available).
- 2) Where there was uncertainty in in-situ water composition (mainly for the experiments involving samples of Cretaceous material), a generic NaCl solution of 35 g/L NaCl was used. We acknowledge that this salinity might not be an accurate representation of that in-situ, and also that many of the lower concentration elements would not be included in the starting solution. However, again we have had to work within the boundaries of what information was available. To partly mitigate this uncertainty, pre-equilibration time of samples was allowed to try and allow this simplified solution to at least partially equilibrate with the rock prior to addition of H₂.
- 3) For the borehole cement experiment, the starting solution was made using de-ionised water reacted with broken pieces of surplus cement at 50°C. This allowed it to become significantly alkaline through the dissolution of portlandite (Ca(OH)₂) ± calcium silicate hydrate (CSH) phases. This step was important, because if pieces of borehole cement were put into e.g., 35 g/L NaCl solution saturated with H₂ gas, then much of the potential change to the surface of the cement blocks would have been due to dissolution into water rather than through chemical interaction with H₂.

Whilst (1) and (2) above might result in some degree of non-equilibrium with minerals in the rock samples, the impact of this was mitigated through the use of pre-equilibration experiments, where the 'raw' solutions were allowed to react with spare pieces of the rocks, such that the solution chemistry evolved to be as close to equilibrium with the rock as was reasonably possible in the time available (Figure 16, Table 7).

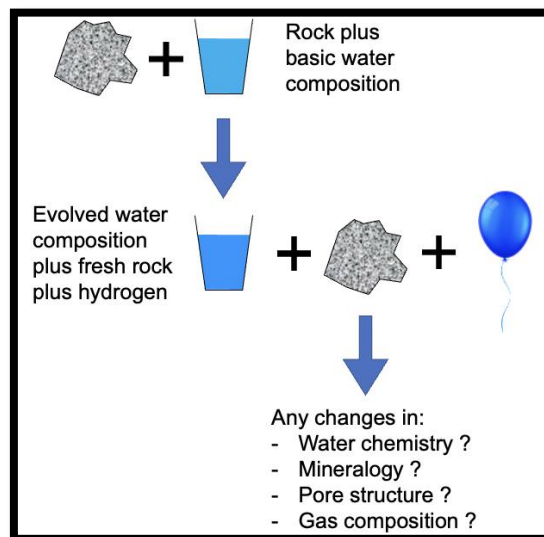


Figure 16: Schematic representation of the experimental approach.

9.1.1.3 GASES

Two gases were used in the experiments: first nitrogen (N₂) and then hydrogen (H₂).

The N₂ was used to pressurise the pre-equilibration experiments. It was obtained from BOC Gases and classified as 'oxygen free' (99.998% pure). It was delivered in a cylinder pressurised to 230 bar (23 MPa). However, the actual experimental pressure was controlled by an ISCO

360D syringe pump. This type of pump allows for the desired pressure stability, but had its pressure transducer ‘zeroed’ at the start of the experiments to maintain its accuracy.

The H₂ used in the ‘simulation’ experiments was also sourced from BOC Gases as a pure gas. As per the N₂ experiments, the actual experimental pressure was controlled by an ISCO 360D syringe pump, which has its pressure transducer periodically ‘zeroed’ to maintain accuracy.

9.1.2 Experimental methodology

The rationale behind these experiments was to scope the potential for reaction in porous media with hydrogen, and its consequent impact on water chemistry, mineral stability, and porosity/permeability. As this was a scoping study, and because this was the first time our lab has worked with high-pressure H₂ in experiments, relatively simple methodologies were employed. A simpler approach would lead to fewer technical issues, and a greater chance of experimental success.

Our approach used PTFE-lined 316-stainless steel batch reactors inside a thermostatically-controlled, fan-assisted incubator at 50 °C. A similar arrangement has been shown to operate reliably with little maintenance for at least 5 years for pressurised systems, and at least 15-20 years for non-pressurised systems (Bateman et al., 2013; Moyce et al., 2014; Rochelle et al., 2016). The basic layout of a typical batch reactor used is shown schematically in Figure 15, alongside a photograph of the key parts of it. This consists of a steel pressure vessel, titanium dip tube with non-reactive filter assembly, and PTFE liner. Note that in this study a simple stirrer bead was used, rather than the caged one in Figure 17, as this gave more room for the rock samples. The PTFE lining is added to prevent corrosion of the 316 stainless steel, and to prevent contamination of the solution with metals such as iron and chromium. Viton O-rings are used between the vessel body and vessel head to prevent loss of pressure. A large retaining ring is screwed onto the top of the vessel to keep the vessel body and vessel head together when pressurised.

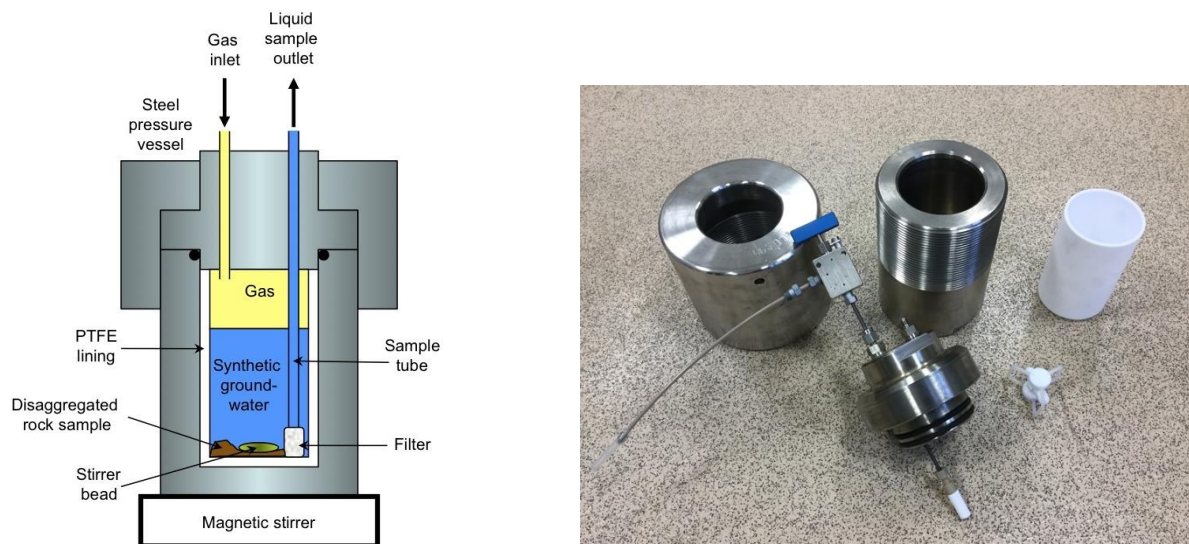


Figure 17: Schematic diagram and photograph of a steel batch reactor, PTFE liner, and magnetic stirrer.

Preparation of the rock samples and loading the vessel consisted of a series of weighing steps that allowed accurate determination of amounts of rock sample and fluid. In summary, the process was:

- Prepare the pressure vessel with a titanium dip tube and non-reactive filter assembly.
- Weigh the PTFE liners
- Weigh (separately) the rock cores, rock chips, and container of granulated material

- Mount the rock cores and chips onto gold wire, and record the combined weight of each group of the same rock type (e.g., one rock core and 2x chips). For some of the smaller chips, it was easier to place them into a 'bag' made from a piece of nylon mesh (Figure 17)
- Add about 75% of the expected water volume to a PTFE liner and weigh it
- Place one set of core/chips into its appropriate water in a PTFE liner and measure the combined weight
- Place the above into a vacuum desiccator and evacuate to about 0.2 bar for a minute, and then allow to return to atmospheric pressure. (This process helped remove air from the dry sandstone samples, but we could not reduce pressure too far or the water would boil at room temperature). Record the combined weight of the PTFE-liner/water/solids
- Weigh stirrer bead and add to PTFE liner
- Record the combined weight of the PTFE-liner/water/solids/stirrer bead
- Add granulated rock
- Add additional solution (water) to the vessel to take the water level to within about 5 mm of the top of the PTFE liner. (This was done to minimise the volume of hydrogen at the top of the vessel, whilst still being able to move the liner around without spilling the water)
- Record the combined weight of the PTFE-liner/water/solids
- Add the granulated material and weigh the empty container
- Record the combined weight of the final PTFE-liner/water/solids/stirrer bead
- Carefully bend the gold wire around the top of the filter so as to hold the rock samples above the stirrer bead at the bottom of the PTFE liner (Figure 18)
- Being careful not to agitate the water around inside the pressure vessel unnecessarily, the top of the vessel was slowly pushed on, and then the retaining ring securely screwed on

Through a process of direct weighings and weight differences, the above process gave accurate information on the weights of material added, and hence the water/rock ratios. Given the different sizes of rock samples used, and the need to minimise the hydrogen volume headspace (for safety reasons, in case of a sudden escape of the hydrogen), each experiment had a slightly different water/rock ratio (Table 7:).

Once, loaded, the vessels were placed onto stirrer plates inside a warmed incubator in two sets of 4 experiments (Figure 19, 20). The vessels were then connected to individual pressurised gas lines. This arrangement meant that half of the experiments could be isolated in case of problems. Each vessel had:

- A valve on top of the dip tube to allow water sampling whilst the experiment was under pressure.
- A valve connected to the gas line.
- A rupture disk, with a burst pressure of 200 bar (i.e., somewhat over the run pressure of 150 bar, but well within the safe working pressure of the pressure vessel).

The small amount of air (i.e., oxygen) was purged from each vessel by gently flushing with a small amount of low-pressure nitrogen (achieved by slackening off the pressure seal around the dip tube). Once all the vessels had been purged of air, the nitrogen was replaced with hydrogen and the nitrogen in each vessel removed with a small flush of low-pressure hydrogen. This process did release a small amount of hydrogen into the lab and was done with the doors of the incubator open to help dissipate it. During this procedure, a dedicated hydrogen detector was used to monitor for any build-up of the gas. Once the headspace of each vessel contained only hydrogen, all seals were tightened down and the vessels warmed to 50°C. Once at temperature, hydrogen gas was slowly (so as not to blow the water around inside the vessels) added to each vessel and the pressure raised to 150 bar. The procedure for this and other pressurisation events was to keep the incubator doors open, and work on one vessel at a time. We considered the highest likelihood of a sudden hydrogen leak would be during pressurisation

(e.g. through O-ring failure), and so maximised the potential for dilution of any leaking H₂ into the lab, whilst keeping the potential leakage volume to a minimum. A dedicated H₂ detector was used to monitor the air around each vessel during pressurisation. Once a stable pressure was reached, each vessel was inspected for any leaks, and then its isolation valve on the gas line closed. Periodic checks of pressure inside each vessel was achieved by opening this isolation valve, and adjusting the pressure as necessary.



Figure 18 : Example of the range of ways samples were introduced into the reactors.



Figure 19: Samples as mounted inside the reactors, adjacent to the filter assembly on the dip tube.



Figure 20: Layout of several batch reactors inside the incubator.

The stirrer bead ensured good mixing between the solution and rock. To minimise mechanical damage, in particular to the granulated rock in the bottom of the vessel, the stirrer bead was only activated for approximately 2 minutes every 4 hours.

9.1.3 Sampling and analysis of reacted fluids

At the end of each experiment, a fluid sample was withdrawn whilst the experiment was still at 50 °C and 150 bar pressure. A syringe was attached to a valve at the top of the titanium sampling tube via a length of polyetheretherketone (PEEK) tubing. The valve was opened slowly and an accurately-known quantity (typically 1-5 ml) of fluid was allowed to flow into the syringe in order to flush the sample tube, valve, and tubing. This syringe was removed and discarded. A second syringe was then attached, and used to withdraw an accurately known amount (typically approximately 15-20 ml) of fluid, this being the sample (Figure 21). This sample was subsequently filtered using a 0.2 µm nylon syringe filter. A further volume (typically approximately 50 ml) was withdrawn into a large syringe and sent for microbiological analysis. The taking of these samples effectively removed all extractable water from the vessels. Upon completion of sampling, the sampling valve was closed, as was the valve to the pressure line, and the vessel removed from the incubator.

A gas sample was taken by attaching a syringe to the now available pressurisation valve, and carefully opening the valve. This syringe was flushed twice with the gas from the experiment before a sample for analysis was taken. A valve at the end of the syringe prevented air contamination.

Once a sample of filtered water was obtained, each was split into several subsamples, with the analysis of pH and alkalinity being conducted as soon as possible.



Figure 21: Sampling arrangement. Note syringe attached to sampling valve, and red gas monitor for hydrogen.

pH was measured at room temperature and pressure on sub-samples using a Thermo Scientific Orion VersaStar meter with an Orion 9103BNWP semi-micro combination pH electrode calibrated using Whatman® NBS traceable buffers at pH 4, 7 and 10.

Analytical sub-samples from the main filtered sample were prepared as follows:

- 8 ml of each of the samples were placed into a polystyrene tube and acidified with 1% (i.e. 0.08 ml) of concentrated 'ARISTAR'® nitric acid. These samples were stored in a fridge (at about 5 °C) prior to analysis. Subsequent analysis was for major and trace cations by inductively coupled plasma – mass spectroscopy (ICP-MS).

- Another 5 ml of the filtered samples were taken and placed in a polyethylene tube for analysis of anions by ion chromatography (IC). Samples were also stored in a fridge prior to analysis.
- 2.7 ml of the filtered samples was added to 0.3 ml dipyriddy solution for the preservation of reduced iron (Fe^{2+}).
- 2 ml of the filtered samples was taken and added to a polystyrene tube with 2 ml of deionised water for analysis of alkalinity by titration against a known strength of sulphuric acid.

9.1.4 Sampling and analysis of starting and reacted solid phases

The petrographic work presented here is primarily based on scanning electron microscope (SEM) techniques (see below), with quantitative mineralogy from X-ray diffraction (XRD) analysis, and trace element chemistry from digestion and ICP-MS analysis.

At the end of experimental runs, the vessels were slowly and carefully depressurised whilst still at near run temperature. The reacted solids were removed from the vessel and rinsed with acetone in order to remove any adherent fluid, preventing subsequent precipitation of solids if the samples dried. All the rock samples showed little or no reaction on their surfaces (Figure 22); however the cement samples showed growth of clear crystals of a secondary phase (Figure 23). The samples were carefully packed into plastic containers and sent for SEM and XRCT analysis.



Figure 22: Typically, the rock samples appeared relatively unchanged at the end of the experiments.

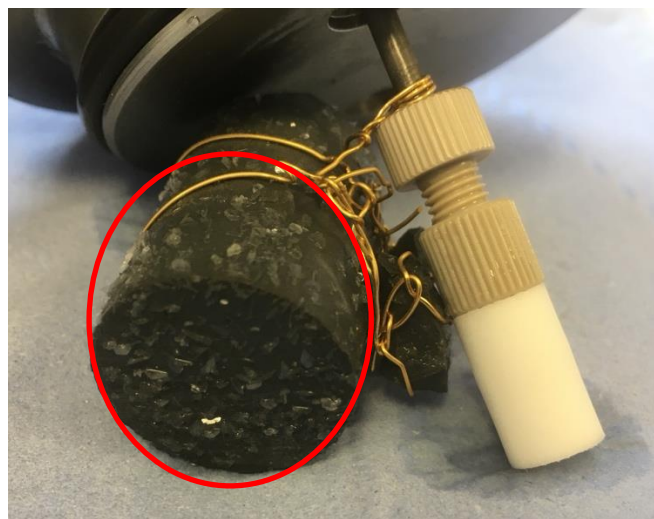


Figure 23: Crystalline secondary minerals were visible at the end of the cement experiment (circled).

9.2 RESULTS

9.2.1 Changes in water composition

Tabulated data obtained from the detailed analyses of the water composition are presented in Appendix 4.

A range of analytes were followed during the experiments, though not all of them showed significant changes during the weeks to months that the samples were reacting. The following sections consider several aspects, aimed at addressing two main questions:

- 1) Did the starting solutions used have realistic chemical compositions?
Answering this requires tackling two sub-questions:
 - Was the starting solution used in approximate equilibrium with the rock sample used?
 - Did pre-reaction under a N_2 -atmosphere allow for closer attainment of equilibrium?
- 2) Did exposure to high pressure hydrogen result in significant fluid chemical changes?

In order to reduce the number of plots/tables, we have used simple comparison plots in the following sections. Changes in water composition are resolved as either positive or negative deviations from a 1:1 relationship between the analyte (usually element) concentrations in the starting solution compared to their concentration in the reacted solution (Figure 24). Adopting this approach allows all analytes from a particular experiment to be compared on the same plot (especially if log axes are used), with addition/removal of elements to/from solution revealed by concentrations deviated from the 1:1 line. Although this approach may be less effective at revealing minor changes in composition (i.e., small amounts of reaction), it will indicate the more important changes.

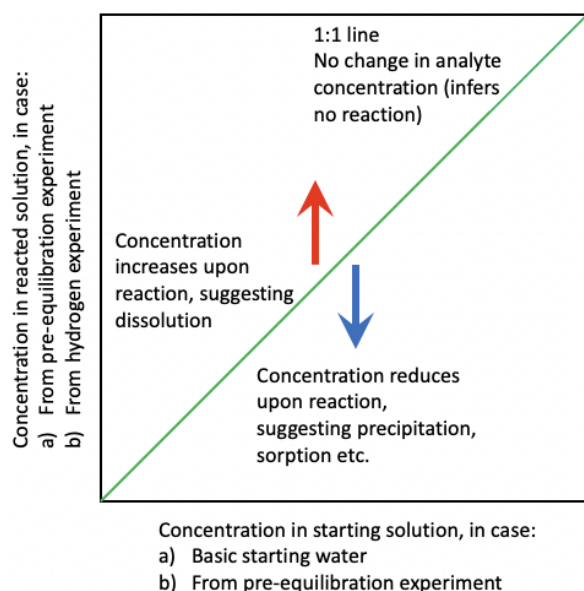


Figure 24: Schematic diagram of a pre-/post-reaction water chemistry plot. Chemical changes are evidenced by departures from the 1:1 line.

It should be noted that if log axes are used, then concentrations in the lower left part of the diagram could be very low, and possibly close to analytical detection limits. As detection limits are approached, uncertainty increases, and so increasing scatter around the 1:1 line might be expected.

9.2.1.1 CHEMICAL COMPOSITION OF STARTING SOLUTIONS

In order to ascertain if the starting waters were in chemical equilibrium with the rock samples, their compositions were compared pre- and post-reaction (i.e., after several weeks) with either Sherwood Sandstone, Lower Greensand or Chalk samples.

Pre-equilibration of the experimental waters

It was postulated that the starting solutions available were not going to be in equilibrium with the sandstone samples, and so we allowed for a period of pre-equilibration under experimental pressure and temperature conditions (150 bar, 50 °C) and under a N₂ atmosphere. This was done to try and better resolve changes purely due to the presence of H₂ in the subsequent experiments. It was not known how long was required to allow for pre-equilibration, but the experiments were constrained by the project timeline, and 9 weeks was considered a reasonable compromise between time available and degree of reaction. Although the timeframe of the study did not allow for longer pre-equilibration (which was preferred), 9 weeks allowed for time to check if this was a reasonable compromise timescale. Run HIL 73 (SSK138919 and UKGEOS water) was sampled several times in order to see if the 9 week 'maturation' period was enough to attain an approximate steady-state composition (a selection of the resulting fluid chemical data are shown in Figure 25).

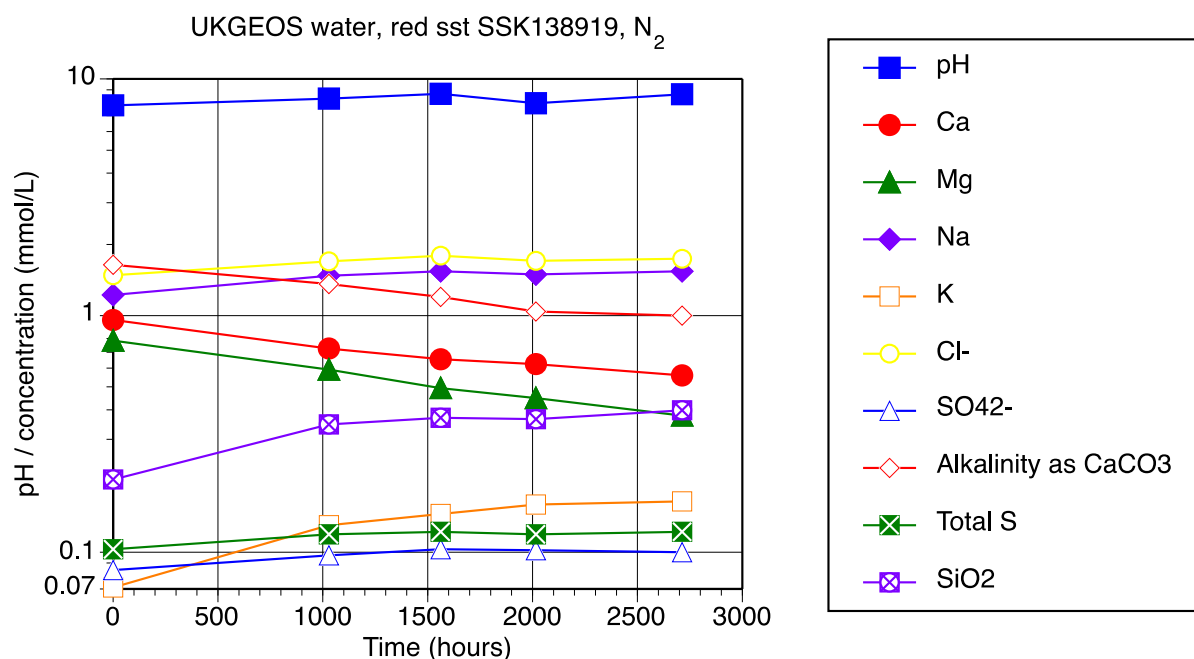


Figure 25: Evolution of pH and selected dissolved analytes upon reacting UKGEOS water with a red Permo-Triassic sandstone SSK138919.

The slight decreases in concentration of Ca, Mg and alkalinity, coupled with increases in pH, suggest equilibrium with respect to dissolved carbonate species, and precipitation of small amounts of a Ca-rich carbonate. That the concentrations involved are relatively small suggests that the amount of material precipitation would be equally small. As a consequence, it might be difficult to detect this during mineralogical observations.

The increases in K and SiO₂ concentrations suggest mineral dissolution. It is tentatively suggested that this may have been a K-rich clay mineral such as illite. There is no direct evidence that illite is this phase, its high surface area would allow for overall more release of elements from it compared to other minerals in the sandstone sample.

Though some reaction was still ongoing after 16 weeks of reaction (c. 2700 hours), much of the initial chemical change had apparently happened within the first 9 weeks (c. 1500 hours).

Indeed, the initial pH increase had stabilised within the first 6 weeks (c. 1000 hours). As such, and given the scoping nature of this initial study, the 9-week pre-equilibration period was considered to be a reasonable compromise between extent of reaction and time available.

As well as the 7 sandstone samples, a single sample of borehole cement was also used in this study. The sample was prepared by Sintef for experiments conducted in the EU SECURE project (Rochelle et al., 2020). It is a Type G borehole cement designed for the elevated temperatures of boreholes exploring deep basinal conditions. Offcuts of this material had been kept wet from the previous study, and so a container of water and broken up pieces of cement was kept at 50 °C for 9 weeks to allow it to equilibrate. Given that portlandite ($\text{Ca}(\text{OH})_2$) is a major component of cement, has retrograde solubility and faster reaction rates, and that the water was already equilibrated at room temperature, it is likely that warming the water to 50 °C resulted in minor precipitation of portlandite.

Sherwood Sandstone samples

After approximately 9 weeks, comparison of pre- and post-reaction water chemistry is shown in Figures 26-28, with no change in analyte represented by the line and deviations from the line represented by distance of the blue dots from the line.

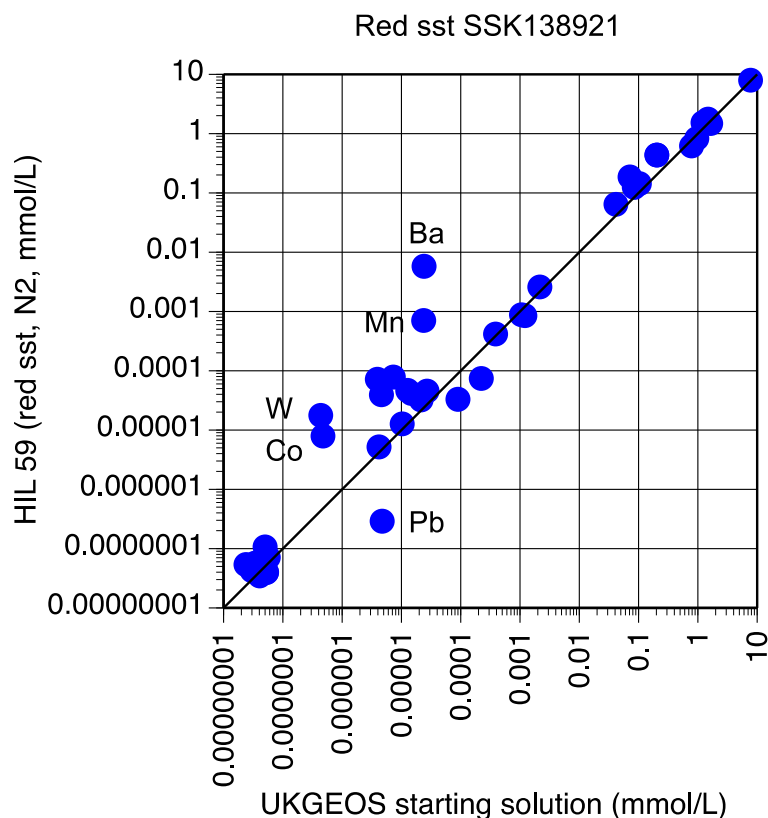


Figure 26: Comparison plot of pre-/post-experiment (line vs blue dot) water chemistry when UKGEOS water is equilibrated with Sherwood Sandstone SSK138921 under N_2 pressure (Run HIL59).

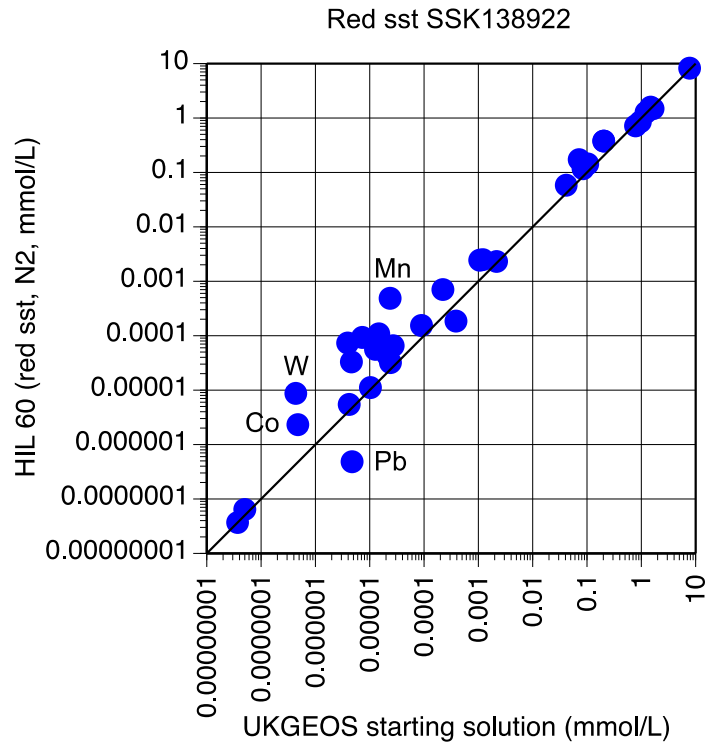


Figure 27: Comparison plot of pre-/post-experiment water chemistry when UKGEOS water is equilibrated with Sherwood Sandstone SSK138922 under N₂ pressure (Run HIL60).

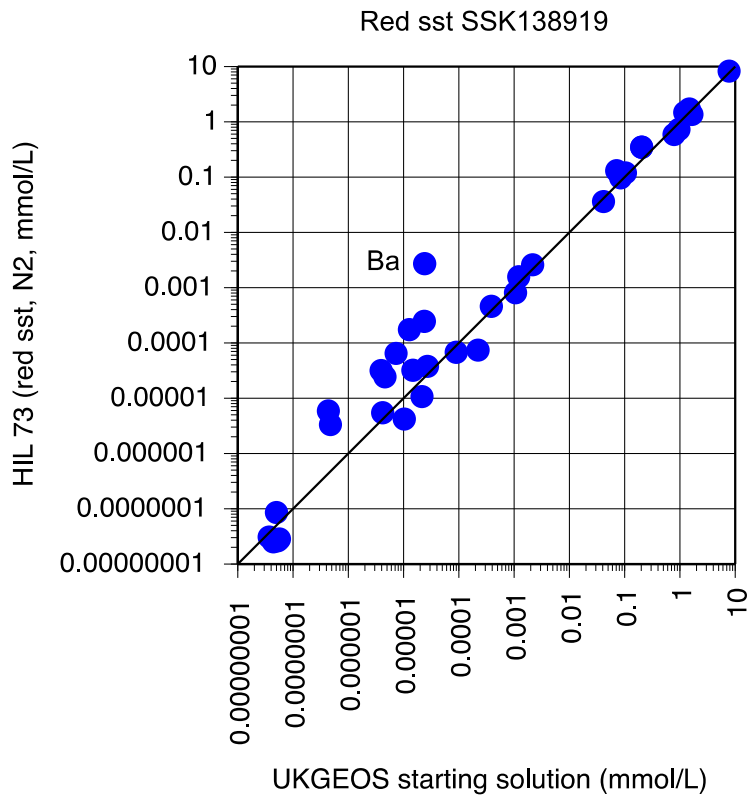


Figure 28: Comparison plot of pre-/post-experiment water chemistry when UKGEOS water is equilibrated with Sherwood Sandstone SSK138919 under N₂ pressure (Run HIL73).

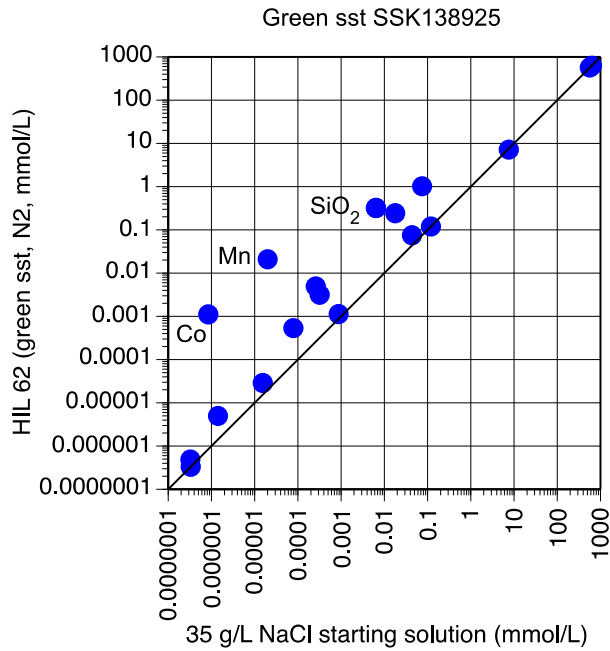


Figure 30: Comparison plot of pre-/post-experiment water chemistry when the NaCl solution is equilibrated with Hythe Formation sandstone SSK138925 under N₂ pressure (Run HIL62).

Most analytes lie along the 1:1 relationship line, representing no change in their concentration on pre-reacting the (relatively simple) NaCl solution with the rock. Some increases in element composition would be expected given the simple starting composition, though reaction kinetics would be sluggish given the relatively low temperature and short timescale. However, there is a consistent increase in SiO₂ concentrations. The low temperature would not favour quartz (or aluminosilicate mineral) dissolution, and so we tentatively suggest that biogenic (i.e. amorphous) silica may be present in the samples, and it is some of this that has dissolved. As per the Sherwood Sandston Group red sandstones, there is an increase in Mn and Co, and potentially similar processes could be operating to those described above.

Sandgate Formation and Glauconitic Marl samples

There are also only two experiments to consider, and comparison of pre- and post-reaction water chemistry after approximately 9 weeks reaction is shown in Figures 31 and 32.

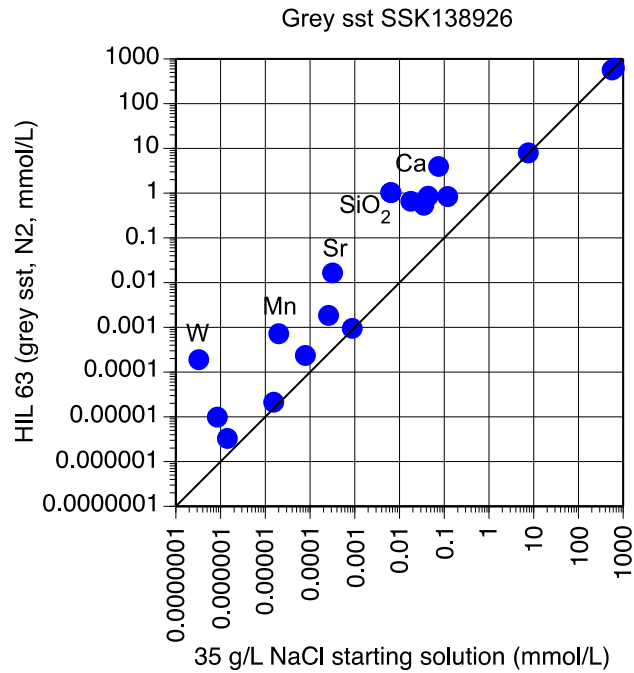


Figure 31: Comparison plot of pre-/post-experiment water chemistry when the NaCl solution is equilibrated with Sandgate Formation sandstone SSK138926 under N₂ pressure (Run HIL63).

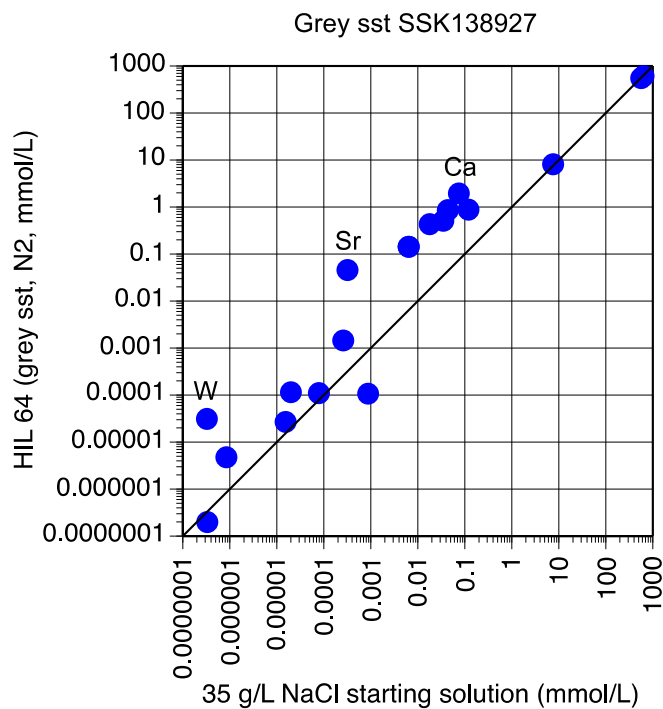


Figure 32: Comparison plot of pre-/post-experiment water chemistry when the NaCl solution is equilibrated with Glauconitic Marl chalk SSK138927 under N₂ pressure (Run HIL64).

Compositional changes are broadly similar to the other rock types in terms of increases in Mn, W, SiO₂, and similar processes to those described above could have been involved. However, this time there are also notable increases in Ca and Sr, and this suggests dissolution of a carbonate mineral, most likely calcite.

9.2.1.2 CHEMICAL COMPOSITIONAL CHANGES UPON ADDITION OF HYDROGEN

As per the section above, it is possible to make an initial assessment of key reactions due to the presence of high-pressure hydrogen – this time through consideration of plots of the compositions of pre-reacted waters (i.e. under an N₂ atmosphere) with the chemistry of waters after 3-months reaction under a hydrogen atmosphere.

Sherwood Sandstone samples

After approximately 3 months reaction, comparison of pre- and post-reaction water chemistry is shown in Figures 33-35.

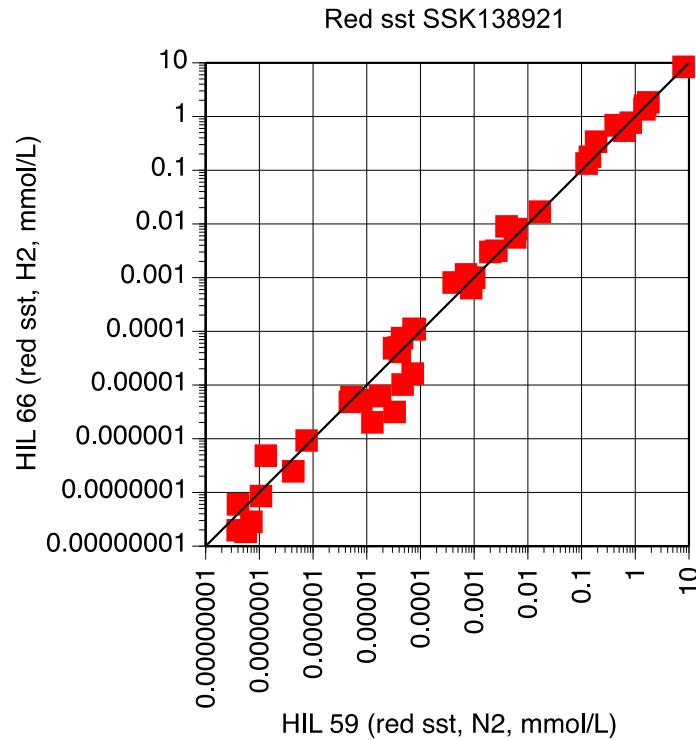


Figure 33: Comparison plot of pre-/post-experiment water chemistry when 'aged' UKGEOS water and Sherwood Sandstone SSK138921 is exposed to high pressure H₂ pressure (Run HIL66).

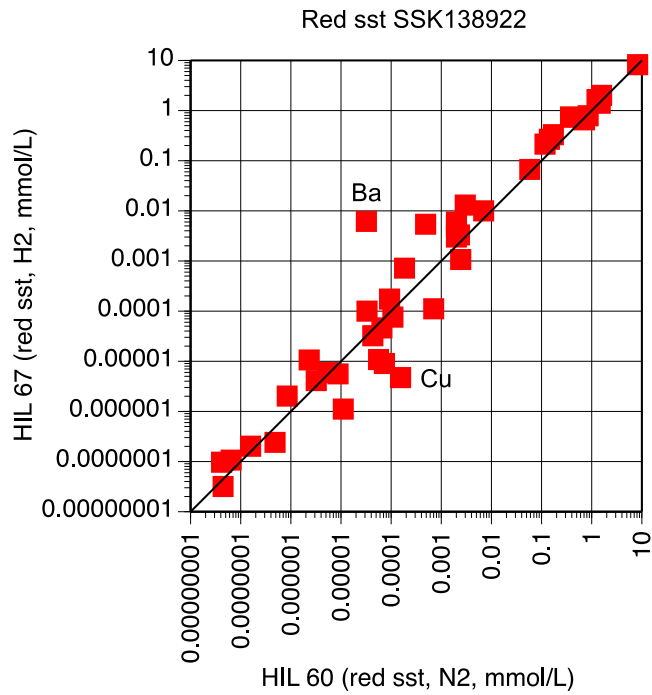


Figure 34: Comparison plot of pre-/post-experiment water chemistry when 'aged' UKGEOS water and Sherwood Sandstone SSK138922 is exposed to high pressure H₂ pressure (Run HIL67).

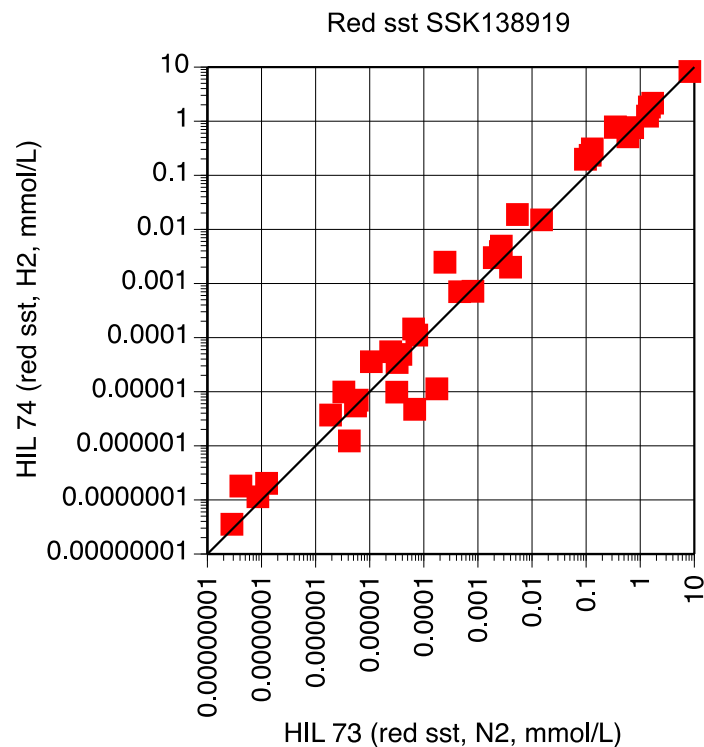


Figure 35: Comparison plot of pre-/post-experiment water chemistry when 'aged' UKGEOS water and Sherwood Sandstone SSK138919 is exposed to high pressure H₂ pressure (Run HIL74).

There was very little apparent reaction during experiments HIL66 and HIL74 (SSK138919) with almost no deviations from the 1:1 Line. As such, and within the time constraints of this study, it is tentatively concluded that the presence of hydrogen did not instigate any significant geochemical reactions with the red sandstone samples involved.

Experiment HIL67 (sandstone sample SSK138922) did show two changes, an increase in Ba, and a decrease in Cu. It is not completely clear why this experiment showed these changes and the other two did not. However, Ba increased during the pre-equilibration experiments, and it is possible that the 9 weeks of pre-reaction was not long enough for the UKGEOS water to have finished reacting with sandstone sample SSK138922, and that some (non H₂-driven) reaction continued to longer timescales. We also note that the stability boundary between the dissolved species Cu²⁺ (at lower pH) and solid phase Cu(OH)₂ (at higher pH) is close to the experimental pH (Rubio-Nieblas *et al.*, 2014). It is possible therefore, that a relatively small increase in pH could lead to Pb removal from solution as a solid phase.

Hythe Formation sandstone samples

There are only two experiments to consider, and comparison of pre- and post-reaction water chemistry after approximately 3 months reaction is shown in Figures 36 and 37.

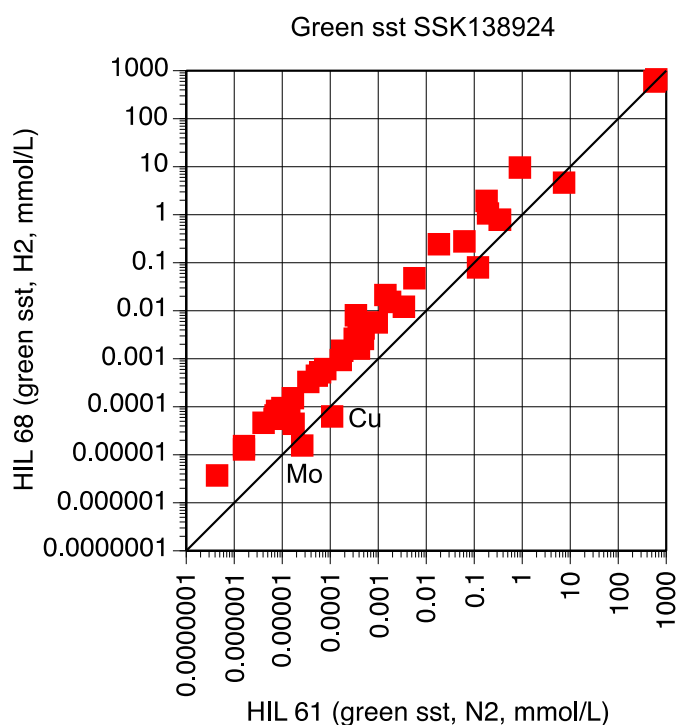


Figure 36: Comparison plot of pre-/post-experiment water chemistry when ‘aged’ NaCl solution and Hythe Formation sandstone SSK138924 is exposed to high pressure H₂ pressure (Run HIL68).

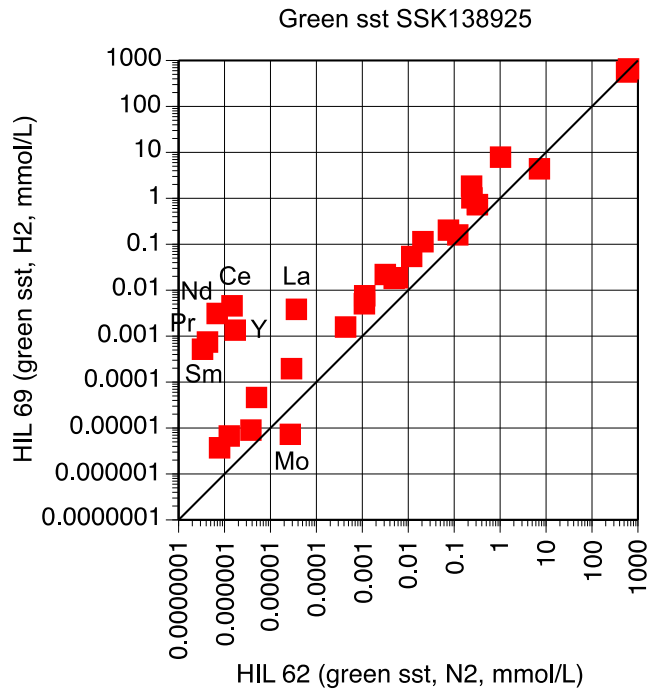


Figure 37: Comparison plot of pre-/post-experiment water chemistry when 'aged' NaCl solution and Hythe Formation sandstone SSK138924 is exposed to high pressure H₂ pressure (Run HIL69).

A feature of these two experiments is that most of the data lie along lines parallel to the 1:1 line. This requires a common process to be affecting almost all of the elements equally, increasing their concentrations in the hydrogen experiments. Given the small size of the hydrogen molecule and its propensity to escape through even slightly imperfect seals, we suggest that slow and continuous (though minor) loss of H₂ occurred through the experiments, and that this would have carried H₂O vapour alongside the H₂. Slow loss of H₂O vapour would have reduced the volume of water in the experiments, increasing element concentrations overall. It is not clear exactly why H₂ loss impacted just these experiments with Hythe Formation sandstones and not others. However, the experiments were assembled one subset at a time, and it is conceivable that minor procedural changes on the day that these 2 experiments were assembled resulted in slightly less perfect sealing.

As per the SSG red sandstone experiments, a decrease in Cu was observed (Run HIL68, SSK138924), and similar processes could have been operating. This time however, there were also decreases in Mo. Again, in the near neutral pH region there can be a change between dissolved and solid phase Mo (Nishimoto *et al.*, 2019; Tkac *et al.*, 2008), but this requires relatively reducing conditions. Though H₂ can be a reducing agent, its slow reaction kinetics at these low temperatures do not favour this process. It is more likely that trace amounts of sulphide minerals (e.g. pyrite) in the samples might have driven the solution towards more reducing conditions. The small, but detectable, amounts of Fe²⁺ in these experiments is indicative of reducing conditions. However, dissolution of pyrite would likely have been limited, otherwise there would have been larger concentrations of Fe²⁺ and total Fe in solution.

Though values are low, the increase in the concentrations of certain lanthanide elements in Run HIL69 (SSK 138925) was unexpected. We currently do not have an explanation for this.

Overall, however, there was relatively little apparent reaction during experiments HIL68 (SSK138924) and HIL69 (SSK138925). As such, and within the time constraints of this study, we can again tentatively conclude that the presence of hydrogen did not instigate any significant geochemical reactions with the green sandstone samples involved.

Sandgate Formation and Glauconitic Marl samples

There are also only two experiments to consider, and comparison of pre- and post-reaction water chemistry after approximately 3 months reaction is shown in Figures 38 and 39.

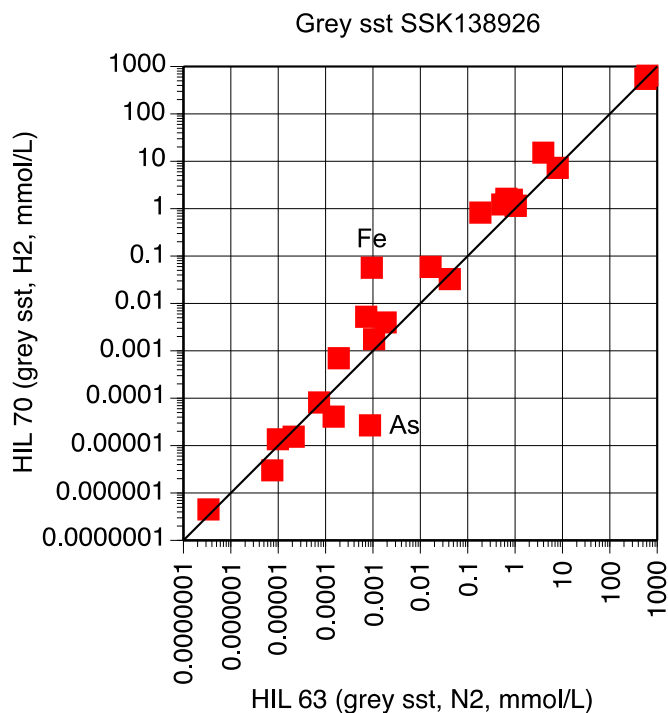


Figure 38: Comparison plot of pre-/post-experiment water chemistry when 'aged' NaCl solution and Sandgate Formation sandstone SSK138926 is exposed to high pressure H₂ pressure (Run HIL70).

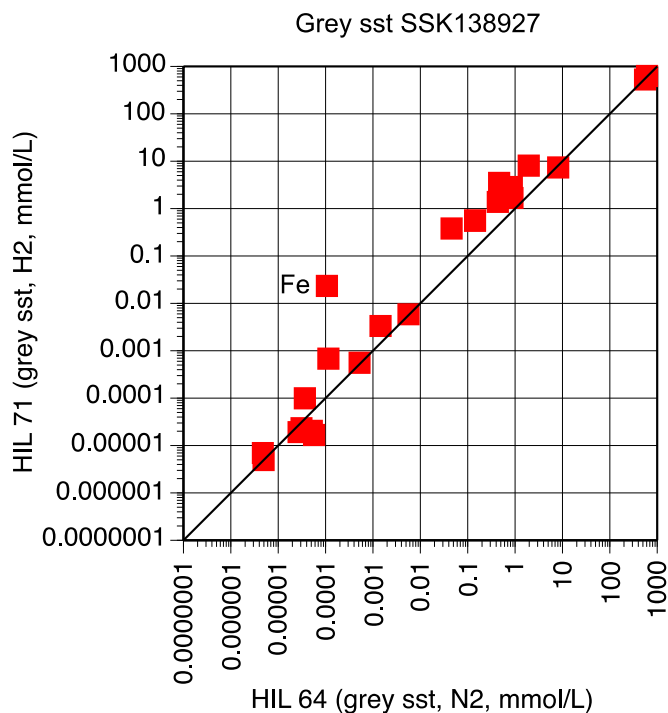


Figure 39: Comparison plot of pre-/post-experiment water chemistry when 'aged' NaCl solution and Glauconitic Marl SSK138927 is exposed to high pressure H₂ pressure (Run HIL71).

As per the Sherwood Sandstone experiments, there was very little apparent reaction during experiments HIL70 and HIL71, with almost no deviations from the 1:1 Line. As such, and within the time constraints of this study, it is tentatively concluded that the presence of hydrogen did not instigate any significant geochemical reactions with the grey sandstone samples involved.

Having said the above, both experiments showed increases in Fe concentrations (ICP data) upon reaction. The most likely explanation is that dissolution of small amounts of reduced minerals (such as pyrite) led to reducing conditions favouring Fe²⁺ in solution (the highest dissolved Fe²⁺ concentrations [colorimetric data] in this study were found in these 2 experiments).

The apparent decrease in As concentration should be treated with caution. This value is almost at the detection limit, and hence is associated with a high degree of uncertainty.

Borehole cement sample

There are also only two experiments to consider, and comparison of pre- and post-reaction water chemistry after approximately 3 months reaction is shown in Figure 40.

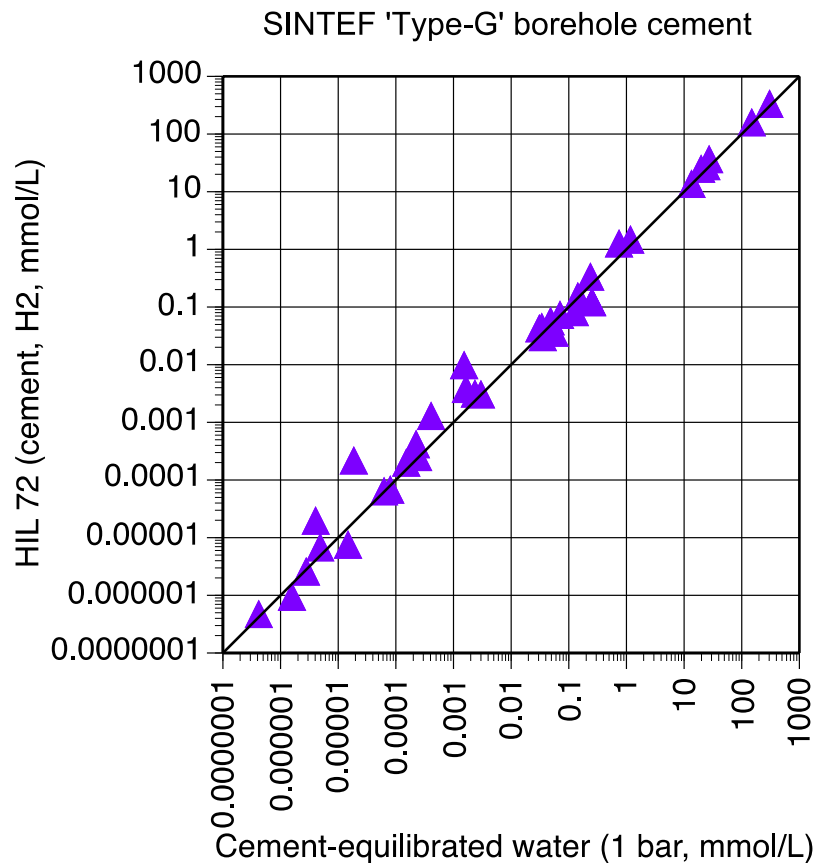


Figure 40: Comparison plot of pre-/post-experiment water chemistry when cement-equilibrated water and borehole cement are exposed to high pressure H₂ pressure (Run HIL72).

Noteworthy for the cement waters is their relatively high pH, alkalinity and Ca concentration. These result from saturation with portlandite (Ca(OH)₂), which is a key cement mineral phase.

There was very little apparent reaction during experiment HIL72, with almost no deviations from the 1:1 Line. As such, and within the time constraints of this study, it is tentatively concluded that the presence of hydrogen did not instigate any significant geochemical reactions with the borehole cement sample involved.

9.2.2 Changes in gas composition

At the end of each experiment, triplicate gas samples were taken whilst the experiments were still at run pressure. The main purpose was to scope the potential for any significant amounts of contaminant gases to form, as these would degrade H₂ quality. A secondary purpose was to develop and test our gas sampling and gas sample handling methodologies. This IDRIC study is one of the first we have undertaken involving H₂-pressurised experiments, and we acknowledge limitations to our gas sampling and analytical approaches. Indeed, the GC used does not have the resolving capabilities of a modern GC-MS instrument.

The analytical data are presented in Table 9: Analyses of headspace gas compositions at the end of the experiments (as a percentage of total gas analysed).

	Relative abundance 4 min (H ₂) (%)	Relative abundance 8 min (%)	Relative abundance 10 min (%)	Relative abundance 12 min (%)	Relative abundance 13 min (%)	Relative abundance 14+ min (%)
HIL66	98.9%	0.1%	0.0%	0.1%	0.5%	0.4%
HIL67	98.3%	0.0%	0.0%	0.0%	0.0%	1.6%
HIL68	99.6%	0.0%	0.0%	0.0%	0.1%	0.3%
HIL69	98.4%	0.0%	0.0%	0.0%	0.4%	1.1%
HIL70	98.0%	0.0%	0.0%	0.0%	0.0%	2.0%
HIL71	98.6%	0.0%	0.0%	0.0%	0.1%	1.2%
HIL72	98.0%	0.0%	0.0%	0.0%	0.5%	1.4%
HIL73/4	89.6%	0.2%	0.4%	1.0%	0.0%	8.7%
HIL74	98.5%	0.0%	0.2%	0.0%	0.0%	1.3%

Table 9: Analyses of headspace gas compositions at the end of the experiments (as a percentage of total gas analysed).

As expected, the gas at the end of the experiments was almost all H₂. In view of limitations in terms of analytical equipment and procedures, we have tried to avoid over-interpretation of the data. The data are output from the GC as a series of peaks at different times as each gas is released from the chromatography column – small gases (like H₂) coming off quickly, larger and more complex ones being released more slowly. One issue is that without a good calibration gas it is not possible to assign every peak to a specific gas, and setting up a full calibration can be time-consuming. For this initial study we only did a limited calibration, focussing on short timescale releases (at about 4 minutes, for H₂) and a single longer-timescale peak (at 14+ minutes, where H₂S would be expected), though other tiny peaks were observed.

Most of the minor peaks in the GC data are close to detection limits, and potentially could be within the range of analytical noise. The only clear anomaly was for the last sample (4) from Run HIL73, where a clear peak at 14+ minutes was observed (making up c. 9% of the gas volume). This is most likely due to an imperfect sampling procedure from the experiment and contamination by air getting into the sample. Although H₂S would also appear at around 14+ minutes, it would have been very easy to smell if it was as abundant as 9% - and there was no strong smell of H₂S.

We did however note if there was an odour when we sampled/opened each experiment. Given that the human nose can be sensitive to H₂S at sub-ppm concentrations and organo-sulphur

compounds (e.g. thiols [mercaptans]) to sub-ppb, or even sub-ppt concentrations (e.g., Guidotti *et al.*, 2017), this can be a useful, albeit a non-quantitative, way to identify if odorants are formed during the reactions. Though odorants are added in minute quantities to the natural gas supply to identify leaks, their uncontrolled generation during H₂ storage in the subsurface might be regarded as a potentially problematic contamination of the H₂.

We found that there was:

- no, or almost no, odour to the gas at the end of the red sandstone experiments (Runs HIL66, HIL67, HIL74) and the cement experiment (Run HIL72) (SSK samples 138919, 138922, 138***).
- little odour, or at most a slightly 'oily odour', to the gas from the green sandstone experiments (Runs HIL68 and HIL69) (SSK samples 138924, 138925).
- a distinctly 'rubbery' odour to the gas from the grey sandstone experiments (Runs HIL70, HIL71) (SSK samples 138936 and 138927).

There does appear to be a link between the strength of smell to the degree of reduction (as evidenced by amount of reduced iron, Fe²⁺, in solution) in the experiments, which could be linked to the amount of reaction of sulphide minerals (e.g. pyrite). Consequently, it is tentatively concluded that contamination of stored H₂ by odorants is likely to be more of a concern in reduced lithologies (e.g. green/grey ones: Greensand and Chalk) where pyrite is present, as opposed to more oxidised sandstones (e.g. red ones: Sherwood Sandstone).

Whilst solely inorganic reactions might not control the production of the smelly compounds, and microbial process may also contribute, it is most likely that breakdown of pyrite provided the energy required for either the inorganic or biogenic reactions. Useful future work would be to identify the precise processes producing the odorants, and whether they are controlled by microbial processes (e.g. through microbial counts or isotopic analysis of potential products).

10 Approach to understanding potential microbial response

10.1 INTRODUCTION

Hydrogen is a valuable energy source to many microbes, leading to interest in the potential impacts that microbial activity could have on hydrogen storage, particularly in porous media. The experiments described in Sections 4-9 were designed primarily as geochemical experiments, but because of this interest some basic microbiological data was collected. Beyond sterile sampling at the end of the experiment no particular microbiological precautions or modifications to design were incorporated into the experiments. Therefore, it must be noted that the following observations are relevant to these particular experiments, and caution needs to be exercised in extrapolating them directly to subsurface storage.

10.2 METHODS

10.2.1 Microbial analysis

At the start of the experiment, between 5 – 10 ml fluid samples were taken from the vessels containing samples SSK138921 - SSK138927 and added to sterile 15 ml tubes. Collection tubing was sterilised by flushing with 60% isopropanol prior to use. 50 ml fluid samples were collected in 50 ml syringes from vessels containing sample SSK138919 (Sherwood Sandstone) at the start and end of the experiment. 50 ml fluid samples were collected in the same way from all other end of experiment vessels. The samples were used for the following assays.

10.2.2 Most probable number counts for iron reducing bacteria and sulphate reducing bacteria

Sterile 2 ml exetainer[®] tubes were used for most probable number (MPN) counts of sulphate-reducing bacteria (SRB) using Postgate's medium B and iron-reducing bacteria (IRB) using IRB#8 medium (see 05 for recipes). A dilution series in 0.9% sterile saline solution (cement sample and starting samples) or sterile PCR water (end of experiment samples) was prepared from the fluid samples and 200 µl of each dilution was used to inoculate 1.8 ml media in triplicate. A positive control (0.1 g soil sediment in 2 ml media) and negative control (2 ml media only) were also set up. Tubes were incubated anaerobically for 25 days. Incubations were carried out at 50 °C. Some of the samples were inadvertently placed in a 30 °C incubator for one (cement and starting samples SSK138921 - SSK138927) or two (end of experiment SSK138927) days. The brief drop to 30 °C was judged likely to have minimal effect on the survival of bacteria present in the experiments, so the incubations were continued as resampling of the experiments was not possible. Growth of the desired microbial group was indicated by the presence of a black precipitate in the Postgate's Medium or a colour change to red or pink in the IRB#8 medium after the addition of 200 µl 2-2'-Bipyridyl solution. MPNs were calculated using the EPA MPN calculator (<https://mostprobablenumbercalculator.epa.gov/mpnForm>) and 95% confidence intervals calculated by the Cornish and Fisher method (Cornish & Fisher, 1938).

10.2.3 Miles Misra counts for aerobic and anaerobic heterotrophic bacteria

Miles Misra counts for total culturable aerobic heterotrophs and anaerobic heterotrophs were performed for all samples. Using the previously described dilution series, eight 15 µl aliquots of each dilution were spotted onto the surface of PTYG medium agar plates (see 05 for recipe). Plates were incubated aerobically or anaerobically at 50 °C for 6 days (cement, starting samples SSK138921 - SSK138927) or 7 days (all other samples). PORTG, starting samples SSK138921 - SSK138927 plates were incubated for one day, and SSK138927 for two days, at 30 °C before the 50 °C incubation. The number of aerobic and anaerobic colony-forming units per ml were calculated from the mean number of colonies in the eight drops on the dilution with 3-30 colonies per spot after this incubation period.

10.3 RESULTS

The results of the aerobic heterotroph, anaerobic heterotroph, SRB and IRB culture-based enumeration tests are presented below.

10.3.1 SRB and IRB

In general, sulphate and iron reducers were present in low numbers at the start of the experiment and were not detected by the experiment end, after a change to a hydrogen headspace. Sulphate reducers were only present in low numbers at the start of the experiment (Figure 41 and Figure 42) with sample SSK138922 (Chester Formation) being the only sample positive for SRB.



Figure 41 MPN counts of SRB per ml starting fluid after 24 days anaerobic incubation at 50 °C. Starting fluid samples had a nitrogen headspace. 95% confidence intervals (Cornish & Fisher, 1938) indicated with error bars.

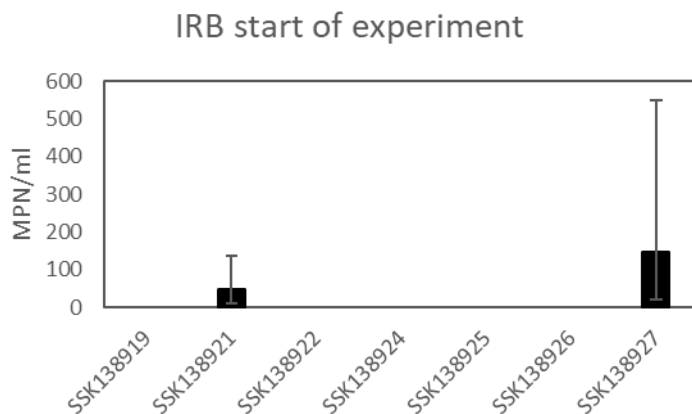


Figure 42. MPN counts of IRB per ml starting fluid after 25 days anaerobic incubation at 50 °C. Starting fluid samples had a nitrogen headspace. 95% confidence intervals (Cornish & Fisher, 1938) indicated with error bars.

Iron reducers were not found in the end of experiment samples and were low numbers detected in only two samples (SSK138919 and SSK138927) at the start of experiment. However, the IRB media for the chalk sample SSK138927 changed colour in non-predictable way (i.e., not as expected in a dilution series), which suggested the colour change may have been chemical rather than microbial and may possibly relate to the pH of this sample. The fact that no aerobic or anaerobic bacteria were detected in the Miles Misra assays SSK138927 chalk sample

(Section 10.3.2) supports the suggestion that the observed colour change was not microbiologically induced.

10.3.2 Total aerobic and anaerobic bacteria

Anaerobes were more numerous than aerobes in all start of experiment samples which showed any growth at the end of the experiment except for SSK138926 where only aerobic bacteria could be detected. At the end of the experiment the number of bacteria detected were considerably lower and disappeared from samples SSK138921 and SSK138924. Bacteria were still detected in SSK138922 but the number of bacteria was approximately 100-fold lower. SSK138922 was the only sample containing aerobic bacteria, which were more numerous than anaerobes. The aerobes that were present in the SSK138926 were not detected by the end of the experiment but a small number of anaerobic bacteria could be detected (Figure 43). The number of heterotrophic bacteria in the other samples was below the detection limits of this assay for both aerobes and anaerobes (SSK138919, SSK138921, SSK138924, SSK138925 and SSK138927).

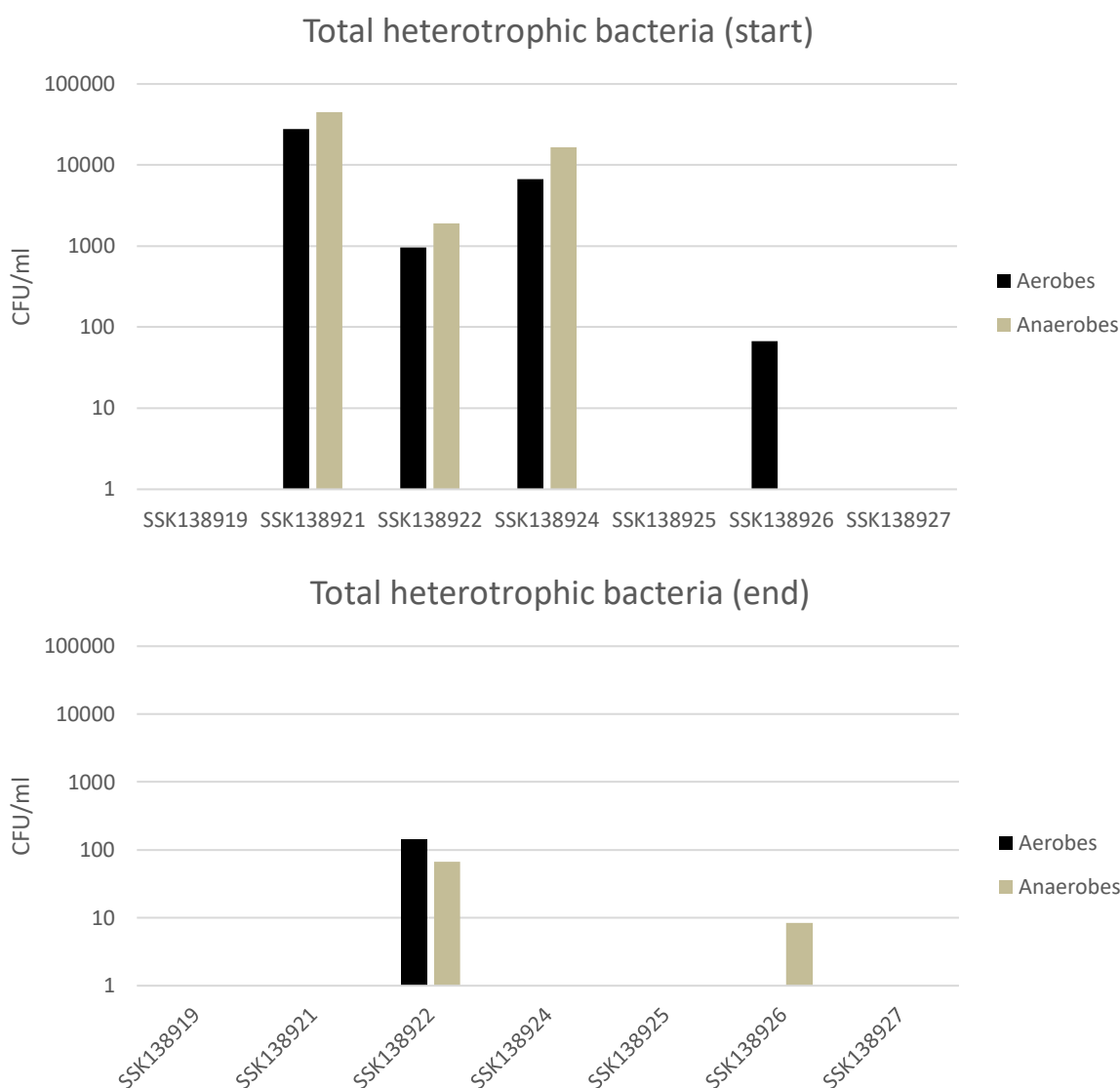


Figure 43. Aerobic and anaerobic Miles Misra in colony forming units per ml fluid (CFU/ml) after 7 days incubation at 50 °C. Upper figure: Fluids taken from end of equilibration phase (nitrogen headspace). Lower: Fluid taken at end of experiment (hydrogen headspace).

10.3.3 Discussion

The number of microorganisms in the lithologies examined in these experiments, particularly of the targeted iron and sulphur reducing bacteria, was consistently low. This may reflect the fact that no specific precautions were taken with regards to maintaining the microbial communities present in the collected samples. No further inoculation with microorganism that are representative of groundwater was carried out. Nothing was added to stimulate microbial activity (other than hydrogen which can act as an electron donor for a variety of microbial processes). The source of microorganisms in these experiments could be those from the rock that survive being exposed to atmosphere and desiccation for a variety of lengths of time between retrieval of sample from the subsurface and experimentation. This would tend to select against anaerobes that are sensitive to oxygen or those that do not survive desiccation well. This might include some SRB and IRB. A second source of microorganisms could be from the groundwater. Groundwater is only a source of microbes in experiments using the Sherwood Sandstone samples SSK138919, SSK138921 and SSK138922, as a 35 g L⁻¹ NaCl solution was used in all other experiments. Such a salt solution would not provide the variety of elements essential to microbial growth that would be found in natural groundwater. Finally, as no precautions were deployed during rock coring, handling and preservation, subsampling or setting up of experiments, the possibility of contamination from the air or from the hands of those involved in each of those stages cannot be ruled out.

Analysis of the groundwater alone showed microbial abundance was low and reduced by the end of the equilibration phase with nitrogen. Changing any environmental conditions, including the gas headspace will perturb the microbial community. In these experiments the microbial community was exposed to a large change in temperature compared to the in situ temperatures and exposed to a change from a nitrogen to a hydrogen environment. The temperature of the groundwater in situ was around 14 °C and the experiments were run at 50 °C. This would exert a selection pressure on the microorganisms in the experiments as the groundwater would have a community of microorganisms that thrive in moderate temperatures which would not be expected to thrive at temperatures of 50 °C. In addition, the groundwater used was oxic and therefore would not be expected to be dominated by the kinds of anaerobic microorganisms (such as sulphate reducers and iron reducers) that are expected to occur within hydrogen storage projects at depths. Most microbial communities with high diversity will contain some members that will benefit from changes and although the microbial community structure will change, microbial activity is likely to continue. When biomass is low, the diversity and capacity to cope with change may also be reduced so that the overall effect was detrimental to microbiology. As a consequence of these two things the microbial biomass entering the stage of the experiment where hydrogen were reduced compared to natural groundwater, in some cases microbial counts were below detection limits. The expected increase in microbial activity in response to exposure to hydrogen was not seen in these experiments. Three samples had both aerobes and anaerobes at the start of the experiment (after nitrogen equilibration); SSK138921, SSK138922 (both Sherwood Sandstone) and SSK138924 (Lower Greensand). No viable microorganisms could be recovered at the end of the hydrogen exposure, and in the remaining sample (Sherwood Sandstone SSK138922) numbers of both aerobes and anaerobes had decreased by approximately one order of magnitude. The results from these experiments alone would suggest that exposure to hydrogen is detrimental to microorganisms, but the extent to which the factors discussed above influenced this, and therefore relevance to the storage of hydrogen in porous media is difficult to ascertain.

Two out of three of the sample with natural groundwater showed the most microbes (UKGEOS water + Cheshire SSG), but microbes were also detected with the NaCl and Hythe and Upper Greensand. Although some microbes can be revived from stored rock core material, the groundwater was expected to be the major source of microorganisms in this experiment. In addition, mixed brines provide a greater variety of nutrients and essential elements required by microorganisms than NaCl.

11 National-scale mapping exercise

A GIS-led exercise was completed to identify potential target locations for underground storage in the Sherwood Sandstone and Lower Greensand (Figure 44). Surfaces for the upper position of the Sherwood Sandstone and Lower Greensand aquifers are sourced from BGS datasets and described in Abesser & Lewis (2015). This analysis has not included a volumetric calculation of hydrogen that could be stored at these locations, and detailed mapping of the extent and character of these closures, beyond the appraisal of the national-scale surfaces, has not been attempted.

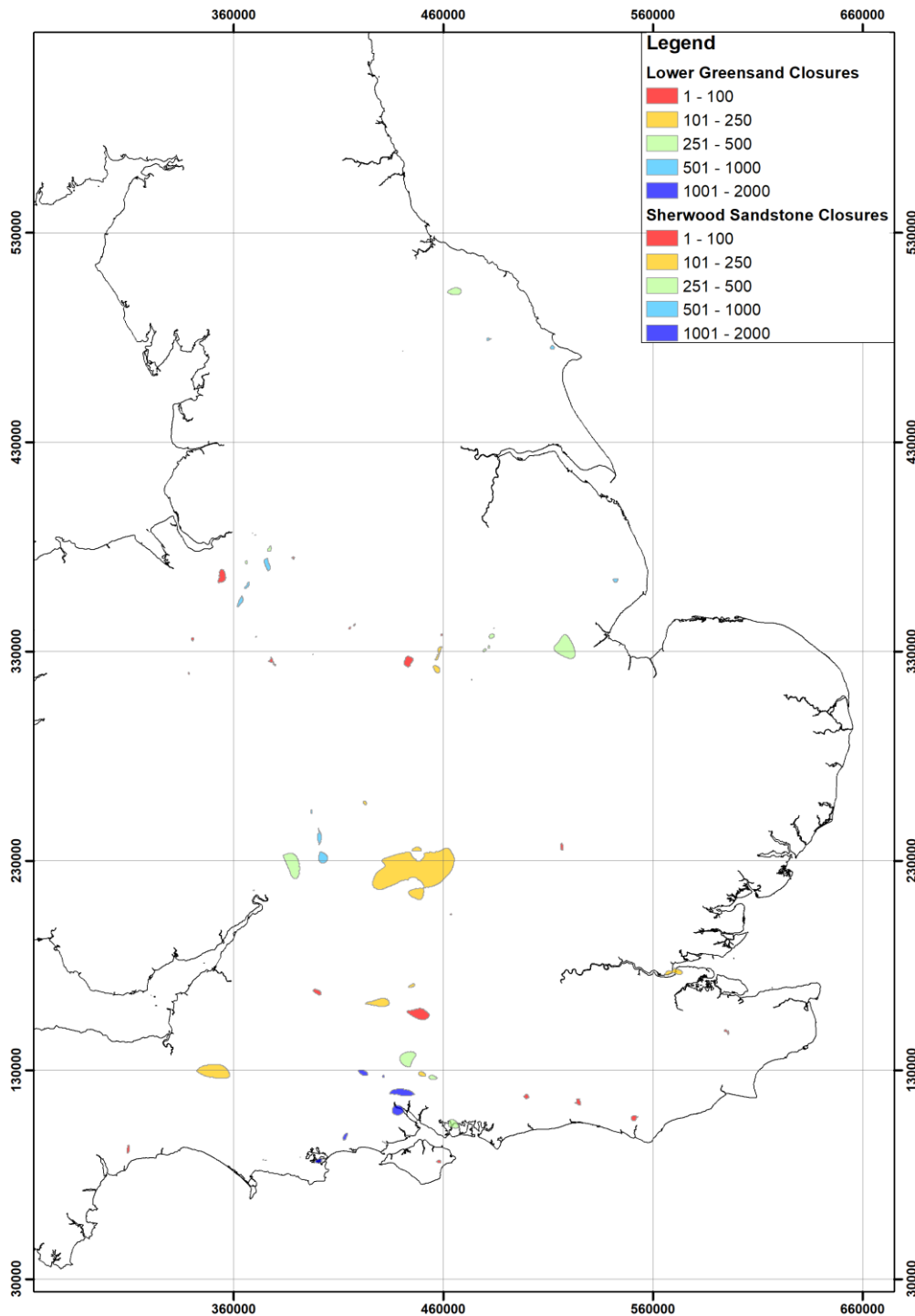


Figure 44 Map showing closures identified from the BGS national scale upper surfaces of the Sherwood Sandstone and Lower Greensand. These are categorised by depth from surface. Contains Ordnance Survey data © Crown copyright and database right 2021

The analysis involved using national-scale surfaces (generated from the BGS Open-Loop ground source heat pump screening tool⁴), for both rock units, and running an automatic script that identified closures in the mapped surface (i.e., areas where structural dips were divergent from a single point, forming upward closures/dome structures). The analysis does not identify structural (e.g., faulted closures), and gives a first-pass analysis of where potential storage locations could be located.

Figure 43, illustrating closures in both the Sherwood Sandstone and Lower Greensand, is derived from individual analysis of individual surfaces for the Sherwood Sandstone (Figure 45) and the Lower Greensand (Figure 46).

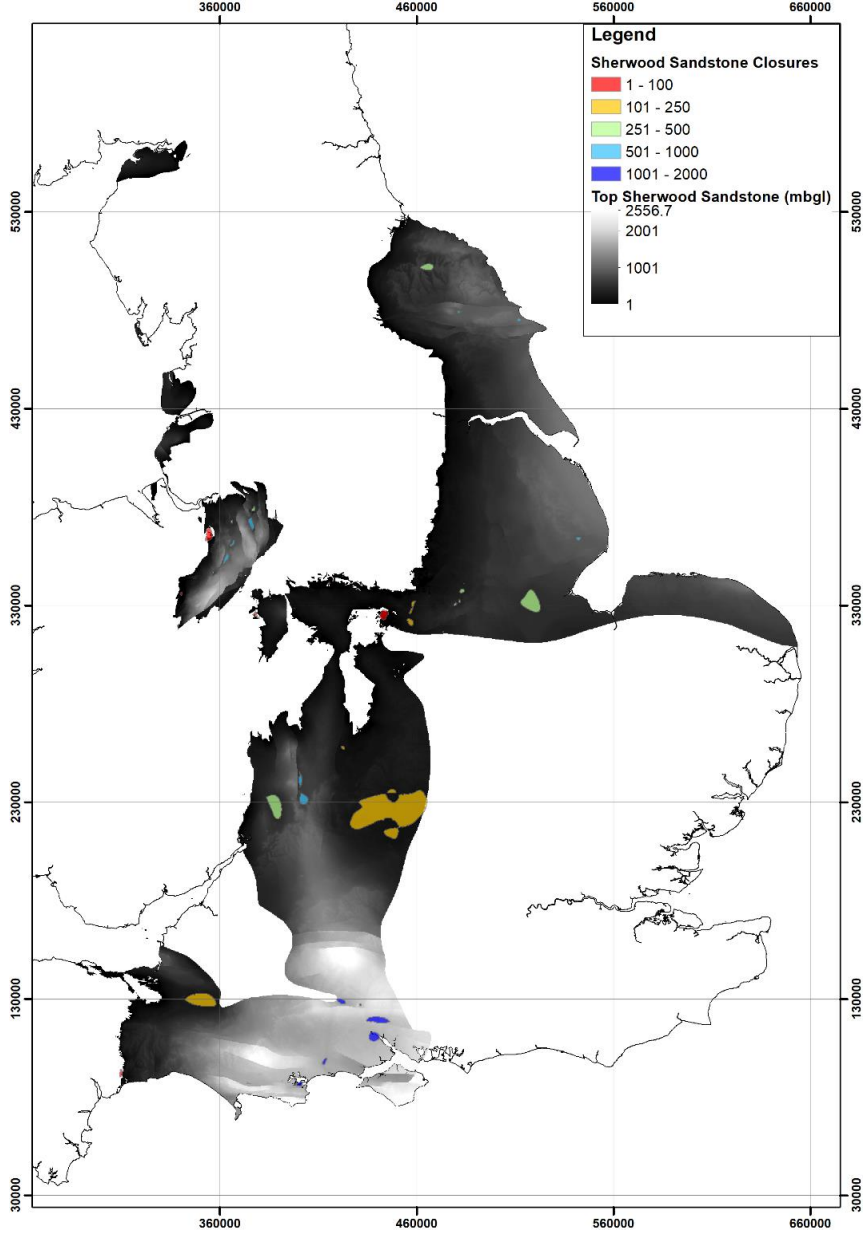


Figure 45: Analysis of closures within the Sherwood Sandstone, with closures categorised by depth from ground surface. *Contains Ordnance Survey data © Crown copyright and database right 2021*

⁴ [https://www.bgs.ac.uk/geology-projects/geothermal-energy/open-loop-gshp-screening-tool/#:~:text=The%20Open%2Dloop%20GSHp%20screening,e.g.%20location%20within%20protection%20zones\).](https://www.bgs.ac.uk/geology-projects/geothermal-energy/open-loop-gshp-screening-tool/#:~:text=The%20Open%2Dloop%20GSHp%20screening,e.g.%20location%20within%20protection%20zones).)

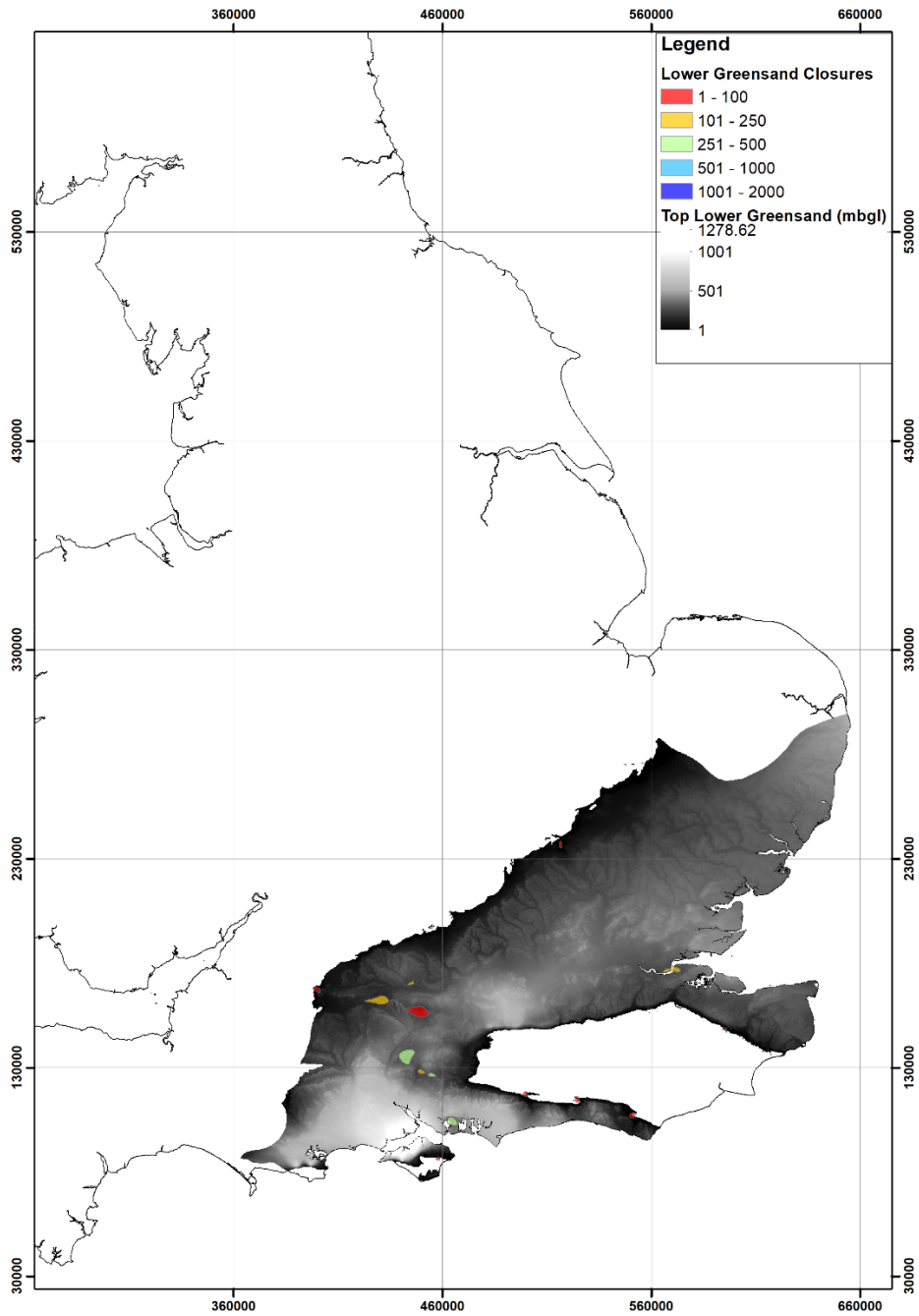


Figure 46 Analysis of closures within the Lower Greensand, with closures categorised by depth from ground surface. *Contains Ordnance Survey data © Crown copyright and database right 2021*

12 Discussion and conclusions

Hydrogen is a difficult gas to work with in laboratory settings, even more so at non-standard conditions of elevated temperatures and pressures. Major outcomes of this research are the confirmation that rock samples can be comprehensively characterised before and after successful exposure to a hydrogen-rich environment at elevated temperatures and pressures. Having an established laboratory method for these experiments allows for repeat experiments, experiments using alternative rock materials and to start designing experiments that consider multiple phases of pressure and/or temperature variations that may better represent the in-situ storage of hydrogen in porous rocks.

Overall, the characterisation of samples used in this study indicates that the changes observed in samples before and following exposure to the hydrogen-rich environment were minor, although there is the potential for different rock types to those analysed to be more reactive with hydrogen.

12.1 PETROGRAPHY- DISCUSSION

The samples of Sherwood Sandstone examined post exposure to hydrogen exhibited a minor loss of sand grains, a movement of finer-grained material and a detachment of areas of diagenetic grain-coating clays. The loss of sand grains and movement of fines is to be expected in experiments that involve movement of fluids. The loss of grain-coating clays is possibly due to a change in clay volume, or displacement of clays through degassing at the end of the experiment; either may be due to sample sensitivity, and a loosening of surface grains could be associated with a clay volume change.

The samples of Cretaceous Lower Greensand and Chalk examined post exposure to hydrogen exhibited a minor loss of grains, a movement of finer-grained material, a change in volume of clay patches, physical local alteration of pyrite and a slight dissolution of some coccoliths. Of these effects, the loss and movement of grains may be due to the experimental design (as with the Sherwood Sandstone). The range of clay minerals may explain the changes in clay volumes observed. The alteration of pyrite is notable as it is a potential result of hydrogen reaction in the rock samples.

The cement sample showed the precipitation of minor quantities of Portlandite. The reasons for this were not clear, but could be due to subtle differences in geochemistry between pre- and post batch experiment exposure of the sample to hydrogen at increased temperatures.

12.2 X-RAY DIFFRACTION- DISCUSSION

Whole-rock powder and <2 μm XRD analyses suggest that the pre-experimental samples are composed of a range of mineralogical assemblages. The Triassic red sandstone samples are quartz-rich with minor proportions of feldspar (plagioclase and K-feldspar), carbonates (calcite and dolomite), phyllosilicates/clay minerals and traces of hematite, pyrite, and halite. Clay mineral assemblages are dominated by approximately similar proportions of illite and smectite/chlorite (R0-ordered, 90%smectite, 10% chlorite interlayers) with trace amounts of discrete chlorite. Possible traces of palygorskite were also detected.

The pre-experimental Cretaceous green sandstones are more quartz-rich with minor quantities of phyllosilicates/clay minerals \pm zeolite and traces of K-feldspar and pyrite. Their clay mineral assemblages are solely or predominantly composed of illite/smectite (R1-ordered, 85% illite, 15% smectite interlayers) glauconite with traces of discrete smectite.

The pre-experimental Cretaceous grey sandstones show differing mineralogies; one is composed of quartz with subordinate calcite, opal-CT, phyllosilicates/clay minerals and traces of pyrite while the other is predominantly composed of calcite with minor proportions of quartz and traces of phyllosilicates/clay minerals. Clay mineral assemblages are composed of illite and smectite \pm minor amounts of chlorite.

Following H₂-interaction, the mineralogies of the post-experimental samples show little, if any, change from the pre-experimental analyses. The differences in concentrations detected are generally within the analytical error of the method. However, the post-experimental samples

show slightly higher quartz and lower phyllosilicate/clay mineral concentrations compared to the pre-experimental materials.

BET/N₂ physisorption measurements reveal a small but consistent reduction in specific surface area for the post-experimental samples compared to the pre-experimental samples.

The reduction in surface area, increase in quartz concentration and reduction in phyllosilicate/clay mineral concentrations are entirely consistent with a loss of fines (likely to be rich in phyllosilicates/clay minerals) due to spalling during the course of the experiment. Much of this fine-grained material would likely have remained in suspension in the experimental fluid and therefore was not retrieved and included in the post-experimental analysis.

12.3 POROSITY AND PERMEABILITY- DISCUSSION

The minor changes in measured porosity (0.6 – 2.85% change) and permeability (0.0 – 6.52 % change) before and after exposure to hydrogen are considered within the margin of experimental error and tolerances of the analytical technique for repeat measurements on the same sample. No firm conclusions can be drawn from the small changes in porosity and permeability observed.

12.4 X-RAY COMPUTERISED TOMOGRAPHY- DISCUSSION

Overall, no conclusive changes were observed in the XCT data regarding the reservoir samples involved in the experiment. Variations in the segmented component volume fractions are within the 5% error tolerance, so cannot be assumed as solely effects of the exposure of hydrogen on samples. Pore networks show no major modification post experiment for any sample. Some fines migrations can be captured in some samples (SSK138924, Hythe Formation). Therefore, the reservoir sandstones investigated in this experiment can be presumed inert to hydrogen exposure.

12.5 EXPERIMENTAL DESIGN AND GEOCHEMISTRY- DISCUSSION

A major outcome of this work is that the experimental design was successful in allowing rock samples to be exposed to a hydrogen-rich environment at elevated temperatures and pressures. Rock samples from prospective storage formations (principal aquifers from the UK) were characterised by multiple techniques both before and following the batch experiments, and for some, the same location of rock sample was repeat analysed (e.g., by SEM).

Overall, for samples of Sherwood Sandstone, Lower Greensand, Chalk and borehole cement, no evidence was found of significant chemical reactions that resulted in large changes in water chemistry. Some evidence of minor calcite dissolution was observed in some of the samples of Glauconitic Marl. Additionally, minor reaction of pyrite was observed in one of the samples of Chester Formation (SSK 138924; although this was not evident in the XRD analysis), leading to a reduction in iron in solution, although it is not possible to be unequivocal in linking this to the presence of hydrogen in the experiment. A slight smell identified following some of the experiments with Lower Greensand was detected but it has not been possible to identify the odorant.

Although major changes in geochemistry were not identified, there remains the potential for rocks of different compositions to show some degree of reaction where certain components (e.g., pyrite, organic matter, anhydrite) may be present at higher amounts.

12.6 MICROBIOLOGY RESPONSE- DISCUSSION

The number of microorganisms in the lithologies examined in these experiments, particularly of the targeted iron and sulphur reducing bacteria, was consistently low. The source of microorganisms in these experiments could be those from the rock that survive being exposed to atmosphere and desiccation for a variety of lengths of time between retrieval of sample from the subsurface and experimentation. Finally, as no precautions were deployed during rock coring, handling and preservation, subsampling or setting up of experiments, the possibility of contamination from the air or from the hands of those involved in each of those stages cannot be ruled out.

Analysis of the groundwater alone showed microbial abundance was low and reduced by the end of the equilibration phase with nitrogen. The expected increase in microbial activity in response to exposure to hydrogen was not seen in these experiments. The results from these experiments alone would suggest that exposure to hydrogen is detrimental to microorganisms, but the extent to which the factors discussed in Section 10 influenced this, and therefore relevance to the storage of hydrogen in porous media is difficult to ascertain.

To fully understand the potential for microbial activity to influence the storage of hydrogen in porous media additional experiments, the following lessons can be learnt from these experiments: The use of groundwater (ideally anoxic) with its microbial community is preferable to NaCl solutions; where possible fresh samples of groundwater (and if possible rock) should be used; and temperature of incubation should be close to the temperature that the microbial community has previously been exposed to.

12.7 NATIONAL-SCALE MAPPING EXERCISE- DISCUSSION

The national-scale mapping exercise identified natural closures in both the Sherwood Sandstone and Lower Greensand at a range of depths and of varying footprints. The analysis did not include an assessment of small-scale faulted structures. The exercise did indicate that there may be closures in these rock units that may be worth further characterisation in terms of nature of closure and character of overburden which are also relevant to understanding their potential for hydrogen storage. Several closures located in the English midlands and in the Wessex Basin may be of particular interest as they could potentially provide an alternative storage solution to cavern storage options, which may be located some distance from these areas, or at considerable depth.

Appendix 1 Images of core materials selected

SSK138919: UKGEOS Ground Investigation Borehole A101
(SJ47NE/141): Chester Formation (Sherwood Sandstone Group)
Channel fill 78.00 – 78.06 m



4



SSK138920: UKGEOS Ground Investigation Borehole A101
(SJ47NE/141): Chester Formation (Sherwood Sandstone Group)
Channel fill 81.70 – 81.80 m



SSK138921: UKGEOS Ground Investigation Borehole A101
(SJ47NE/141): Chester Formation (Sherwood Sandstone Group)
Channel top 89.97 – 90.07 m



SSK138922: UKGEOS Ground Investigation Borehole A101
(SJ47NE/141): Chester Formation (Sherwood Sandstone Group)
Channel fill 106.42 – 106.52 m



SSK138923: UKGEOS Ground Investigation Borehole A101
(SJ47NE/141): Chester Formation (Sherwood Sandstone Group)
Channel fill 117.73 – 117.83 m



SSK138924: A3 Hindhead 29R Borehole (SU83NE/17):
Hythe Formation (Lower Greensand Group) 47.01 – 47.11 m



9



SSK138925: A3 Hindhead 29R Borehole (SU83NE/17):
Hythe Formation (Lower Greensand Group) 51.55 – 51.65 m



SSK138926: Laporte 360 Borehole (TQ25SE-247): Sandgate Formation (Lower Greensand Group): 4 plugs taken between 33.9 and 34.3 m



SSK138927: Faircross Borehole (SU66SE/21): Glauconitic Marl Member, West Melbury Chalk Formation 320.3 – 320.4 m



Appendix 2 Sedimentary logs: Cretaceous borehole material

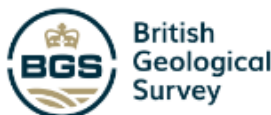
Appendix 1.1: Hindhead A3

SEDIMENTARY LOG: HINDHEAD SSK138924 and SSK138925

OS Grid Ref: 135842 489042
BGS ID: SU83NE/17

Litho-stratigraphy	Depth (mMDD)	Lithology & Grain-size <small>chalk sl vt f m c vc g p c</small>	Sedimentary Features	Porosity [%]:		Corrected perm [mD]:	Description
				Pre and post treatment [post in bold]	Pre and post treatment [post in bold]		
Hythe Formation, Lower Greensand Group	40m						
	41m		▨				40.9 - 41.14m: SDST: Beige-buff, with speckles of v dark green grains of glauconite; fine grained, sub-rounded, moderate to well-sorted. 41.14 - 41.22m: SDST: Pale
			▨				41.22 - 41.25m: SDST: pale beige grey, very friable to loose rubble; v fine to fine grained, moderately sorted, sub-angular to sub-rounded. Very friable to loose sand. Sporadic small flecks of glauconite
			▨				41.26 - 41.82m: SDST: pale ash grey to creamy buff beige; very fine to fine sandstone, some very faint parallel cross-bedding in places but otherwise massive. Homogenous. Blocky in core but extremely friable when handled. 2% sporadic flecks of v dark glauconite
	42m		▨				41.82 - 41.84m: SDST: pale ash grey to very pale brown and buff. Fine-grained, moderately sorted, sub-angular sandstone with very cluster of glauconite grains, very friable to loose running sand. 41.84 - 41.9m: Core loss
			▨				41.9 - 41.98m: SDST: Pale ash grey with greenish tinge; 2% scattered isolated glauconite grains no structure seen. Sub-angular to sub-rounded and well sorted. 41.98 - 42.2m: Core loss
			▨				42.2 - 42.54m: SDST: Pale buff and grey with greenish tinge very fine sandstone; well sorted and sub-rounded. 42.54 - 42.7m: Core loss
			▨				42.7 - 43m: SDST: Pale grey cream with greenish tinge. Very fine grained. Sub-rounded and well sorted.
	43m		▨				43 - 43.07m: SDST: Pale grey cream with greenish tinge. Very fine grained. Sub-rounded and very well sorted. 43.07 - 43.7m: SDST: Pale cream buff with greenish tinge; very fine to fine sandstone, 5% glauconite. Sub-rounded and very well sorted.
	44m		▨				43.7 - 44.1m: Core loss
			▨				44.1 - 45m: SDST: Pale buff with greenish tinge, very fine sandstone some glauconite bedding seen and glauconite pockets and isolated floating 5mm pebble clast. Sub-rounded and very well sorted.
	45m		▨				45 - 45.9m: SDST: Pale cream to buff, medium with 10% glauconite staining; glauconite concentrated in layers; very rubbly so structure etc impossible to see. Sub-angular and moderately sorted.
	46m		▨				45.9 - 45.95m: SDST: Pale cream to buff, medium grained with 5% glauconite grains. Sub-rounded and well sorted. 45.95 - 46m: Core loss
			▨				46 - 46.2m: SDST: Pale cream to buff, silty to fine sandstone with mm scale laminations. 46.2 - 46.54m: SDST: Pale cream to buff, silty to fine sandstone with mm scale laminations, very rubbly. Well rounded and well-sorted.
47m		▨				46.64 - 46.95m: SDST: Pale grey green medium grained, with highly speckled appearance (glauconite) showing faint tough cross-bedding. Well rounded and well-sorted. 46.95 - 47m: Core loss	
		▨				47 - 47.25m: SDST: Pale grey green, with highly speckled appearance (glauconite grains) showing faint tough cross-bedding. Well rounded and well-sorted. 47.25 - 47.5m: SDST: Pale cream and buff to very pale grey, fine	

LOGGED BY: Cath Cripps
IDRIC Project



Lithology:
 sandstone
 core loss

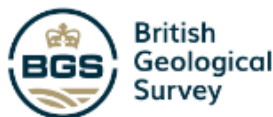
Sedimentary Features:
 isolated floating clasts
 parallel laminations
 planar cross bedding
 trough cross bedding

SEDIMENTARY LOG: HINDHEAD SSK138924 and SSK138925

OS Grid Ref: 135842 489942
BGS ID: SU83NE/17

Litho-stratigraphy	Depth (mMDD)	Lithology & Grain-size <small>chak sl vf f m c vc g p c</small>	Sedimentary Features	Porosity [%]:		Corrected perm [mD]:	Description
				Pre and post treatment [post in bold]	Pre and post treatment [post in bold]		
Hythe Formation, Lower Greensand Group	48m		 	33%	32.5%	1098mD 1025mD	<p>grained, small amount of glauconite, basically rubble, showing faint laminations. Well rounded and well-sorted.</p> <p>47.5 - 47.8m: SDST: Pale cream and buff to very pale grey, fine grained, small amount of glauconite, very friable, showing faint laminations. Well-rounded and well sorted.</p> <p>47.8 - 48m: SDST: Pale cream and buff to very pale grey, fine grained, small amount of glauconite, very friable, showing faint laminations. Well rounded and well-sorted.</p> <p>48 - 48.35m: SAND: Pale grey with green flecks loose running medium sand. Sub-rounded and well sorted.</p>
	49m						<p>48.35 - 49.07m: SDST: Pale grey green medium sandstone with speckled appearance of glauconite (dark green/black). Sub-rounded and well sorted.</p>
	50m						<p>49.07 - 50.85m: SDST: Pale cream and buff, fine sandstone with glauconite, very friable and lumpy; clay drapes/layers of finer material seen (but diff to see b/c of friable nature). Sub-rounded, moderately sorted.</p>
	51m						<p>50.85 - 52m: SDST: Pale grey with speckled green flecks; loose fine to med sand; running sand. Well sorted.</p>
	52m						<p>52 - 53.6m: SDST: Pale cream and buff, sub-angular, fine grained, blocky; well sorted.</p>
	53m						
	54m						

LOGGED BY: Cath Cripps
IDRIC Project



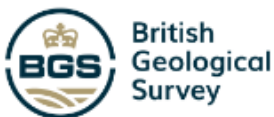
Lithology:
 sandstone
 core loss

Sedimentary Features:
 isolated floating clasts
 parallel laminations
 planar cross bedding
 trough cross bedding

Appendix 1.2: Laporte 360

SEDIMENTARY LOG: LAPORTE SSK138926					OS Grid Ref: 151120 529570 BGS ID: TQ25SE/247	
Litho-stratigraphy	Depth (mMMD)	Lithology & Grain-size <small>chalk sl sh f m c vc g p c</small>	Sedimentary Features	Porosity [%]: Pre and post treatment (post in bold)	Corrected perm (mD): Pre and post treatment (post in bold)	Description
Sandgate Formation, Lower Greensand Group	28.4m	sandy siltstone				28.2 - 28.6m: SANDY SILTSTONE. Medium to medium dark grey-green, massive, friable.
	28.8m					
	29.2m					
	29.6m					
	30m					
	30.4m					
	30.8m					
	31.2m					
	31.6m	sandstone	☪			28.6 - 34.67m: SANDSTONE, pale green-grey, massive, highly glauconitic (30-40%), highly fossiliferous/bioturbated [highly porous/permeable; sprayed water instantly disappears].
	32m					
32.4m						
32.8m						
33.2m						
33.6m						
34m						
34.4m				38.9%	38.4%	Result not available
34.8m						
35.2m	sandy siltstone					34.67 - 35.96m: SANDY SILTSTONE. Medium to medium dark grey-green, massive, friable
35.6m						
36m						
36.4m	sandstone	☪				35.96 - 36.4m: SANDSTONE, pale green-grey, massive, highly glauconitic (30-40%), highly fossiliferous/bioturbated

LOGGED BY: Cath Cripps
IDRIC Project



Lithology:

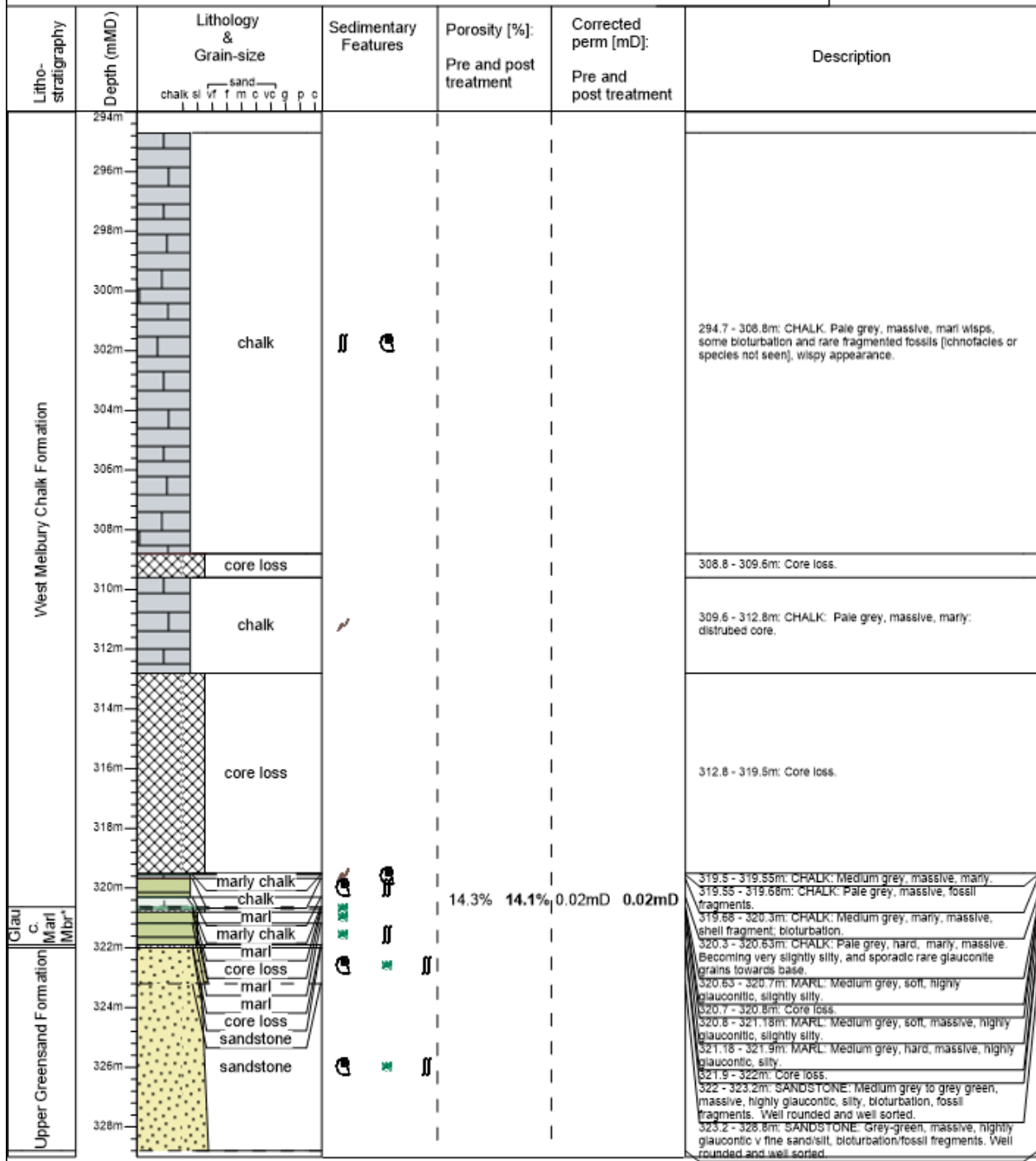
- sandy siltstone
- sandstone

Sedimentary Features:

- fossil
- moderate bioturbation

SEDIMENTARY LOG: FAIRCROSS SSK138927

OS Grid Ref: 163220 469720
BGS ID: SU66SE/21



LOGGED BY: Cath Cripps
IDRIC Project



- Lithology:**
- sandstone
 - marly chalk
 - core loss
 - marl
 - chalk
- *=Glauconitic Marl Member

- Sedimentary Features:**
- fossil
 - marl rich
 - moderate bioturbation
 - frequent glauconite grains
 - n

Appendix 3 Porosity and Permeability results

Table 10: Porosity data of 9 rock samples: pre-batch experiments

	IDRIC								
	26 November 2021								
Aq Props Number	IDRIC project number	Dry weight (g)	Sat.wt. (fluid) (g)	Sat.wt. (air) (g)	Fluid density (g/cm3)	DryBulk density (g/cm3)	SatBulk density (g/cm3)	Grain density (g/cm3)	Porosity (%)
1746/1H	SSK138919	48.414	33.98	52.803	0.790	2.032	2.265	2.650	23.3
1746/2H	SSK138920	42.009	29.418	45.67	0.790	2.042	2.267	2.636	22.5
1746/3H	SSK138921	37.17	26.31	39.135	0.790	2.290	2.443	2.704	15.3
1746/4H	SSK138922	41.101	28.84	44.567	0.790	2.065	2.285	2.648	22.0
1746/5H	SSK138923	47.009	32.964	50.825	0.790	2.079	2.293	2.644	21.4
1746/6H	SSK138924	40.155	28.173	45.027	0.790	1.882	2.171	2.648	28.9
1746/7H	SSK138925	30.057	21.064	34.478	0.790	1.770	2.100	2.640	33.0
1746/8H	SSK138926	12.176	8.351	14.609	0.790	1.537	1.926	2.515	38.9
1746/9H	SSK138927	48.075	34.007	50.428	0.790	2.313	2.456	2.700	14.3

Table 11: Permeability data of 9 rock samples: pre-batch experiments

Aquifer Props Lab Sample number	IDRIC project number	Length (mm)	Diameter (mm)	Pressure (mB)	Flow rate (ml/min)	Atmos. pressure (mB)	Gas viscos. (cP)	Gas perm. (mD)	Corrected perm. (mD)	Hydraulic conductivity (m/d)	Flowrate (cc/sec)	CSArea (mm ²)	Up Pressure (atm)	Down Pressure (atm)	Meter
1746/1	SSK138919	52.07	24.53	200	388	1020.7	0.0174	572.04	543.69	3.68E-01	6.467	472.59	1.205	1.007	AALBORG
1746/2	SSK138920	44.52	24.62	200	119	1020.7	0.0174	148.91	130.55	9.57E-02	1.983	476.06	1.205	1.007	AALBORG
1746/3	SSK138921	36	23.79	900	0.73	1020.7	0.0174	0.13	0.08	8.61E-05	0.012	444.51	1.896	1.007	AALBORG
1746/4	SSK138922	42.57	24.66	300	449.00	1020.7	0.0174	341.76	314.94	2.20E-01	7.483	477.61	1.303	1.007	AALBORG
1746/5	SSK138923	48.96	24.66	200	457.00	1020.7	0.0174	626.87	599.08	4.03E-01	7.617	477.61	1.205	1.007	AALBORG
1746/6	SSK138924	46.94	24.48	80	413.00	1020.7	0.0174	1455.83	1455.83	9.36E-01	6.883	470.67	1.086	1.007	AALBORG
1746/7	SSK138925	38.31	24.47	100	486.00	1020.7	0.0174	1109.01	1096.76	7.13E-01	8.100	470.28	1.106	1.007	AALBORG
1746/8	SSK138926														
1746/9	SSK138927	43.67	24.67	1000	0.17	1020.7	0.0174	0.03	0.02	1.97E-05	0.003	478.00	1.994	1.007	AALBORG

Table 12: Porosity data of 9 rock samples: post-batch experiments

	IDRIC								
	12 July 2022								
Aq Props	IDRIC project	Dry	Sat.wt.	Sat.wt.	Fluid	DryBulk	SatBulk	Grain	Porosity
Number	number	weight	(fluid)	(air)	density	density	density	density	
		(g)	(g)	(g)	(g/cm3)	(g/cm3)	(g/cm3)	(g/cm3)	(%)
1751/1H	SSK138919	48.309	34.074	52.478	0.790	2.074	2.300	2.681	22.7
1751/3H	SSK138921	37.1	26.382	39.053	0.790	2.313	2.467	2.735	15.4
1751/4H	SSK138922	41.058	28.965	44.39	0.790	2.103	2.319	2.682	21.6
1751/6H	SSK138924	40.108	28.267	44.842	0.790	1.912	2.197	2.676	28.6
1751/7H	SSK138925	29.657	20.893	33.877	0.790	1.804	2.129	2.673	32.5
1751/8H	SSK138926	12.186	8.391	14.553	0.790	1.562	1.946	2.537	38.4
1751/9H	SSK138927	48.024	34.126	50.3	0.790	2.346	2.486	2.730	14.1

Table 13: Permeability data of 9 rock samples: post-batch experiments

Aquifer Props Lab	IDRIC project	Leng th	Diame ter	Press ure	Flow	Atmo s.	Gas	Gas	Correc ted	Hydrauli c	Flowr ate	CSAr ea	Up	Down	Meter
Sample number	number	(mm)	(mm)	(mB)	rate (ml/m in)	press ure (mB)	visc os. (cP)	perm . (mD)	perm. (mD)	conducti vity (m/d)	(cc/se c)	(mm 2)	Press ure (atm)	Press ure (atm)	
1751/1	SSK138 919	51.96	24.6	200	364	1026.7	0.0178	545.01	516.49	3.50E-01	6.067	475.29	1.211	1.013	AALBO RG
1751/3	SSK138 921	36	23.84	900	0.77	1026.7	0.0178	0.14	0.08	9.27E-05	0.013	446.38	1.902	1.013	AALBO RG
1751/4	SSK138 922	42.7	24.62	300	418.00	1026.7	0.0178	327.78	301.30	2.11E-01	6.967	476.06	1.309	1.013	AALBO RG
1751/6	SSK138 924	46.96	24.46	200	1052.63	1026.7	0.0178	1440.76	1440.76	9.26E-01	17.544	469.90	1.211	1.013	HM1
1751/7	SSK138 925	38.14	24.37	100	444.00	1026.7	0.0178	1040.63	1025.21	6.69E-01	7.400	466.45	1.112	1.013	AALBO RG
1746/8	SSK138 926														
1751/9	SSK138 927	43.56	24.67	1000	0.16	1026.7	0.0178	0.03	0.02	1.90E-05	0.003	478.00	2.000	1.013	AALBO RG

Appendix 4 Changes in water chemistry, pre- and post experiment

Table 14: Starting solutions and nitrogen runs: geochemical changes

Sample code or lab run number		UKGEOS water	35 g/L NaCl	Cement water		HIL 59/1	HIL 60/1	HIL 73/1		HIL 61/1	HIL 62/1	HIL 63/1	HIL 64/1
Comments		Starting solution = UKGEOS water	Starting solution = 35 g/L NaCl sln	Starting solution - cement-equilibrated water (50°C)		N2 pressurised expt, UKGEOS water	N2 pressurised expt, UKGEOS water	N2 pressurised expt, UKGEOS water		N2 pressurised expt, 35 g/L NaCl sln			
Elapsed time (h)		0	0	0		1606	1628	1029		1566	1585	1588	1589
pH		7.74	7.58	13.5		7.95	8.22	8.26		7.47	7.19	7.95	8.14
Ca	mg l ⁻¹	38.4	3	47		33.10	34.00	29.10		36	41	158	78
Mg	mg l ⁻¹	19.1	<0.2	<0.2		15.05	17.42	14.36		4.4	5.8	4.5	11.2
Na	mg l ⁻¹	28.1	13007	6978		35.10	29.20	33.90		13083	13078	12981	12677
K	mg l ⁻¹	2.79	0.7	1064		7.26	6.73	5.08		7.6	9.5	25.7	16.9
Cl ⁻	mg l ⁻¹	52.5	22575	26.5		62.13	55.93	60.13		22003	22145	22065	21688
SO ₄ ²⁻	mg l ⁻¹	8.11	3.36	2341		11.86	11.20	9.34		<25	<25	51.5	49.1
NO ₃ ⁻	mg l ⁻¹	2.57	<0.3	3.56		3.98	3.60	2.24		<15	<15	<15	<15
Br ⁻	mg l ⁻¹	<0.1	2.52	0.235			0.13	<0.1		<5	<5	<5	<5
NO ₂ ⁻	mg l ⁻¹	<0.05	<0.05	<0.1		0.11	0.09	0.16		<2.5	<2.5	<2.5	<2.5
HPO ₄ ²⁻	mg l ⁻¹	0.101	<0.1	13.8		<0.1	0.26	<0.1		<5	<5	9.84	11.2
F ⁻	mg l ⁻¹	<0.05	<0.05	0.871		0.07	0.13	0.28		<2.5	<2.5	<2.5	<2.5
Fe ²⁺ (assumed = 0 at start)		0	0	0		0.00	0.00	0.00		0	0	0	0
Sample code or lab run number		UKGEOS water	35 g/L NaCl	Cement water		HIL 59/1	HIL 60/1	HIL 73/1		HIL 61/1	HIL 62/1	HIL 63/1	HIL 64/1
Comments		Starting solution = UKGEOS water	Starting solution = 35 g/L NaCl sln	Starting solution - cement-equilibrated water (50°C)		N2 pressurised expt, UKGEOS water	N2 pressurised expt, UKGEOS water	N2 pressurised expt, UKGEOS water		N2 pressurised expt, 35 g/L NaCl sln			
Total P	mg l ⁻¹	0.037	<0.07	<0.07		0.03	0.08	0.05		<0.07	<0.07	0.08	<0.07
Total S	mg l ⁻¹	3.3	1.4	634		4.60	4.60	3.80		2.0	2.4	27.3	27.5
Si	mg l ⁻¹	5.71	0.18	7.10		12.22	10.58	9.74		9.64	9.02	29.0	4.01
SiO ₂	mg l ⁻¹	12.2	0.385	15.2		26.14	22.63	20.84		20.6	19.3	62.0	8.58
Ba	µg l ⁻¹	3.3	<2	225		794.00	4.40	372.70		782	1631	5769	775
Sr	µg l ⁻¹	92.5	28	2704		77.20	214.10	70.90		155	278	1443	4009
Mn	µg l ⁻¹	1.3	1.1	<0.6		38.70	26.70	13.50		1010	1150	39.6	6.3
Fe	µg l ⁻¹	1.2	49	<5		1.80	2.40	0.60		52	63	53	6
Li	µg l ⁻¹	15	<37	1644		18.00	16.00	18.00		<37	<37	<37	<37
Be	µg l ⁻¹	<0.08	<0.1	<0.1		<0.08	<0.08	<0.08		1.5	<0.1	<0.1	<0.1
B	µg l ⁻¹	<53	<502	764		180.00	<53	58.00		<502	<502	<502	<502
Al	µg l ⁻¹	6	<12	3458		2.00	19.00	2.00		13	<12	<12	<12
Ti	µg l ⁻¹	<0.2	<2	3		<0.2	<0.2	<0.2		<2	<2	<2	<2
V	µg l ⁻¹	0.20	<0.7	1.1		3.66	3.74	1.61		<0.7	0.9	16.9	4.1
Cr	µg l ⁻¹	0.66	0.8	1839		2.42	2.91	9.03		0.9	1.5	1.1	1.4

Co	µg l ⁻¹	0.028	0.05	0.24	0.47	0.14	0.20	20.2	65.6	0.58	0.28
Ni	µg l ⁻¹	0.27	<0.2	1.1	2.31	1.94	1.43	202	342	8.7	3.0
Cu	µg l ⁻¹	5.7	5	26	2.10	9.80	4.30	7	34	15	7
Zn	µg l ⁻¹	25.3	17	100	27.20	12.10	30.10	92	323	121	95
Ga	µg l ⁻¹	<0.3	<3	17	<0.3	<0.3	<0.3	<3	<3	<3	<3
As	µg l ⁻¹	1.1	<2	6	3.10	8.10	2.40	<2	<2	65	8
Se	µg l ⁻¹	0.33	<0.09	12.0	0.41	0.43	0.43	<0.09	0.10	5.77	2.89
Rb	µg l ⁻¹	2.31	<0.8	2908	3.88	5.59	3.22	33.9	36.9	91.0	44.7
Y	µg l ⁻¹	<0.006	<0.03	<0.03	0.04	0.01	0.01	44.0	0.13	0.03	<0.03
Sample code or lab run number		UKGEOS water	35 g/L NaCl	Cement water	HIL 59/1	HIL 60/1	HIL 73/1	HIL 61/1	HIL 62/1	HIL 63/1	HIL 64/1
Comments		Starting solution = UKGEOS water	Starting solution = 35 g/L NaCl sln	Starting solution - cement-equilibrated water (50°C)	N2 pressurised expt, UKGEOS water	N2 pressurised expt, UKGEOS water	N2 pressurised expt, UKGEOS water	N2 pressurised expt, 35 g/L NaCl sln			
Zr	µg l ⁻¹	<0.009	<0.07	<0.07	0.01	<0.009	<0.009	<0.07	<0.07	<0.07	<0.07
Nb	µg l ⁻¹	<0.01	<0.04	<0.04	0.01	<0.01	<0.01	<0.04	<0.04	<0.04	<0.04
Mo	µg l ⁻¹	0.7	<0.4	4650	7.50	8.90	6.20	2.5	2.6	20.2	5.5
Ag	µg l ⁻¹	<0.04	<0.2	<0.2	<0.04	<0.04	<0.04	1.1	0.5	0.2	0.3
Cd	µg l ⁻¹	<0.007	0.16	0.55	0.10	0.01	<0.007	0.46	0.56	0.37	<0.08
Sn	µg l ⁻¹	<0.08	0.16	0.33	0.09	0.10	<0.08	<0.09	<0.09	<0.09	<0.09
Sb	µg l ⁻¹	<0.04	<0.4	1.8	0.59	0.39	0.23	<0.4	<0.4	1.2	0.6
Cs	µg l ⁻¹	0.07	<0.3	312	<0.3	<0.3	<0.3	<0.3	0.5	1.0	0.5
La	µg l ⁻¹	<0.01	<0.2	<0.2	<0.01	<0.01	<0.01	54.3	5.1	<0.2	<0.2
Ce	µg l ⁻¹	0.007	<0.05	<0.05	0.02	0.01	0.01	25.0	0.24	<0.05	<0.05
Pr	µg l ⁻¹	0.008	<0.05	<0.05	0.01	<0.004	0.00	11.1	0.06	<0.05	<0.05
Nd	µg l ⁻¹	<0.005	<0.06	<0.06	0.02	0.01	0.01	46.8	0.10	<0.06	<0.06
Sm	µg l ⁻¹	0.008	0.05	<0.03	0.01	<0.005	<0.005	7.91	0.05	<0.03	0.03
Eu	µg l ⁻¹	0.008	<0.04	<0.04	0.01	<0.003	0.00	1.53	<0.04	<0.04	<0.04
Gd	µg l ⁻¹	<0.005	<0.05	<0.05	0.01	0.01	<0.005	9.72	<0.05	<0.05	<0.05
Tb	µg l ⁻¹	0.007	<0.04	<0.04	0.01	<0.004	0.00	1.10	<0.04	<0.04	<0.04
Dy	µg l ⁻¹	0.006	<0.02	<0.02	0.01	0.01	0.01	5.69	<0.02	0.03	<0.02
Ho	µg l ⁻¹	0.005	<0.05	<0.05	0.01	<0.005	<0.005	1.20	<0.05	<0.05	<0.05
Er	µg l ⁻¹	0.004	<0.04	<0.04	0.01	<0.004	<0.004	2.79	<0.04	<0.04	<0.04
Tm	µg l ⁻¹	<0.005	<0.06	<0.06	0.01	<0.005	<0.005	0.27	<0.06	<0.06	<0.06
Yb	µg l ⁻¹	0.007	<0.04	<0.04	0.01	<0.004	<0.004	1.35	<0.04	<0.04	<0.04
Lu	µg l ⁻¹	0.006	<0.06	<0.06	0.01	<0.006	<0.006	0.28	<0.06	<0.06	<0.06
Hf	µg l ⁻¹	<0.008	<0.09	<0.09	<0.008	<0.008	<0.008	<0.09	<0.09	<0.09	<0.09
Ta	µg l ⁻¹	<0.006	<0.06	<0.06	0.01	<0.006	<0.006	<0.06	<0.06	<0.06	<0.06
Sample code or lab run number		UKGEOS water	35 g/L NaCl	Cement water	HIL 59/1	HIL 60/1	HIL 73/1	HIL 61/1	HIL 62/1	HIL 63/1	HIL 64/1
Comments		Starting solution = UKGEOS water	Starting solution = 35 g/L NaCl sln	Starting solution - cement-equilibrated water (50°C)	N2 pressurised expt, UKGEOS water	N2 pressurised expt, UKGEOS water	N2 pressurised expt, UKGEOS water	N2 pressurised expt, 35 g/L NaCl sln			
W	µg l ⁻¹	0.08	0.06	0.29	3.25	1.60	1.08	<0.06	0.09	34.9	5.71
Tl	µg l ⁻¹	<0.02	<0.07	<0.07	0.02	0.02	<0.02	0.09	0.16	0.23	0.22
Pb	µg l ⁻¹	0.98	<0.4	46.5	0.06	0.10	<0.04	2.9	<0.4	<0.4	<0.4
Bi	µg l ⁻¹	<0.08	<0.2	<0.2	<0.08	<0.08	<0.08	<0.2	<0.2	<0.2	<0.2
Th	µg l ⁻¹	<0.03	<0.05	<0.05	<0.03	<0.03	<0.03	<0.05	<0.05	<0.05	<0.05
U	µg l ⁻¹	2.45	<0.03	0.10	3.03	2.65	1.00	<0.03	<0.03	0.24	0.69

Table 15: Nitrogen equilibrium test: geochemical changes

Sample code or lab run number		UKGEOS water		HIL 73/1	HIL 73/2	HIL 73/3	HIL 73/4
Comments		Starting solution = UKGEOS water		N2 pressurised expt, UKGEOS water			
Elapsed time (h)		0		1029	1562	2016	2713
pH		7.74		8.26	8.66	7.90	8.62
Ca	mg l ⁻¹	38.4		29.1	26.2	25.0	22.4
Mg	mg l ⁻¹	19.1		14.4	12.0	10.9	9.20
Na	mg l ⁻¹	28.1		33.9	35.4	34.3	35.4
K	mg l ⁻¹	2.79		5.08	5.66	6.21	6.43
Cl ⁻	mg l ⁻¹	52.5		60.1	63.5	60.4	61.6
SO ₄ ²⁻	mg l ⁻¹	8.11		9.34	9.87	9.77	9.63
NO ₃ ⁻	mg l ⁻¹	2.57		2.24	3.88	3.33	3.38
Br	mg l ⁻¹	<0.1		<0.1	<0.1	0.126	0.120
NO ₂ ⁻	mg l ⁻¹	<0.05		0.164	0.149	0.157	0.190
HPO ₄ ²⁻	mg l ⁻¹	0.101		<0.1	0.210	<0.1	<0.1
F ⁻	mg l ⁻¹	<0.05		0.281	0.288	0.266	0.249
Alkalinity as CaCO ₃ (mg/L)		164.1		136.1	120.1	104.1	100.1
Fe ²⁺ (assumed = 0 at start)		0		0	0.000	0.100	0.050
Total P	mg l ⁻¹	0.037		0.049	0.044	0.036	0.034
Total S	mg l ⁻¹	3.3		3.8	3.9	3.8	3.9
Si	mg l ⁻¹	5.71		9.74	10.4	10.2	11.2
SiO ₂	mg l ⁻¹	12.2		20.8	22.2	21.9	23.9
Ba	µg l ⁻¹	3.3		373	886	477	486
Sr	µg l ⁻¹	92.5		70.9	71.1	63.3	60.9
Mn	µg l ⁻¹	1.3		13.5	17.7	21.9	25.3
Fe	µg l ⁻¹	1.2		0.6	0.8	1.2	1.5
Li	µg l ⁻¹	15		18	17	17	18
Be	µg l ⁻¹	<0.08		<0.08	<0.08	<0.08	<0.08
B	µg l ⁻¹	<53		58	122	53	134
Al	µg l ⁻¹	6		2	3	3	8
Ti	µg l ⁻¹	<0.2		<0.2	<0.2	<0.2	<0.2
V	µg l ⁻¹	0.20		1.61	2.16	1.99	2.04
Cr	µg l ⁻¹	0.66		9.03	7.62	7.32	6.26
Co	µg l ⁻¹	0.028		0.196	0.295	0.287	0.333
Ni	µg l ⁻¹	0.27		1.43	1.32	1.40	1.19
Cu	µg l ⁻¹	5.7		4.3	4.6	5.3	4.7
Zn	µg l ⁻¹	25.3		30.1	25.1	28.7	24.4
Ga	µg l ⁻¹	<0.3		<0.3	<0.3	<0.3	<0.3
As	µg l ⁻¹	1.1		2.4	2.6	2.4	2.4
Se	µg l ⁻¹	0.33		0.43	0.42	0.45	0.47

Sample code or lab run number		UKGEOS water		HIL 73/1	HIL 73/2	HIL 73/3	HIL 73/4
Comments		Starting solution = UKGEOS water		N2 pressurised expt, UKGEOS water			
Rb	µg l ⁻¹	2.31		3.22	4.03	3.86	4.07
Y	µg l ⁻¹	<0.006		0.011	0.015	0.019	0.014
Zr	µg l ⁻¹	<0.009		<0.009	<0.009	0.027	0.031
Nb	µg l ⁻¹	<0.01		<0.01	<0.01	<0.01	<0.01
Mo	µg l ⁻¹	0.7		6.2	6.5	7.9	8.4
Ag	µg l ⁻¹	<0.04		<0.04	<0.04	<0.04	<0.04
Cd	µg l ⁻¹	<0.007		<0.007	<0.007	<0.007	0.010
Sn	µg l ⁻¹	<0.08		<0.08	1.01	0.64	0.36
Sb	µg l ⁻¹	<0.04		0.23	0.27	0.25	0.27
Cs	µg l ⁻¹	0.07		<0.3	<0.3	<0.3	<0.3
La	µg l ⁻¹	<0.01		<0.01	<0.01	<0.01	<0.01
Ce	µg l ⁻¹	0.007		0.012	0.012	0.010	0.006
Pr	µg l ⁻¹	0.008		0.004	0.004	<0.004	<0.004
Nd	µg l ⁻¹	<0.005		0.006	<0.005	0.009	<0.005
Sm	µg l ⁻¹	0.008		<0.005	<0.005	<0.005	0.011
Eu	µg l ⁻¹	0.008		0.004	<0.003	<0.003	<0.003
Gd	µg l ⁻¹	<0.005		<0.005	0.005	<0.005	<0.005
Tb	µg l ⁻¹	0.007		0.004	<0.004	<0.004	<0.004
Dy	µg l ⁻¹	0.006		0.005	<0.003	0.004	<0.003
Ho	µg l ⁻¹	0.005		<0.005	<0.005	<0.005	<0.005
Er	µg l ⁻¹	0.004		<0.004	<0.004	<0.004	<0.004
Tm	µg l ⁻¹	<0.005		<0.005	<0.005	<0.005	<0.005
Yb	µg l ⁻¹	0.007		<0.004	<0.004	<0.004	<0.004
Lu	µg l ⁻¹	0.006		<0.006	<0.006	<0.006	<0.006
Hf	µg l ⁻¹	<0.008		<0.008	<0.008	<0.008	<0.008
Ta	µg l ⁻¹	<0.006		<0.006	<0.006	<0.006	<0.006
W	µg l ⁻¹	0.08		1.08	1.21	1.11	1.08
Tl	µg l ⁻¹	<0.02		<0.02	<0.02	<0.02	<0.02
Pb	µg l ⁻¹	0.98		<0.04	<0.04	<0.04	<0.04
Bi	µg l ⁻¹	<0.08		<0.08	<0.08	<0.08	<0.08
Th	µg l ⁻¹	<0.03		<0.03	<0.03	<0.03	<0.03
U	µg l ⁻¹	2.45		1.00	0.594	0.430	0.281

Table 16 : Final hydrogen runs: geochemical changes

Sample code or lab run number			HIL 66/1	HIL 67/1	HIL 68/1	HIL 69/1	HIL 70/1	HIL 71/1	HIL 72/1	HIL 74/1
Comments			H2 pressurised expt, UKGEOS water	H2 pressurised expt, UKGEOS water	H2 pressurised expt, 35 g/L NaCl sln	H2 pressurised expt, Cement Water	H2 pressurised expt, UKGEOS water			
Elapsed time (h)			2516	2518	2496	2498	2495	2349	2441	1373
pH			8.39	8.23	4.67	4.39	7.28	7.40	13.4	8.29
Ca	mg l ⁻¹		30.8	31.5	386	316	610	324	58	30.5
Mg	mg l ⁻¹		13.3	15.9	47.3	44.9	20.1	84.9	<0.2	12.5
Na	mg l ⁻¹		36.6	37.9	13662	12928	12590	12197	7496	42.1
K	mg l ⁻¹		13.2	12.9	41.6	39.9	63.2	54.1	1402	12.1
Cl ⁻	mg l ⁻¹		64.9	71.2	23405	23324	22736	22357	43.9	76.1
SO ₄ ²⁻	mg l ⁻¹		12.7	20.5	<25	<25	118	249	2615	19.0
NO ₃ ⁻	mg l ⁻¹		<0.3	4.14	<15	<15	<15	<15	2.19	<0.3
Cat1	meq l ⁻¹		4.56	4.86	619	583	581	555	365	4.69
Cat2	meq l ⁻¹		0.016	0.018	0.143	0.175	0.353	0.853	0.419	0.015
Ani1	meq l ⁻¹		2.10	2.50	660	658	644	636	55.7	2.54
Ani2	meq l ⁻¹		0.032	0.044	0.000	0.000	0.000	0.000	0.343	0.030
Meas. Cations	meq l ⁻¹		4.57	4.87	619	583	582	556	365	4.70

Sample code or lab run number			HIL 66/1	HIL 67/1	HIL 68/1	HIL 69/1	HIL 70/1	HIL 71/1	HIL 72/1	HIL 74/1
Comments			H2 pressurised expt, UKGEOS water	H2 pressurised expt, UKGEOS water	H2 pressurised expt, 35 g/L NaCl sln	H2 pressurised expt, Cement Water	H2 pressurised expt, UKGEOS water			
Meas. Anions	meq l ⁻¹		2.13	2.55	660	658	644	636	56.1	2.57
Br ⁻	mg l ⁻¹		0.610	0.264	<5	<5	<5	<5	0.214	0.248
NO ₂ ⁻	mg l ⁻¹		0.136	0.223	<2.5	<2.5	<2.5	<2.5	0.135	0.105
HPO ₄ ²⁻	mg l ⁻¹		0.599	1.21	<5	<5	<5	<5	14.3	0.446
F ⁻	mg l ⁻¹		0.163	0.196	<2.5	<2.5	<2.5	<2.5	0.760	0.282
Alkalinity as CaCO ₃ (mg/L)			136.1	140.1	8.00	16.0	132.1	168.1	15633.7	124.1
Fe ²⁺ (assumed = 0 at start)			0.000	0.000	0.160	0.530	3.51	1.43	0.000	0.000
Total P	mg l ⁻¹		0.040	0.172	0.08	<0.07	<0.07	<0.07	<0.07	0.088
Total S	mg l ⁻¹		5.7	8.6	8.9	6.5	49.6	91.3	783	7.5
Si	mg l ⁻¹		19.4	20.8	22.1	20.5	32.3	15.7	3.35	21.8
SiO ₂	mg l ⁻¹		41.4	44.5	47.2	43.8	69.2	33.5	7.17	46.6
Ba	µg l ⁻¹		768	843	6544	7451	4489	807	510	673
Sr	µg l ⁻¹		55.7	94.0	1338	1929	5173	33305	3650	62.7
Mn	µg l ⁻¹		63.0	297	13345	6236	288	37.5	<0.6	136
Fe	µg l ⁻¹		2.7	1.8	319	423	3165	1305	<5	2.0
Li	µg l ⁻¹		22	23	<37	<37	<37	74	2276	27
Be	µg l ⁻¹		<0.08	<0.08	8.5	12.8	<0.1	<0.1	<0.1	<0.08
B	µg l ⁻¹		183	166	<502	<502	<502	564	773	203
Al	µg l ⁻¹		3	3	70	226	<12	<12	2153	3

Sample code or lab run number			HIL 66/1	HIL 67/1	HIL 68/1	HIL 69/1	HIL 70/1	HIL 71/1	HIL 72/1	HIL 74/1
Comments			H2 pressurised expt, UKGEOS water	H2 pressurised expt, UKGEOS water	H2 pressurised expt, 35 g/L NaCl sln	H2 pressurised expt, Cement Water	H2 pressurised expt, UKGEOS water			
Ti	µg l ⁻¹		<0.2	<0.2	<2	<2	<2	<2	3	0.2
V	µg l ⁻¹		0.83	0.46	<0.7	<0.7	<0.7	<0.7	<0.7	0.50
Cr	µg l ⁻¹		0.53	0.56	2.3	10.2	0.8	1.0	1526	0.59
Co	µg l ⁻¹		0.309	0.627	475	299	0.80	0.41	1.14	0.583
Ni	µg l ⁻¹		2.94	5.88	711	1098	2.4	1.2	12.5	3.22
Cu	µg l ⁻¹		0.2	0.3	4	<3	<3	<3	80	0.3
Zn	µg l ⁻¹		52.9	47.0	1392	1176	260	218	629	46.0
Ga	µg l ⁻¹		<0.3	<0.3	4	4	<3	<3	17	<0.3
As	µg l ⁻¹		3.1	5.7	<2	<2	2	<2	5	2.6
Se	µg l ⁻¹		0.47	0.47	0.63	0.53	6.42	7.86	15.4	0.43
Rb	µg l ⁻¹		6.36	3.95	139	135	150	47.6	3757	4.17
Y	µg l ⁻¹		0.022	0.018	381	407	0.04	0.06	<0.03	0.018
Zr	µg l ⁻¹		0.044	0.044	<0.07	<0.07	<0.07	<0.07	<0.07	0.048
Nb	µg l ⁻¹		<0.01	<0.01	<0.04	<0.04	<0.04	<0.04	<0.04	<0.01
Mo	µg l ⁻¹		10.5	16.7	1.5	0.7	<0.4	1.6	5328	13.8
Ag	µg l ⁻¹		<0.04	<0.04	<0.2	<0.2	<0.2	<0.2	<0.2	<0.04
Cd	µg l ⁻¹		<0.007	0.009	5.21	5.20	<0.08	<0.08	0.75	0.010
Sn	µg l ⁻¹		0.11	0.24	<0.09	<0.09	<0.09	<0.09	0.30	0.46
Sb	µg l ⁻¹		0.59	0.50	<0.4	<0.4	<0.4	0.6	0.9	0.45
Cs	µg l ⁻¹		<0.3	<0.3	1.3	1.2	0.4	<0.3	410	<0.3
La	µg l ⁻¹		<0.01	<0.01	395	533	<0.2	<0.2	<0.2	<0.01

Sample code or lab run number			HIL 66/1	HIL 67/1	HIL 68/1	HIL 69/1	HIL 70/1	HIL 71/1	HIL 72/1	HIL 74/1
Comments			H2 pressurised expt, UKGEOS water	H2 pressurised expt, UKGEOS water	H2 pressurised expt, 35 g/L NaCl sln	H2 pressurised expt, Cement Water	H2 pressurised expt, UKGEOS water			
Ce	µg l ⁻¹		0.012	0.015	206	189	<0.05	<0.05	<0.05	0.016
Pr	µg l ⁻¹		0.004	0.005	86.1	105	<0.05	<0.05	<0.05	0.005
Nd	µg l ⁻¹		<0.005	0.014	377	450	0.06	<0.06	<0.06	0.026
Sm	µg l ⁻¹		0.009	0.007	66.8	78.2	<0.03	<0.03	<0.03	<0.005
Eu	µg l ⁻¹		0.003	<0.003	14.3	17.0	<0.04	<0.04	<0.04	<0.003
Gd	µg l ⁻¹		<0.005	0.005	82.3	92.8	<0.05	<0.05	<0.05	<0.005
Tb	µg l ⁻¹		<0.004	<0.004	8.93	10.2	<0.04	<0.04	<0.04	<0.004
Dy	µg l ⁻¹		0.003	<0.003	53.5	62.3	<0.02	<0.02	0.02	<0.003
Ho	µg l ⁻¹		<0.005	<0.005	10.9	12.5	<0.05	<0.05	<0.05	<0.005
Er	µg l ⁻¹		<0.004	<0.004	25.3	28.2	<0.04	<0.04	<0.04	<0.004
Tm	µg l ⁻¹		<0.005	<0.005	2.57	3.08	<0.06	<0.06	<0.06	<0.005
Yb	µg l ⁻¹		<0.004	<0.004	14.2	17.8	<0.04	<0.04	<0.04	0.004
Lu	µg l ⁻¹		<0.006	<0.006	2.25	3.06	<0.06	<0.06	<0.06	<0.006
Hf	µg l ⁻¹		<0.008	<0.008	<0.09	<0.09	<0.09	<0.09	<0.09	<0.008
Ta	µg l ⁻¹		<0.006	<0.006	<0.06	<0.06	<0.06	<0.06	<0.06	<0.006
W	µg l ⁻¹		1.15	1.03	0.12	<0.06	128	4.29	0.17	1.28
Tl	µg l ⁻¹		<0.02	<0.02	0.76	0.76	<0.07	<0.07	<0.07	<0.02
Pb	µg l ⁻¹		<0.04	0.05	18.5	39.7	<0.4	<0.4	84.6	<0.04
Bi	µg l ⁻¹		<0.08	<0.08	<0.2	<0.2	<0.2	<0.2	<0.2	<0.08
Th	µg l ⁻¹		<0.03	<0.03	<0.05	<0.05	<0.05	<0.05	<0.05	<0.03
U	µg l ⁻¹		0.482	0.264	<0.03	0.05	<0.03	<0.03	0.11	0.293

Appendix 5 Microbiological growth media

Postgate's medium B (for sulphate reducing bacteria): KH_2PO_4 0.5 g L⁻¹, CaSO_4 1.0 g L⁻¹, NH_4Cl 1.0 g L⁻¹, $\text{MgSO}_4 \cdot 7\text{H}_2\text{O}$ 2.0 g L⁻¹, Yeast extract 1.0 g L⁻¹, $\text{FeSO}_4 \cdot 7\text{H}_2\text{O}$ 0.5 g L⁻¹, 60 % sodium lactate solution 3.5 ml L⁻¹, sodium thioglycolate 0.1 ml L⁻¹ and 0.5 ml L⁻¹ 0.2 µm filter sterile 20 % ascorbic acid solution added after autoclaving. Media prepared using tap water

IRB#8 medium (for iron reducing bacteria): NaHCO_3 2.5 g L⁻¹, NH_4Cl 1.5 g L⁻¹, NaH_2PO_4 0.6 g L⁻¹, $\text{CaCl}_2 \cdot 2\text{H}_2\text{O}$ 0.1 g L⁻¹, KCl 0.1 g L⁻¹, $\text{MgCl}_2 \cdot 6\text{H}_2\text{O}$ 0.1 g L⁻¹, Ferric EDTA sodium salt hydrate 1.84 g L⁻¹, Peptone 1.5 g L⁻¹ and 1 ml L⁻¹ TE solution containing 5.0 g L⁻¹ $\text{MnCl}_2 \cdot 4\text{H}_2\text{O}$ and 1.0 g L⁻¹ $\text{NaMoO}_4 \cdot 2\text{H}_2\text{O}$. Media prepared using deionised water

5% PTYG medium (for heterotrophic bacteria): Peptone 0.25 g L⁻¹, Tryptone 0.25 g L⁻¹, yeast extract 0.25 g L⁻¹, $\text{MgSO}_4 \cdot 7\text{H}_2\text{O}$ 0.03 g L⁻¹, $\text{CaCl}_2 \cdot 2\text{H}_2\text{O}$ 0.004 g L⁻¹, agar 15 g L⁻¹ and 2.5 ml L⁻¹ 0.2 µm filter sterile 20 % glucose solution added after autoclaving. Media prepared using deionised water

References

British Geological Survey holds most of the references listed below, and copies may be obtained via the library service subject to copyright legislation (contact libuser@bgs.ac.uk for details). The library catalogue is available at: <https://of-ukrinerc.olib.oclc.org/folio/>.

Abesser, C & Lewis, M. 2015. A semi-quantitative technique for mapping potential aquifer productivity on the national scale: example of England and Wales (UK). *Hydrogeology Journal*, 23(8), pp.1677-1694.

Aftab, A, Hassanpouryouzband, A, Xie, Q, Machuca, LL & Sarmadivaleh, M. 2022. Toward a Fundamental Understanding of Geological Hydrogen Storage. *Ind. Eng. Chem. Res.* 2022, 61, 9, 3233–3253.

Bateman, K, Rochelle, CA, Purser, G, Kemp, SJ & Wagner, D. 2013. Geochemical interactions between CO₂ and minerals within the Utsira caprock: A 5-year experimental study. *Energy Procedia*, 37, 5307-5314, 10.1016/j.egypro.2013.06.448

Bloomfield, JP & Williams, AT. 1995. An empirical liquid permeability-gas permeability correlation for use in aquifer properties studies. *Quarterly Journal of Engineering Geology*, 28, S143-S150.

Bloomfield, JP, Brewerton, LJ & Allen, DJ. 1995. Regional trends in matrix porosity and dry density of the Chalk of England. *Quarterly Journal of Engineering Geology*, 28, S131-S142.

Bruaner, S, Emmet, PH & Teller, E. 1938. Adsorption of Gases in Multimolecular Layers. *Journal of the American Chemical Society*, 60, 309–319.

Cornish, EA, & RA Fisher. 1938. Moments and cumulants in the specification of distributions. *Revue de l'Institut international de Statistique*, 307-320.

Evans, DJ & West, JM. 2008. An appraisal of underground gas storage technologies and incidents, for the development of risk assessment methodology. Health and Safety Executive Research Report RR605.

Guidotti TL. 2010. Hydrogen Sulfide: Advances in Understanding Human Toxicity. *International Journal of Toxicology*, 29(6) 569-581. DOI:10.1177/1091581810384882

Hallsworth, CR, and Knox, RWO'B. 1999. BGS Rock Classification Scheme Volume 3 Classification of sediments and sedimentary rocks. British Geological Survey Research Report, RR 99–03.

Heinemann, N. et al., 2021. Enabling large-scale hydrogen storage in porous media - the scientific challenges. *Energy & Environmental Science*, Issue 14, pp. 853-864.

Hetherington, D, Damaschke, M, Thompson, J, Hough, E, Kingdon, A, Spence, M, Cripps, C, Elsome, J, Burgess, D & Fellgett, M. 2022. UKGEOS Cheshire - BHA-101 Initial Borehole Information Pack. NERC EDS National Geoscience Data Centre. (Dataset). <https://doi.org/10.5285/98432556-c319-495a-a0e0-711806a0a237>

Hillier, S. 1999. Use of an air-brush to spray dry samples for X-ray powder diffraction. *Clay Minerals*, 34, 127-135.

Hopson, PM. 2005. A stratigraphical framework for the Upper Cretaceous Chalk of England and Scotland, with statements on the Chalk of Northern Ireland and the UK Offshore Sector. British Geological Survey Research Report RR/05/01 102pp.

Hopson, PM, Wilkinson, IP, & Woods, M A. 2008. A stratigraphical framework for the Lower Cretaceous of England. British Geological Survey. British Geological Survey Research Report, RR/08/03.

Howard, AS, Hough E, Crofts, RG, Reeves, HJ & Evans, D. J. 2007. Geology of the Liverpool district—a brief explanation of the geological map. Sheet Explanation of the British Geological Survey. 1:50 000 Sheet 96 Liverpool (England and Wales).

- Ihsanullah, I, Sajid, M, Kabeer, M, Shemsi, AM & Atieh MA. 2020. First Investigations on the Removal of Tungsten Species from Water Using Multi-walled Carbon Nanotubes. *Water Air Soil Pollution*, 231, 119. DOI: <https://doi.org/10.1007/s11270-020-04485-2>
- Ketcham, RA. & Carlson, WD. 2001. Acquisition, optimization and interpretation of X-ray computed tomographic imagery: applications to the geosciences. *Computers & Geosciences*, Volume 27, pp. 381-400.
- Kim, SH, Lee, JH, Jung, K, Yang, JY, Shin, HS, Lee, JP, Jeong, J, Oh, JH & Lee, JK. 2019. Copper and Cobalt Ions Released from Metal Oxide Nanoparticles Trigger Skin Sensitization. *Front Pharmacol*. 2021 Apr 14;12:670581. PMID: 33679407; PMCID: PMC7933575.
- Milodowski, AE & Rushton, JC. 2008. Mineralogical and porosity characterisation of potential aquifer and seal units for carbon capture and storage methodologies for the CASSEM Project. British Geological Survey Report, CR/08/153.
- Moore, DM & Reynolds, RC. 1997. *X-Ray Diffraction and the Identification and Analysis of Clay Minerals, Second Edition*. Oxford University Press, New York.
- Mouli-Castillo, J, Heinemann, N & Edlmann, K. 2021. Mapping geological hydrogen storage capacity and regional heating demands: An applied UK case study. *Applied Energy*, vol. 283, p. 116348, 2021.
- Moyce, E, Rochelle, CA, Morris, K, Milodowski, AE, Chen, X, Thornton, S & Small, J. 2014. Rock alteration in alkaline cement waters over 15 years and its relevance to the geological disposal of nuclear waste. *Applied Geochemistry*, 50, 91-105.
- Newell, AJ. 2018. Rifts, rivers and climate recovery: A new model for the Triassic of England. *Proceedings of the Geologists' Association*. 129. 352-371.
- Nishimoto, M, Muto, I, Sugawara, Y & Hara, N. 2019. Pit Initiation Behavior at Sulfide Particles in Sintered Stainless Steels. *Electrochemical Society Meeting Abstracts* 236, 844-844.
- Plant, JA, Jones, DG & Haslam, HW. (editors). 1999. *The Cheshire Basin: Basin evolution, fluid movement and mineral resources in a Permo-Triassic rift setting*. Keyworth, Nottingham: The British Geological Survey.
- Reynolds Jr., R.C. & Reynolds III, R.C. 2013. Description of Newmod II™. The calculation of one-dimensional X-ray diffraction patterns of mixed layered clay minerals. R C Reynolds III, 1526 Farlow Avenue, Crofton, MD 21114.
- Rochelle, CA, Milodowski, AE, Bateman, K, Moyce, EBA & Kilpatrick, A. 2016. A long-term experimental study of the reactivity of basement rock with highly alkaline cement waters: Reactions over the first 15 months. *Mineralogical Magazine*, 80(6), 1089-1113.
- Rochelle, CA, Liddy, T, Lacinska, A, Ji, Y, Agofack, N & Cerasi, P. 2020. Report on the small-scale processes occurring during engineered precipitation and models to assist in the upscaling. Deliverable report 5.5, Subsurface Evaluation of Carbon Capture and Storage and Unconventional Risks (SECURE) project. <https://www.securegeoenergy.eu/>.
- Rubio-Nieblas, V, Pérez-Tello, M, Jacobs, RA, Herrera-Urbina, R. & Moreno-Zazueta, SA. 2014. Two-Dimensional Computational Modeling of the Electrokinetic Remediation of a Copper-Contaminated Soil. Part I: Model Validation". *Dyna (Medellin, Colombia)*. 81. 199-207. 10.15446/dyna.v81n183.36896.
- Snyder, R.L. & Bish, DL. 1989. Quantitative analysis. In: Bish, DL & Post, JE. (Editors), *Modern Powder Diffraction, Reviews in Mineralogy*, Volume 20, Mineralogical Society of America, USA, pp. 101-144 (Chapter 5).
- Tarkowski, R. 2019. Underground hydrogen storage: Characteristics and prospects. *Renewable and Sustainable Energy Reviews*, Volume 105, pp. 86-94
- Tkac, P & Paulenova, A. 2008. Speciation of Molybdenum (VI) In Aqueous and Organic Phases of Selected Extraction Systems, *Separation Science and Technology*, 43:9-10, 2641-2657, DOI: 10.1080/01496390802122261

UKGEOS. 2022. Data pack for borehole A101. Dataset available from <https://webapps.bgs.ac.uk/services/ngdc/accessions/index.html#item175587> .
<https://doi.org/10.5285/98432556-c319-495a-a0e0-711806a0a237>.

Van Gessel, S & Hajibeygi, H (eds). 2023. Hydrogen TCP- Task 42 Underground Hydrogen Storage. IEA Technology Monitor Report 2023.